



TECHNISCHE
UNIVERSITÄT
WIEN

Vienna University of Technology

Diplomarbeit

Structure and Extinction of Flames Mixtures of Biofuels and Hydrocarbon Fuels

ausgeführt zum Zwecke der Erlangung des akademischen Grades eines
Diplom-Ingenieurs unter der Leitung von

Ao.Univ.Prof. Dipl.-Ing Dr.techn. Ernst Pucher

Institut für Fahrzeugantriebe und Automobiltechnik
Technische Universität Wien

und

Prof. Dr. Kalyanasundaram Seshadri

Department of Mechanical and Aerospace Engineering
University of California, San Diego

eingereicht an der Technischen Universität Wien
Fakultät für Maschinenwesen und Betriebswissenschaften

von

Philipp Mairhofer

Matrikel Nr. 0926129
Sechshauserstraße 97/24
A – 1150 Wien

Wien, Mai 2015

Structure and Extinction of Flames Mixtures of Biofuels and Hydrocarbon Fuels

Diploma Thesis

Philipp Mairhofer

Institute for Powertrains and Automotive Technology
Faculty of Mechanical and Industrial Engineering

Vienna University of Technology

Advisors:

Ao. Univ-Prof. Dipl.-Ing. Dr.techn. Ernst Pucher
Institute for Powertrains and Automotive Technology
Vienna University of Technology, Austria

Prof. Dr. Kalyanasundaram Seshadri
Department of Mechanical and Aerospace Engineering
University of California, San Diego, USA

San Diego, May 2015

Abstract

Experimental, numerical and analytical studies are conducted to gain a better understanding of the influence of the stoichiometric mixture fraction ξ_{st} on the structure and critical conditions of extinction of non-premixed methane and non-premixed dimethyl ether flames.

Experimental studies were carried out using a counterflow setup, consisting of an oxidizer duct and a fuel duct. A steady, laminar and axisymmetric flow leaves each duct and stagnates against the flow of the opposed duct. In this way a stagnation plane is produced by the two reactant streams, leading to a reaction zone at the boundary layer. By diffusion the oxidant and the fuel form a flammable mixture.

The combustion in a counter flow burner mainly depends on the chemical reaction time, the velocity of the flow of the fuel and the flow of the oxidizer. The characteristic chemical time depends on the adiabatic temperature and the stoichiometric mixture fraction, whereas the characteristic flow time is given by the strain rate. If the fuel and oxidizer velocities exceed a certain value the reaction ends abruptly. This state is called extinction. In order to elucidate the effect of ξ_{st} , the mass fractions of the reactants were so chosen that T_{st} is fixed.

For methane, it was found that the strain rate at extinction continually increased with increasing ξ_{st} , signifying that with decreasing fuel mass fraction and rising oxygen mass fraction the flame becomes harder to extinguish. This was confirmed by numerical studies and asymptotic analysis. The predictions of the analysis show that with increasing values of ξ_{st} , the scalar dissipation rate at extinction $\chi_{st,q}$ first increases and then decreases. A key outcome of the analysis is that with increasing stoichiometric mixture fraction, the thickness of the regions where oxygen and fuel are consumed first increases and then decreases. Numerical computations using the San Diego Mechanism show a full consumption of fuel and a leakage of oxygen for all

values of ξ_{st} , whereas computations using one-step chemistry show a leakage of fuel from the reaction zone at low values of ξ_{st} and a leakage of oxygen at low $(1 - \xi_{st})$.

Results of extinction experiments in the counterflow burner with dimethyl ether show a decrease followed by an increase in the strain rate at extinction with increasing values of ξ_{st} . This behavior is observed at different oxidizer and fuel mass fractions obtained using various Lewis numbers in the calculation of the mixture fraction. Numerical computations were performed but do not match the experimental results, showing a much more significant decrease in strain rates at extinction.

Kurzfassung

Experimentelle, numerische und analytische Studien werden durchgeführt um ein besseres Verständnis des Einflusses des stöchiometrischen Mischungsverhältnisses ξ_{st} auf die Struktur und die kritischen Bedingungen der Erlöschung von nicht vorgemischten Methan- und nicht vorgemischten Dimethylether-Flammen zu erlangen.

Experimentelle Untersuchungen wurden mit einem Gegenstrombrenner durchgeführt, welcher aus einem Oxidationskanal und einem Brennstoffkanal besteht. Ein stetiger, laminarer und axialsymmetrischer Strom wird von jedem Kanal dem Brennraum zugeführt und führt zur Entstehung einer Stauebene. Durch die zwei reaktionsfähigen Ströme entsteht in der Nähe der Stauebene eine dünne viskose Grenzschicht, in der die Ströme in einem stöchiometrischem Verhältnis stehen.

Die Verbrennung in einem Gegenstrombrenner ist abhängig von der chemischen Reaktionszeit (abhängig von der adiabaten Flammentemperatur und dem Mischungsverhältnis) und der Verweilzeit der Reaktionspartner (abhängig von der Strömungsgeschwindigkeit der Gase). Wenn die Strömungsgeschwindigkeiten des Oxidationsstroms und des Brennstoffstroms einen kritischen Wert übersteigen endet die Reaktion abrupt. Dieser Zustand wird als Erlöschung bezeichnet. Um den Einfluss des stöchiometrischen Mischungsverhältnisses auf die Erlöschung zu untersuchen werden die Massenanteile der Reaktionspartner so gewählt, dass die adiabate Flammentemperatur T_{st} einen konstanten Wert annimmt.

Die Experimente mit Methan als Brennstoff zeigen, dass die Strain-Rate im Punkt der Erlöschung kontinuierlich steigt mit zunehmendem stöchiometrischem Mischungsbruch. Das bedeutet, dass die Flamme mit abnehmendem Brennstoffmassenanteil und steigendem Sauerstoffmassenanteil schwieriger erlischt. Dies wird durch die numerischen Berechnungen und die asymptotische Analyse bestätigt. Die Vorhersagen der asymptotischen Analyse zeigen, dass die skalare Dissipationsrate χ_{st} , mit

steigendem ξ_{st} zuerst zunimmt und dann abfällt. Parallel dazu nehmen auch die Reaktionsebenen in ihrer Stärke zu, um dann bei hoher stöchiometrischer Mischungsrate abzunehmen. Numerische Berechnungen mit dem San Diego Mechanismus deuten darauf hin, dass über die gesamte Bandbreite der Mischungsverhältnisse ein Entweichen von Sauerstoff von der Reaktionszone vorliegt. Berechnungen mit einem einfachen reduzierten Mechanismus hingegen zeigen ein Entweichen von Brennstoff bei niedrigem ξ_{st} , sowie ein Entweichen von Sauerstoff bei niedrigem $(1 - \xi_{st})$.

Verbrennungsversuche mit Dimethylether in dem Gegenstrombrenner zeigen eine Abnahme der Strain-Rate zum Zeitpunkt der Erlöschung, gefolgt von einer Zunahme mit steigendem Mischungsverhältnis. Dieses Verhalten kann bei unterschiedlichen Massenanteilen von Oxidationsmittel und Kraftstoff beobachtet werden, welche sich durch eine Variation der Lewis-Zahl ergeben. Die Ergebnisse der numerischen Simulation stimmen nicht mit den Ergebnissen überein, sie zeigen eine signifikante Abnahme der Strain-Rate über nahezu die gesamte Bandbreite des Mischungsverhältnisses.

Acknowledgements

First of all I would like to thank the persons who granted me the opportunity to conduct research and write my diploma thesis at the University of California in San Diego. My utmost appreciation goes to Professor Ernst Pucher, my advisor at Vienna University of Technology, who offered me to write my diploma thesis abroad. His persistent efforts to establish and maintain international relationships are remarkable! Furthermore, I would like to express my gratitude toward Professor Kalyanasundaram Seshadri, my advisor at the University of California San Diego, who invited me to join his team and conduct research in his facilities. His knowledge in combustion is unsurpassable and I am glad that I could learn from him.

Moreover, I would like to thank Gerald Mairinger, my co-worker in the lab. His support, knowledge and advice during my research were of great value.

I would like to express my gratitude toward the Austrian Marshallplan Foundation and the Federation of Austrian Industries for their financial support.

My special thanks goes out to my family, who have continually supported me during my time in the United States, as well as throughout the last years of studying. Their advice and encouragement are key to my success.

Last, but certainly not least, I would like to thank my fiancée Lisa for her never ending patience and support. Thank you for allowing me to embark on my journey and for sharing this adventure!

Table of Contents

List of Symbols	VIII
Subscripts	XI
Nomenclature	XII
1. Introduction.....	1
1.1. Tested Fuels	3
1.1.1. Methane	4
1.1.2. Dimethyl Ether	5
1.2. Counter Flow Configuration.....	7
1.3. Strain Rate	9
1.4. The S-shaped Curve	10
1.5. Arrhenius Equation.....	12
2. Experimental Setup.....	14
2.1. Lower Part of the Burner	15
2.2. Upper Part of the Burner	16
2.3. Gas Supply.....	17
2.4. LabVIEW Controlling Software.....	18
2.4.1. Fixed Parameters.....	20
2.4.2. Calculated Parameters	20
2.5. Controlling Units	22
2.5.1. Mass Flow Controllers.....	22
2.5.2. Temperature Measurement.....	23
3. Extinction Experiments	25
3.1. Experimental Procedure and Preparation	25
3.2. Adiabatic Flame Temperature	26
3.2.1. Adiabatic Flame Temperature of Methane.....	26
3.2.2. Adiabatic Flame Temperature of Dimethyl Ether	27
3.3. Mixture Fraction.....	28
3.4. Determining the Mass Fractions	31
3.4.1. Boundary Values at $T_{st} = 2000\text{K}$ for non-premixed Methane Flames	31
3.4.2. Boundary Values at $T_{st} = 2100\text{K}$ for non-premixed Methane Flames	33

3.4.3.	Boundary Values at $T_{st} = 2000\text{K}$ for non-premixed Dimethyl Ether Flames.....	34
4.	Computational Simulations.....	38
4.1.	Numerical Computations.....	38
4.2.	Rate-Ratio Asymptotic Analysis.....	39
4.2.1.	The Outer Structure.....	40
4.2.2.	Reduced Mechanism.....	41
4.2.3.	The Structure of the Reaction Zone.....	43
4.2.4.	The Scalar Dissipation Rate.....	47
5.	Experimental and Numerical Results.....	49
5.1.	Extinction of Methane.....	49
5.1.1.	Results of the Rate-Ratio Asymptotic Analysis.....	59
5.2.	Extinction of Dimethyl Ether.....	64
6.	Concluding Remarks.....	68
	References.....	i
	List of Figures.....	iv
	List of Tables.....	vii
	Appendix A.....	viii
A.1	Experimental Data: Extinction of Methane at $T_{st} = 2000\text{K}$	viii
A.2	Experimental Data: Extinction of Methane at $T_{st} = 2100\text{K}$	xii
A.3	Experimental Data: Extinction of Dimethyl Ether with $Le = 1.5$	xv
A.4	Experimental Data: Extinction of Dimethyl Ether with $Le = 1.4$	xviii
A.5	Experimental Data: Extinction of Dimethyl Ether with $Le = 1.6$	xx
	Appendix B.....	xxii

List of Symbols

A	pre-exponential factor for Arrhenius equation
A_1	fuel duct area [m ²]
A_2	oxidizer duct area [m ²]
$A_{curt,1}$	fuel curtain area [m ²]
$A_{curt,2}$	oxidizer curtain area [m ²]
a_1	fuel duct strain rate [1/s]
a_2	oxidizer duct strain rate [1/s]
c_p	specific heat capacity (isobaric) [J/kgK]
d_{sc}	diameter of the oxidizer screen [m]
d_w	diameter of the thermocouple wire [m]
D_i	coefficient of diffusion of species i [-]
Da	Damköhler number [-]
E_A	activation energy [cal/mole]
E_b	activation energy for a backward reaction [cal/mole]
E_f	activation energy for a forward reaction [cal/mole]
F_{sc}	view factor of the oxidizer screen [-]
$F_{sur,upper}$	view factor of the upper surroundings [-]
$F_{sur,lower}$	view factor of the lower surroundings [-]
ΔH	heat of reaction [cal/mole]
k	reaction rate constant
f_k	thermal conductivity of air [W/mK]
L	distance between the fuel duct and the oxidizer duct [mm]
Le_{dme}	Lewis number dimethyl ether [-]
Le_{CH_4}	Lewis number methane [-]
\dot{m}_1	mass flux of the fuel stream [kg/s]
\dot{m}_2	mass flux of the oxidizer stream [kg/s]
Nu_{cyl}	Nusselt number [-]
p	ambient pressure [Pa]
Q_F	heat release of fuel [J/mole]
Q_{CH_4}	heat release of methane [J/mole]

Q_{dme}	heat release of dimethyl ether [J/mole]
\dot{Q}_{cat}	heat flow loss due to surface-induced catalytic reactions [W]
\dot{Q}_{cond}	heat flow loss due to conduction [W]
\dot{Q}_{conv}	heat flow loss due to convection [W]
\dot{Q}_{rad}	heat flow loss due to radiation [W]
R	gas constant [J/moleK]
Re	Reynolds number of air [-]
T	absolute temperature (Arrhenius equation) [K]
T_1	temperature of the stream at the fuel duct exit [K]
T_2	temperature of the stream at the oxidizer duct exit [K]
T_u	temperature of the unburnt mixture [K]
T_{ref}	reference temperature [K]
T_{surr}	surrounding temperature [K]
T_{st}	adiabatic flame temperature [K]
T_{tc}	temperature measured by the thermocouple [K]
t_c	chemical reactive time [s]
t_m	time of convection and diffusion [s]
V	volume [m ³]
V_1	normal component of the velocity of the fuel stream at the duct exit [m/s]
V_2	normal component of the velocity of the oxidizer stream at the duct exit [m/s]
$\dot{V}_{O_2,2}$	volume stream of oxygen [m ³ /s]
$\dot{V}_{F,1}$	volume stream of fuel [m ³ /s]
$\dot{V}_{CURT,1}$	volume stream of the fuel curtain [m ³ /s]
$\dot{V}_{CURT,2}$	volume stream of the oxidizer curtain [m ³ /s]
$\dot{V}_{DME,1}$	volume stream of dimethyl ether [m ³ /s]
$\dot{V}_{CH_4,1}$	volume stream of dimethyl ether [m ³ /s]
$\dot{V}_{N_2,1}$	volume stream of nitrogen (fuel stream) [m ³ /s]
$\dot{V}_{N_2,2}$	volume stream of nitrogen (oxidizer stream) [m ³ /s]
$\dot{V}_{SLM,i,j}$	volume stream scaled to the normal temperature [m ³ /s]
$u_{rel,curt}$	relative velocity of the curtain to the inner duct [-]

W_F	molecular weight of fuel [g/mole]
W_{O_2}	molecular weight of oxygen [g/mole]
W_{CH_4}	molecular weight of methane [g/mole]
W_{DME}	molecular weight of dimethyl ether [g/mole]
W_{N_2}	molecular weight of nitrogen [g/mole]
$X_{O_2,2}$	oxygen mole fraction of oxidizer stream [-]
$X_{CH_4,1}$	methane mole fraction of fuel stream [-]
$X_{DME,1}$	dimethyl ether mole fraction of fuel stream [-]
$X_{N_2,1}$	nitrogen mole fraction of fuel stream [-]
$X_{N_2,2}$	nitrogen mole fraction of oxidizer stream [-]
$Y_{O_2,2}$	oxygen mass fraction of oxidizer stream [-]
$Y_{CH_4,1}$	methane mass fraction of fuel stream [-]
$Y_{DME,1}$	dimethyl ether mass fraction of fuel stream [-]
$Y_{N_2,1}$	nitrogen mass fraction of fuel stream [-]
$Y_{N_2,2}$	nitrogen mass fraction of oxidizer stream [-]
Z	mixture fraction [-]
Z_{st}	stoichiometric mixture fraction [-]
β	temperature exponent [-]
λ	coefficient of thermal conductivity [-]
ρ	density [kg/m ³]
ρ_1	density at the fuel duct exit [kg/m ³]
ρ_2	density at the oxidizer duct exit [kg/m ³]
ξ	mixture fraction [-]
ξ_{st}	stoichiometric mixture fraction [-]
ξ_{dme}	dimethyl ether mixture fraction [-]
ω_{dme}	reaction rate of dimethyl ether [1/m ³ s]

Subscripts

1	fuel duct side
2	oxidizer duct side
u	unburned
b	burned
q	extinction

Nomenclature

CH ₃ OCH ₃	Dimethyl ether
CIDI	Compression-Ignition Direct-Injection
CNG	Compressed natural gas
CH ₄	Methane
CO	Carbon monoxide
CO ₂	Carbon dioxide
DME	Dimethyl ether
H ₂ O	Water
LHV	Lower heating value
LNG	Liquefied natural gas
LPG	Liquefied petroleum gas
MFC	Mass flow controllers
NO _x	Nitrous oxides
O ₂	Oxygen
PID	Proportional integral derivative
RON	Research octane number
UCSD	University of California, San Diego

Chapter 1

Introduction

In our modern-day, fast moving society, a world without combustion is no longer imaginable. Combustion of fossil-fuels is the basis for transportation, manufacturing and electricity production in power plants and was the foundation of the industrial and economic progress in the 20th century. As mobility is a basis for economic development and a fundamental human need, a global increase in demand of transport of commodities and individuals can be observed. Due to the presently inadequate storage capacities of modern batteries for electric vehicles, the internal combustion engine still serves as a universal propulsion system for passenger cars, trucks, and navigation. Fossil fuels serve as the main fuel supply, challenging the current climate and emission situation and leading to severe restrictions of ground transportation and aviation.

Combustion is a complex process, in which a substance reacts rapidly with oxygen and gives off heat. From a chemical perspective, it can be simplified to the transformation of chemical bond energy into thermal energy by conversion of reactants to products. This simplification illustrates the two main challenges combustion faces today: the constant supply of crude oil to meet the ever increasing demand for energy consumption and the safe and sustainable handling of the products with regard to their impact on the global climate. Fossil fuels are a limited resource that will eventually deplete, and with large countries entering the phase of intensified industrialization the need for alternative fuel sources is pressing. In addition, numerous governments want to lower their dependency on crude oil due to their limited access to fossil fuel reserves. This calls for the search of alternatives and creating an infrastructure that can support the gradual replacement of fossil fuels. The

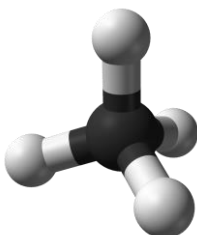
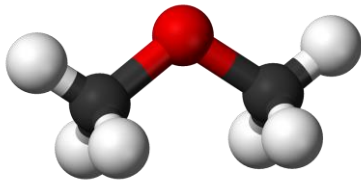
second challenge of fossil fuel combustion, dealing with the products and the resulting change in climate has become one of the biggest challenges of the 21st century. The environmental impact due to the increasing consumption of fossil fuels can be felt and seen throughout the world, imposing a serious threat to the health of many. Especially in the booming economies of China and India, air pollution from traffic and industry has become a serious concern. Hence, various governments, especially in highly developed regions, have introduced restrictions for vehicles and industries to regulate emissions and decelerate climate change.

With ever growing concerns on future oil supplies, environmental pollution and energy security, it is essential to find non-petroleum based alternative fuels, along with more advanced energy technologies to increase the efficiency of energy use. A promising alternative fuel must show severe improvements in major impact areas such as well-to-wheel greenhouse gas emissions, fuel versatility, infrastructure, availability, economics and safety. Two leading alternative fuel candidates with the potential to decrease the dependency on petroleum are dimethyl ether and methane. Dimethyl ether is being studied as an oxygen-rich fuel additive or replacement for diesel in an effort to decrease emissions in compression ignition engines and methane has been considered an alternative fuel for many years. For a better understanding of the combustion behavior of these two fuels, the critical conditions of extinction of these fuels are studied under ambient pressure.

1.1. Tested Fuels

In this thesis the combustion behavior of methane and dimethyl ether is analyzed. Methane plays an important role in the biofuel sector, as it is the main constituent of compressed natural gas (CNG). Dimethyl ether is considered a promising alternative to diesel fuel due to its high cetane number of 55 to 60. Both fuels are the most simple compounds of their type, methane being the most basic alkane and dimethyl ether being the most elementary ether. This makes the comparison of these fuels very interesting. The properties of methane and dimethyl ether can be found in table 1.1.

Table 1.1: Properties of Methane and Dimethyl Ether [18,19]

	Methane	Dimethyl Ether
Chemical Structure		
Chemical formula	CH ₄	CH ₃ OCH ₃
Molar mass (g/mole)	16.04	46.07
Density	0.656 g/L (298.15 K, 1 atm) 0.716 g/L (273.15 K, 1 atm)	1.860 g/L (298.15K, 1 atm) 2.115 g/L (273.15K, 1 atm)
Melting point (°C)	-182.5	-141.49
Boiling point (°C)	-161.49	-24.81
LHV (MJ/kg)	50.01	28.62
Carbon content (wt%)	74	52.2
Sulfur content (ppm)	7-25	0

1.1.1. Methane

Methane is a colorless, odorless, non-toxic and flammable gas with the chemical formula CH_4 . It is classified as a hydrocarbon, being an organic compound consisting entirely of hydrogen and carbon. Methane, being the most elementary alkane, is composed entirely of single bonds and is saturated with hydrogen, therefore belonging to the group of saturated hydrocarbons.

Due to its relative abundance methane is considered an attractive fuel. It is used as such in various forms and states, predominantly in a compressed state or liquid state. Natural gas consists primarily of methane and is used not only as an energy source for cooking, heating and power generation, but also as a fuel for motor vehicles. Natural gas vehicles (NGVs) were first introduced in Italy in the 1930's, but remained widely disregarded until the oil crisis in the 1970's and 1980s. Their promotion ceased rapidly after the crisis had been overcome, and interest in NGVs remained low until reducing air pollution became a priority and the expansion of alternative fuels was backed by local governments.

Gasoline can be substituted by compressed natural gas (CNG), which is made by compressing natural gas to less than 1% of its volume at standard pressure. CNG is either used in conventional internal combustion engines that have been adapted to allow operation with natural gas, or in vehicles specifically manufactured for CNG use. Compressed natural gas offers number of advantages, first and foremost the environmental benefits of reducing local air pollution. Natural gas vehicles have the potential of emitting lower levels of carbon monoxide, nitrous oxides, particulate matter and air toxics as well as lowering cold-start emissions [23]. In addition, CNG mixes evenly with air due to its gaseous state. The drawback of CNG use is the storage difficulty, requiring a greater amount of space for fuel storage than

conventional gasoline powered vehicles due to the high pressure of the storage tanks.

Naturally occurring methane is primarily produced by the process of methanogenesis. Microbes known as methanogens are organisms capable of producing methane in the final step of decomposition of biomass. Methane or methane-rich gases produced by the anaerobic decay of non-fossil organic matter are often referred to as biogas.

Methane can also be produced by power-to-gas technology, converting electrical power to a gaseous fuel. Electricity is used to split water into hydrogen and oxygen by means of electrolysis. The resulting hydrogen is combined with carbon dioxide to form methane using a methanation reaction, such as the Sabatier reaction or biological methanation. Natural gas, however, is so abundant that the intentional industrial production is relatively rare.

1.1.2. Dimethyl Ether

Dimethyl Ether (DME) is the simplest ether and has the chemical formula CH_3OCH_3 , occasionally simplified to $\text{C}_2\text{H}_6\text{O}$. It burns with a visible blue flame and, unlike methane, it does not require an odorant due to its typical sweet ether-like odor. Due to its low normal boiling point, DME is gaseous at 20°C and 1 atm and liquid above 6.1 atm. Although dimethyl ether is considered a volatile organic compound, it is non-carcinogenic, non-mutagenic and non-toxic [19].

Dimethyl Ether is a promising alternative for standard petroleum fuels and has been promoted as a oxygen-rich fuel additive or replacement of diesel in compression ignition engines. Advantages of DME are the decreased pollutant emissions, shown in CIDI engine tests comparing dimethyl ether and diesel. The results reveal substantially lower emissions of NO_x , hydrocarbons and carbon monoxide together with a soot-free combustion [20]. In addition,

its higher cetane number (55-60) makes it an attractive substitute for diesel (55). Only minor modifications are necessary to convert a diesel engine to burn dimethyl ether. Negative aspects are the lack of lubrication of DME as well as the higher fuel consumption, due to the lower energy by mass of DME (28.62 kJ/kg) compared to the energy by mass of diesel (41.66 kJ/kg). Therefore a larger volume of dimethyl ether must be injected into the cylinder to obtain the same combustion performance as diesel and larger fuel storage tanks are required.

Currently two different methods for the production of DME exist, the conventional indirect synthesis and the recently developed direct synthesis. Both require synthesis gas (syngas) as primary feedstock. Indirect synthesis is a two step process, in which syngas is first converted to methanol and subsequently dehydrated to DME. Direct synthesis merges these two steps into one step. The methanol synthesis and dehydration take place in the same process unit, with no methanol isolation and purification. Since the thermodynamic limitations of methanol synthesis can be bypassed this method proves to be more efficient [20-22]. Dimethyl ether produced from bio sources or bio gas is referred to as BioDME.

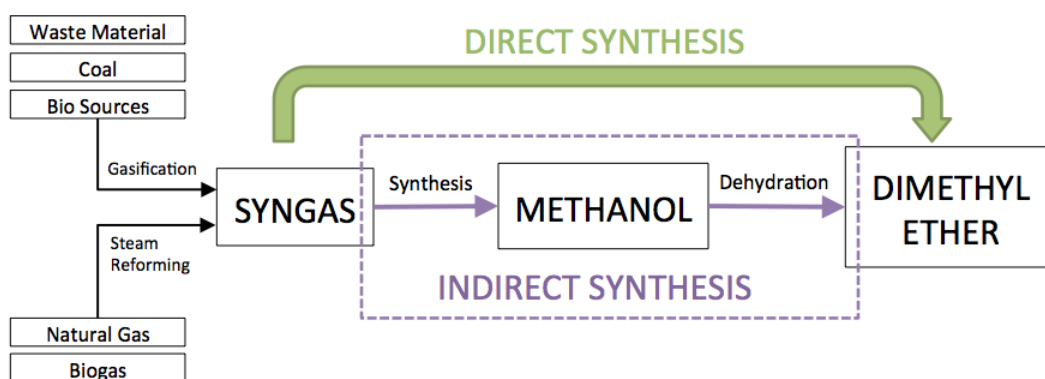


Figure 1.1: DME Production Methods: Direct and Indirect Synthesis

1.2. Counter Flow Configuration

For convenience, combustion processes are considered to be either premixed or non-premixed.

In premixed combustion, the reactants are mixed before they reach the reaction zone. In order to create a premixed stream in a counter flow configuration, the oxidizer would be added to the fuel stream. This would result in the oxidizer, the fuel and nitrogen entering the reaction zone through the fuel duct, and an inert nitrogen stream entering through the oxidizer duct. Premixed flames are used in spark ignition engines for instance, when intense combustion is necessary within small volume. The flame in a premixed system propagates with finite velocity. [1, 2]

Any system in which fuel and oxidizer enter separately into the combustion area is called non-premixed. The mixing occurs at the same time the reaction takes place, through convection and diffusion. Chemical reactions can only occur when mixing takes place at a molecular level, the rate of diffusion being the crucial factor. For this reason non-premixed flames are also referred to as diffusion flames.

A simple example of a diffusion flame, where mixing occurs simultaneously with the combustion process, is a candle flame. The paraffin of the candle melts through the heat of the flame and rises the wick through capillary forces. There it evaporates into paraffin vapor, acting as the gaseous fuel supply. Surrounding air diffuses into the flame due to buoyancy, functioning as oxidizer. By blowing air into the candle, the flame temperature rises due to the increase in oxygen. If, however, the velocity of the influx exceeds a certain limit, the flame is extinguished. This demonstrates the effect a change of flow velocity can have in a combustion process. This phenomenon can also be observed in internal combustion engines, and is referred to as quenching. [1, 3]

In this thesis, all combustion experiments are carried out using a non-premixed flame setup. To investigate the combustion behavior, the extinction experiments are conducted using a counter flow configuration.

This counter flow configuration consists of two ducts, an oxidizer duct and a fuel duct. The two ducts are arranged in a vertically opposing position, the distance between the ends of the ducts varying for different experiments. Pure oxygen or oxygen diluted with nitrogen enters through the upper duct, hence called oxidizer duct. The lower duct is referred to as fuel duct, as a mixture of fuel and nitrogen enters the combustion area from this side. The combustion zone is guided by nitrogen curtains to screen the reaction from the outside environment. A detailed description of the counter flow burner is given in chapter 2.

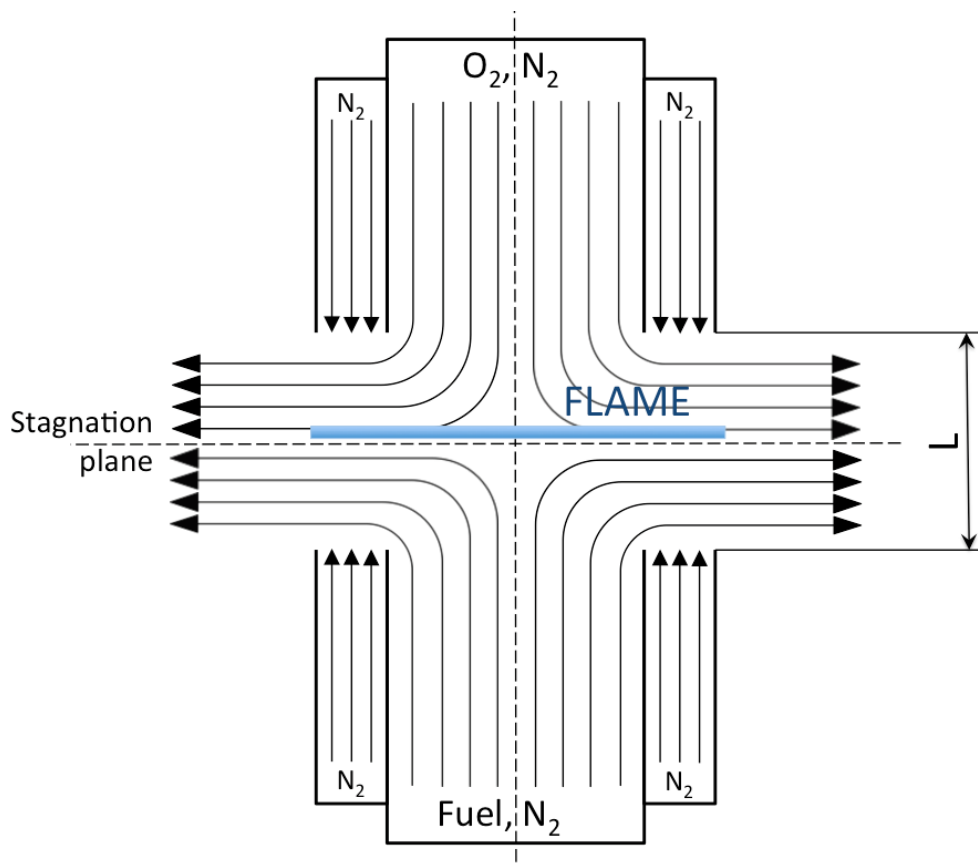


Figure 1.2: Schematic illustration of the counterflow burner with an established flame

A steady, laminar and axisymmetric flow leaves each duct and stagnates against the flow of the opposed duct. In this way a stagnation plane is

produced by the two reactant streams, leading to a reaction zone at the boundary layer. By diffusion the oxidant and the fuel form a flammable mixture in the region with the maximum energy output. This is the region where the fluxes of the streams are in stoichiometric proportions.

The combustion in a counterflow burner is mainly determined by the chemical reaction time as well as the velocity of the flow of the fuel and the flow of the oxidizer. Similar to the candle flame example, the reaction of the fuel and oxidizer ends abruptly if the fuel and oxidizer velocity exceed a certain value.

1.3. Strain Rate

To provide an accurate characterization of the flow field and quantify the velocity of the flows the strain rate, „ a “, is introduced. It is defined as the normal gradient of the normal component of the flow velocity and changes from the exit of the fuel duct to the exit of the oxidizer duct [11]. It is the reciprocal of the characteristic flow time in the flow field of a counterflow flame and is discontinuous across the stagnation plane [26]. The strain rate is obtained from an asymptotic theory where the Reynolds numbers of the laminar flow at the boundaries are presumed to be large [4].

The strain rate a_2 of the oxidizer duct at the stagnation plane is given by

$$a_2 = \frac{2 |V_2|}{L} \left(1 + \frac{|V_1| \sqrt{\rho_1}}{|V_2| \sqrt{\rho_2}} \right) \quad (1.1)$$

where index 1 indicates the conditions of the fuel side and index 2 the oxidizer side. L is the distance between the two ducts [m], ρ_1 and ρ_2 the densities of the fuel and oxidizer streams at the boundaries [kg/m^3] and V_1 and V_2 the normal components of the flow velocities for the fuel and oxidizer side [m/s].

The quantity a_2 is a good measure of the characteristic residence time for $0 < \xi_{st} < 0.5$. On the fuel side of the stagnation plane, the strain rate is

$$a_1 = a_2 \sqrt{\frac{\rho_2}{\rho_1}} \quad (1.2)$$

and represents a better measure for the characteristic residence time for $0.5 < \xi_{st} < 1$. The strain rates of these two measures are discontinuous.

By using the momentum balance, equation (1.1) can be reduced to

$$V_2 = \frac{a_2 L}{4} \quad (1.3)$$

According to equation (1.3), the velocity of the oxidizer stream can be calculated for a given oxidizer strain rate.

1.4. The S-shaped Curve

A diffusion flame in a counter flow configuration has two burning limits; the point of autoignition and the point of extinction. To illustrate these two limits, the S-shaped curve can be a useful aid. It is determined by calculating the maximum temperature T_{max} in a flow field as a function of the strain rate.

The curve consists of a stable upper-, an unstable middle- and a stable lower branch. The upper branch describes the temperature of a burning flame at different strain rates, whereas the lower branch represents the temperature of a non-burning mixture before ignition at different strain rates.

For a better understanding of the S-shaped curve, the Damköhler-number Da is introduced. It describes the ratio of the characteristic time of convection and diffusion t_m (residence time) to the characteristic chemical reaction time t_c of combustion. The residence is dependent on the properties of the flow field, whereas the chemical reaction time is specified by the fuel and indicates its reactivity.

$$Da = \frac{t_m}{t_c} \quad (1.4)$$

Slow chemical reactions have low Damköhler numbers, fast chemical reactions have high Damköhler numbers. Diffusion flames typically have large Damköhler numbers, as the time of transport and mixing of the reactants t_m is very high.

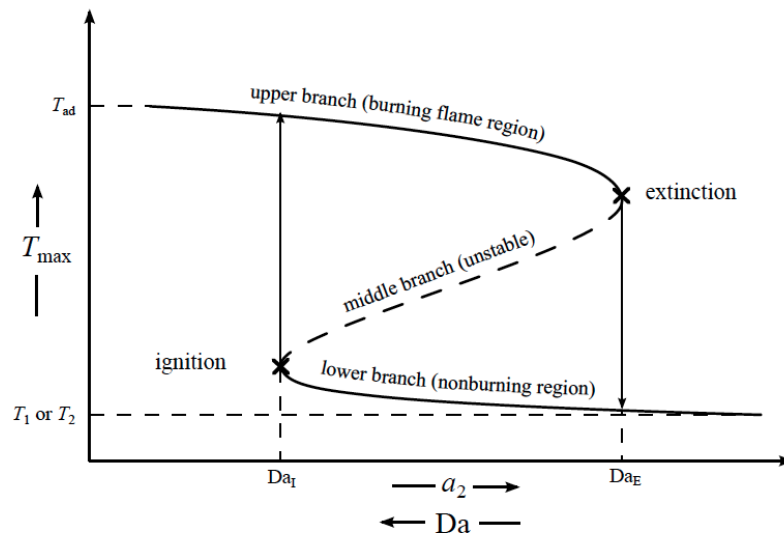


Figure 1.3: The maximum temperature T_{max} as a function of the Damköhler number - the characteristic S-shaped curve. T_1 is the temperature of the fuel boundary, T_2 the temperature of the oxidizer boundary, T_{ad} the adiabatic flame temperature, Da_I the Damköhler number at ignition, Da_E the Damköhler number at extinction.

On the lower branch of the S-shaped curve, the flows are considered frozen because chemical reactions are not significant. At high strain rates, the two opposing streams mix, the temperature of the frozen flow equaling the higher temperature of the two streams. By decreasing the strain rate, the residence time of the reactants increases and thus the Damköhler number. The temperature rises accordingly, leading to a critical point where the mixture autoignites. The maximum temperature of the flame is now represented on the upper branch. Autoignition can equally be attained by increasing the temperature at a constant strain rate.

By increasing the strain rate of the established flame on the upper branch, the residence time of the reactants decreases, leading to a lower maximum flame temperature. At a certain strain rate the flame extinguishes and the

temperature drops immediately to the lower branch. This point is referred to as the point of extinction.

The middle branch is physically unstable, thus no flames can be observed. [3]

1.5. Arrhenius Equation

In order to understand the temperature dependency of the reaction rate on a molecular basis the Arrhenius equation is helpful. The reaction rate constant k is given by Arrhenius as

$$k = AT^\beta e^{-\frac{E_A}{RT}} \quad (1.5)$$

where A is the pre-exponential factor [$1/K^\beta s$], β is the temperature exponent [-], T is the absolute temperature [K], R is the gas constant [J/moleK] and E_A is the activation energy [J/mole].

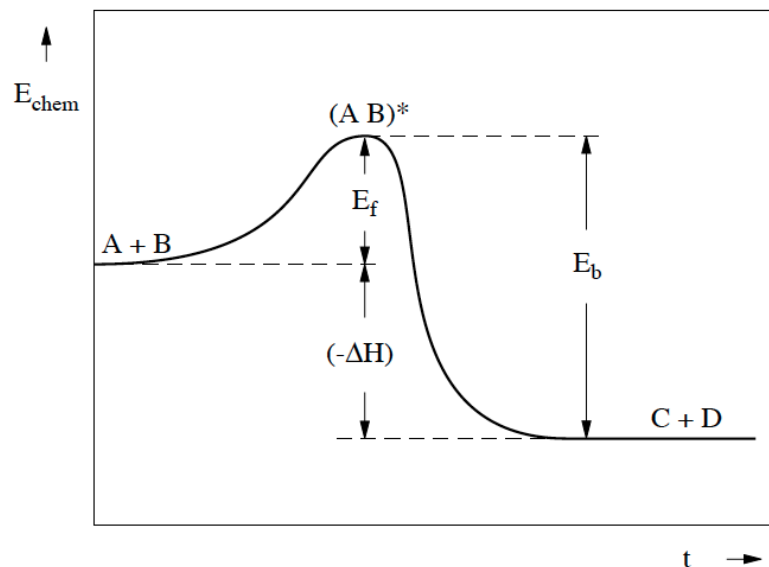


Figure 1.4: Schematic illustration of the chemical energy contained in the reactants, the activated complex and the products of the reaction [7]

The activation energy is the minimum amount of energy needed in a chemical system with potential reactants to start a chemical reaction. As described in Figure 1.4, the reactants A and B form an activated complex $(A B)^*$ with a higher energy level. The energy level of this transition term is higher by the

amount E_f than the energy contained in the single reactants. Assuming an exothermic reaction, the enthalpy of the products C + D is lower than the enthalpy of the reactants, as the activation energy as well as the heat of the reaction ΔH are released. E_b is the energy of the backward reaction needed to obtain the energy level of the activated complex and is the sum of E_f and ΔH . The heat of reaction is the maximum amount of energy that can be generated by an exothermic reaction. [7, 8]

Chapter 2

Experimental Setup

The experimental setup, as shown in Figure 2.1, consists of the counterflow burner, the gas supply for the oxidizer and the fuel duct, the mass flow controllers, the exhaust system as well as the control software. The counterflow burner is made up of two parts, the fuel duct and the oxidizer duct. The various components are discussed in the following chapters.

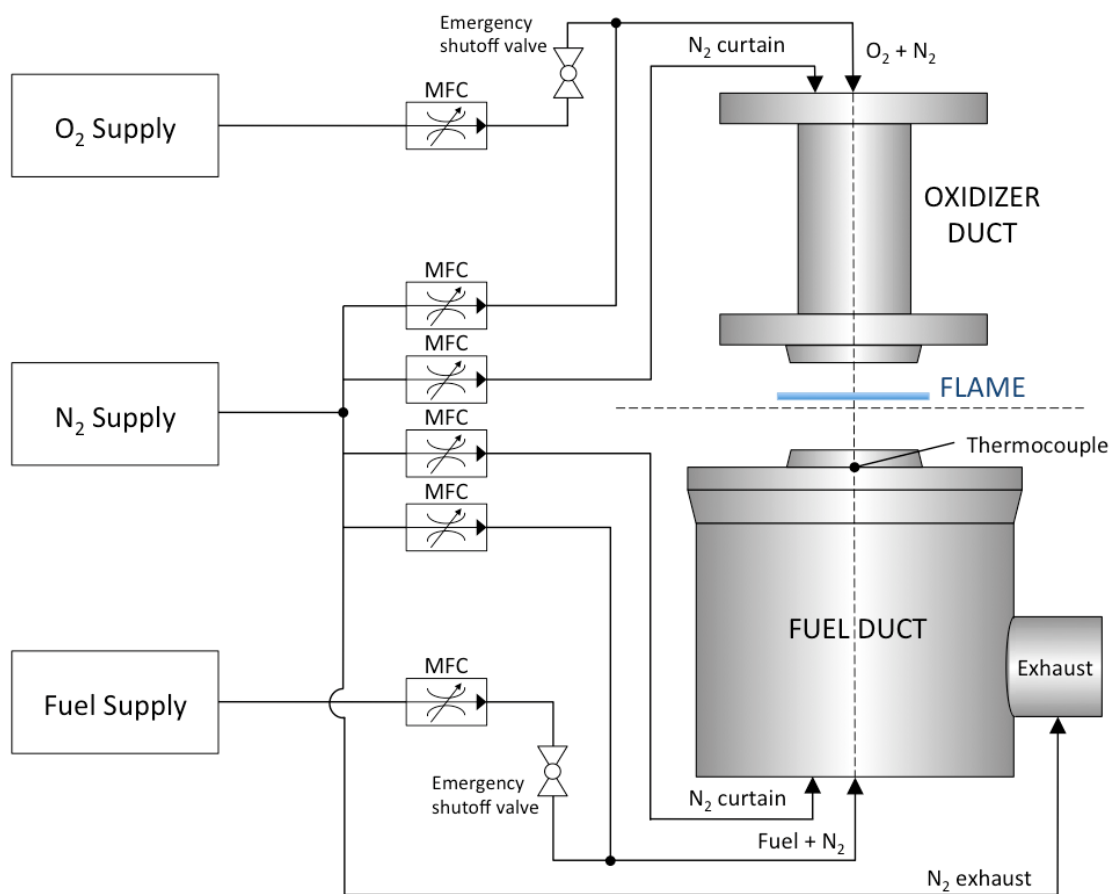


Figure 2.1: Schematic illustration of the experimental setup, showing the counterflow burner, the mass flow controllers and the gas supply.

2.1. Lower Part of the Burner

The purpose of the lower part of the burner is directing the fuel stream to the reactive flow field, hence called the fuel duct. The fuel is guided through the main duct into the reaction zone. At the exit of the fuel duct, 3 screens are arranged to ensure a uniform velocity profile (plug flow profile) and to prevent flashback. They consist of stainless steel mesh of 200 lines per inch and are held in place by 4 steel rings, reducing the effective diameter of the duct to 23mm.

The main duct is surrounded by a second concentric duct, which is referred to as the curtain duct. Nitrogen flows through the curtain duct toward the reaction zone, shielding it from the environment. The hot combustion products are sucked away from the reaction zone into an annular concentric section around the curtain duct. The exhaust is connected to the internal building extraction system, ensuring a safe disposal of the reaction products. To prevent further reactions in the outlying exhaust the exhaust gases are cooled by 6 water spray nozzles.

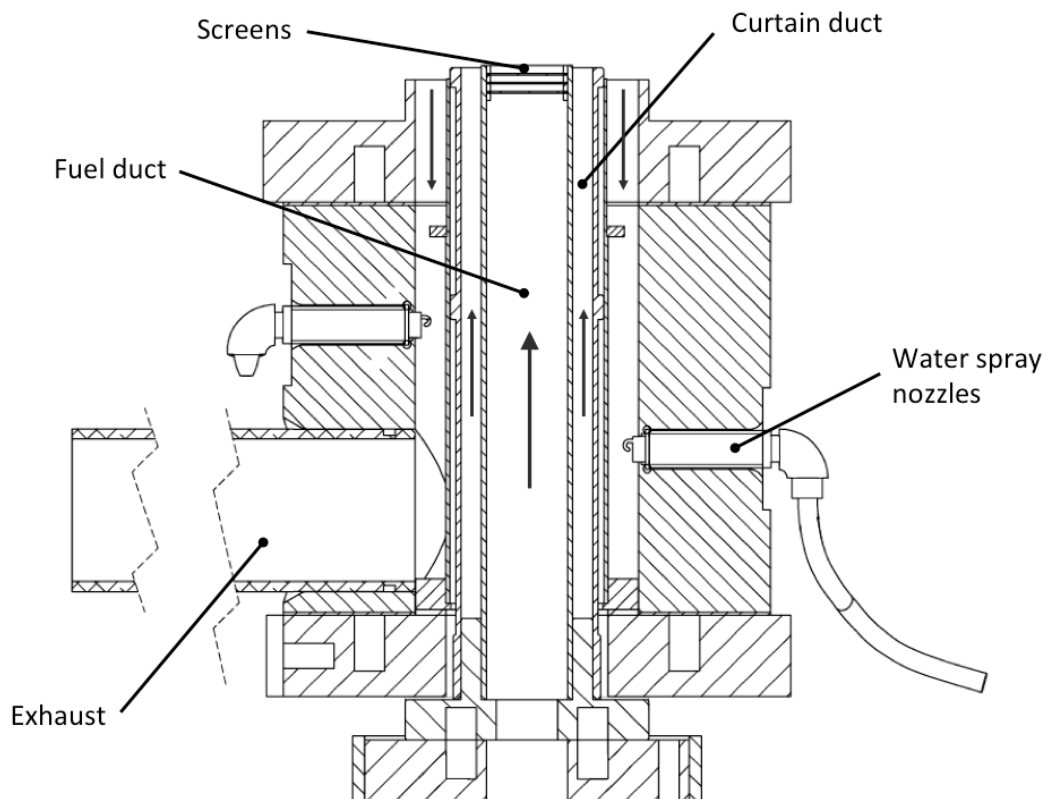


Figure 2.2: Section view of the lower part of the burner

2.2. Upper Part of the Burner

The upper part of the burner, also referred to as the oxidizer duct, guides the oxygen toward the reactive flow field. Its composition is similar to that of the fuel duct, consisting mainly of two concentric ducts. Oxygen or oxygen diluted with nitrogen enters the reaction zone through the main duct, whereas the surrounding curtain duct ensures the formation of a nitrogen curtain. Three screens are arranged at the exit of the oxidizer duct, held in place by 4 steel rings. A water-jet cut honeycomb ring is inserted close to the exit of the nitrogen curtain in the annular duct to produce a smooth, uniform flow. No cooling or heating of the oxidizer stream is necessary.

The oxidizer duct is attached to the fuel duct using 3 adjustable pins. By turning the pins, the distance between the two ducts can be varied and their axes aligned. The distance between the last screen of the oxidizer duct and the last screen of the fuel duct is 12.5mm.

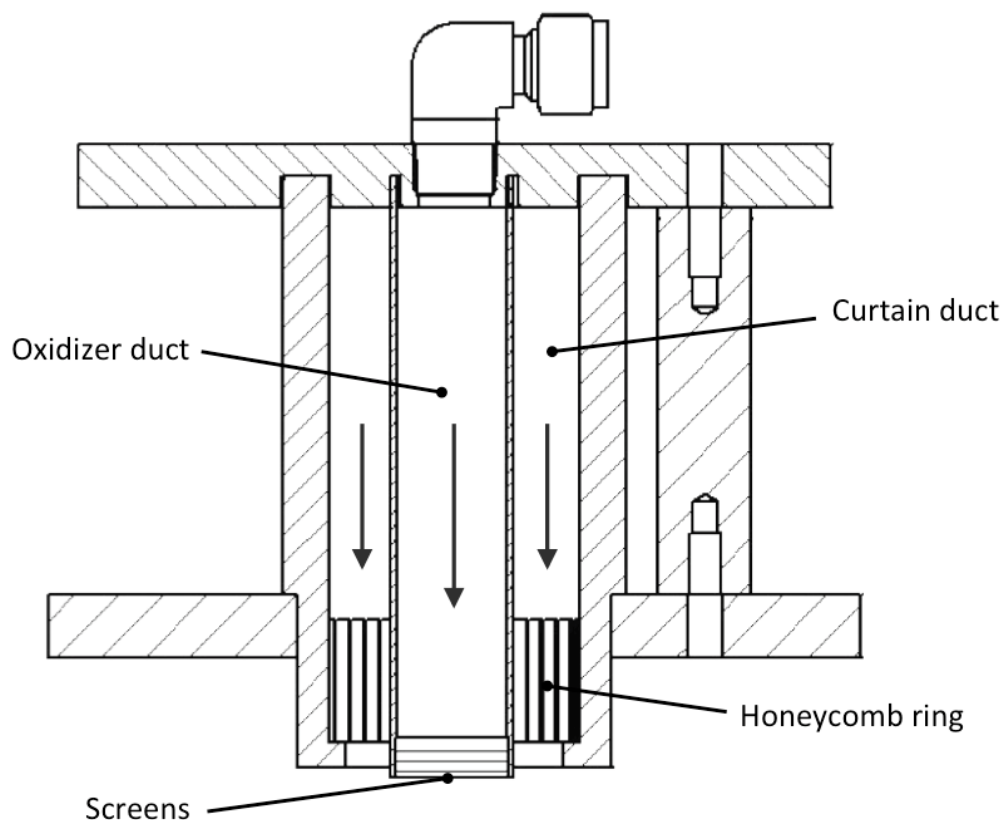


Figure 2.3: Section view of the extinction top

2.3. Gas Supply

All reactants in the extinction experiments are gaseous and are supplied from high pressure gas cylinders with an initial pressure of 150 bars. Pressure reducing valves ensure a steady supply pressure. To provide a constant flow of all reaction participants every flow controller has its own gas supply.

Due to the high mass fraction of oxygen in the oxidizer stream at the higher stoichiometric mixture fractions, a separate flow of nitrogen is induced into the exhaust to minimize the risk of oxygen reacting with hot soot afterproducts. A series of shut-off valves are installed for emergency shut off of the fuel and oxygen supply.

2.4. LabVIEW Controlling Software

To guarantee reliable and reproducible results it is essential to have full control over the counterflow setup and the combustion experiments. In order to regulate and monitor the gas flows, a computer with a reliable and sturdy, but nevertheless accurate and detailed software is necessary. For this purpose, a control software was developed using the program LabVIEW and improved throughout the last years. LabVIEW (Laboratory Virtual Instrument Engineering Workbench), a graphical programming language developed by National Instruments, enables full control over all input and output parameters.

Up to 5 reactants can be controlled in each stream, as well as an additional liquid reactant. The data is reprocessed every two seconds, to react to sudden changes in the experiment. To avoid human errors, error loops were implemented to prevent too high strain rates or notify the user when the maximum flow of a mass flow controller is reached. A recent extension allows the user to calibrate the mass flow controllers using the same program by processing the data input of the wet test meter.

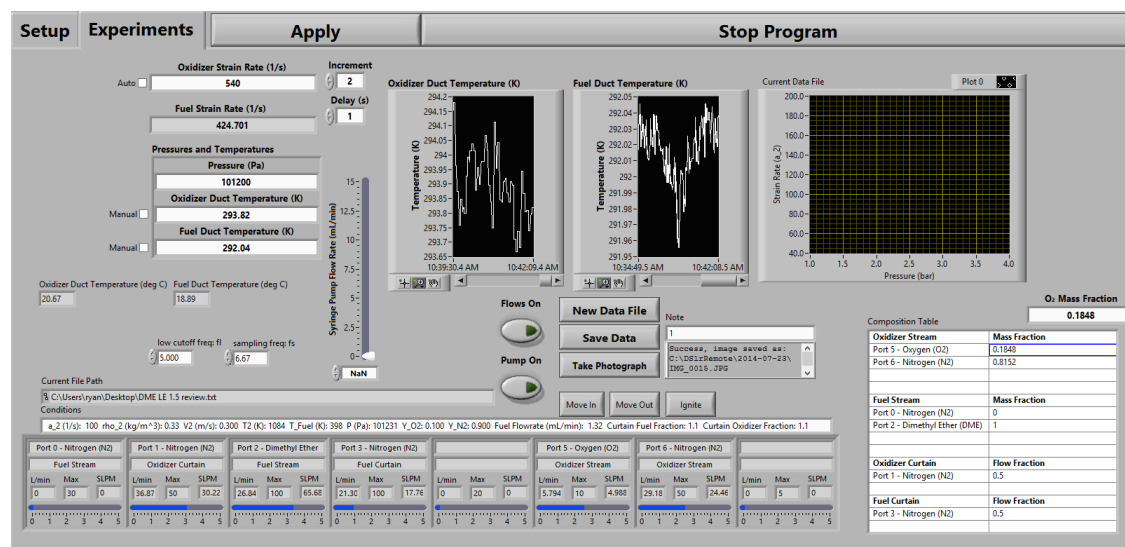


Figure 2.4: Experiment control screen of the Lab View program. The user can control reactant mass fractions, gaseous flow rates, temperatures and data saving routines.

Chapter 2: Experimental Setup

Figure 2.4 shows the main control screen of the LabVIEW software. The area in the top left allows the user to set and control the temperatures of the streams, the pressure and the strain rate. For the extinction experiments, the strain rate can be set to increase automatically at a rate designated by the user. The program then calculates the change in the mass flows for each stream and adapts the flows to the values at the desired increments.

On the lower left hand side the mass flow controllers can be supervised. The flows are displayed for each controller, as well as the maximum flow and the ratio of the current flow to the maximum flow.

The segment on the lower right enables the user to set the mass fractions of each reactant. As soon as one mass fraction of one stream is set and the “apply”- button is pressed, the software sets the mass fraction of the other reactant in the same stream accordingly.

The graphs on the top right display the course of the oxidizer and fuel duct temperatures.

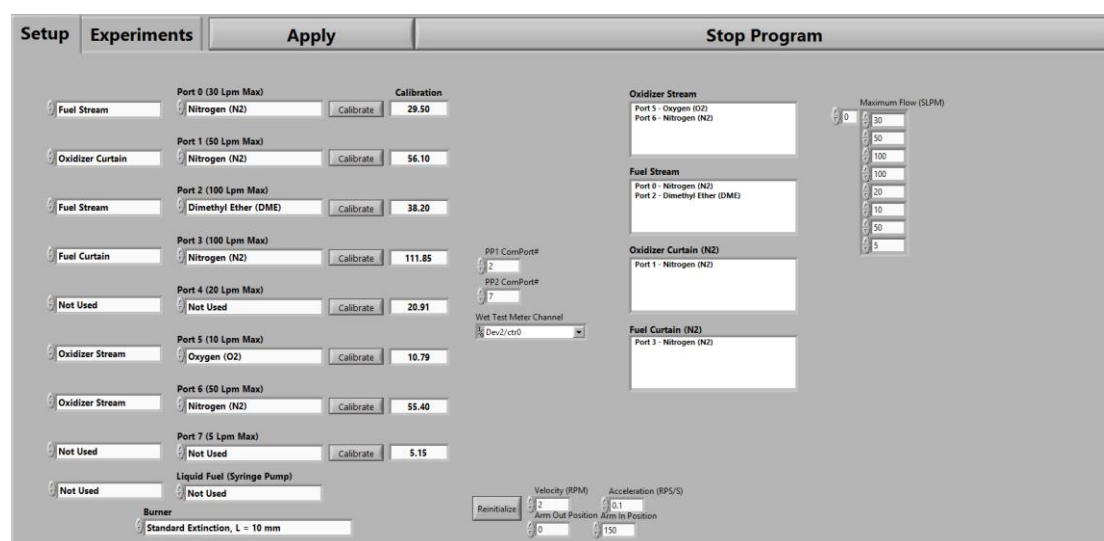


Figure 2.5: Control setup screen of the Lab View software. The User can select the computation program for the desired experiments, assign the gas inputs to the different ports and start the calibration procedure for the mass flow controllers.

Figure 2.5 shows the setup screen of the LabVIEW program. This is mainly used to assign the various ports to the different mass flow controllers. Throughout the different experiments, the mass flows of the streams change with differing stoichiometric mixture fractions. To guarantee precise and

reliable results, the mass flow of each stream must be within the designated flow range of the individual mass flow controller. Due to a large variation in the fuel and oxidizer flows over the spectrum of the stoichiometric mixture fractions, a frequent change of mass flow controllers is necessary and performed in the setup screen of the program. With every change of the reactant used in a mass flow controller, it needs to be recalibrated. By pressing the calibration button the maximum flow of the mass flow controller can be altered after processing the data received from the wet test meter. At the bottom of the screen the calculation mode can be switched between autoignition and extinction experiments.

2.4.1. Fixed Parameters

The following input parameters are maintained constant throughout the course of the experiments.

- The distance L between the fuel duct and the oxidizer duct. This value is preset by selecting either the autoignition or the extinction mode.
- The pressure is set to 101200 Pa, as the experiments are carried out under constant ambient pressure.
- The areas of the duct exits A_1 and A_2 as well as the curtain exits A_{curt1} and A_{curt2} are identical to obtain a steady state flame.

2.4.2. Calculated Parameters

The fuel and oxidizer mass fractions are given by the calculated stoichiometric mixture fractions and limited by the temperatures in the ducts as well as the maximum flow rates of the mass flow controllers. The N_2 mass fractions of fuel and oxidizer streams are calculated using the following equation.

$$Y_{N_2,1} = 1 - Y_{F,1} \quad (2.1)$$

$$Y_{N_2,2} = 1 - Y_{O_2,2} \quad (2.2)$$

Index 1 refers to the fuel duct, index 2 the oxidizer duct.

The mole fractions are given by (2.3) and (2.4), M_i being the molecular weight of the regarding element.

$$X_{i,1} = \frac{\frac{Y_{i,1}}{W_{i,1}}}{\sum_{F,N_2} \frac{Y_{i,1}}{W_{i,1}}} \quad (2.3)$$

$$X_{i,2} = \frac{\frac{Y_{i,2}}{W_{i,2}}}{\sum_{O_2,N_2} \frac{Y_{i,2}}{W_{i,2}}} \quad (2.4)$$

Using the ideal gas equation, the densities ρ_i of the fuel and oxidizer stream [kg/m³] can be calculated.

$$\rho_1 = \frac{p \sum_{i=F,N_2} X_{i,1} W_{i,1}}{RT_1} \quad (2.5)$$

$$\rho_2 = \frac{p \sum_{i=O_2,N_2} X_{i,2} W_{i,2}}{RT_2} \quad (2.6)$$

The temperature of the fuel stream T_1 [K] is measured using a thermocouple, placed in the fuel duct directly below the screens at the exit of the duct. The oxidizer duct temperature T_2 [K] is determined using a thermocouple measuring the ambient temperature. $R = 8.314$ [J/molK] is the ideal gas constant and p the ambient pressure [Pa].

The velocity of the fuel stream is calculated using the momentum balance, since the velocity of the oxidizer stream can be derived from the oxidizer strain rate a_2 .

$$V_1 = \frac{V_2}{\sqrt{\frac{\rho_1}{\rho_2}}} \quad (2.7)$$

Following equation 2.7, the necessary volume fluxes of the reactant streams can be calculated.

$$\dot{V}_{F,1} = X_{F,1}V_1A_1 \quad (2.8)$$

$$\dot{V}_{N_2,1} = X_{N_2,1}V_1A_1 \quad (2.9)$$

$$\dot{V}_{O_2,2} = X_{O_2,2}V_2A_2 \quad (2.10)$$

$$\dot{V}_{N_2,2} = X_{N_2,2}V_2A_2 \quad (2.11)$$

The curtain velocities are set relative to the duct velocities, as the curtain stream must adjust to a change in the reactant stream. This way, the curtain velocity increases with an increase in the reactant velocity and vice versa.

$$\dot{V}_{curt,1} = v_{rel,1}V_1A_1 \quad (2.12)$$

$$\dot{V}_{curt,2} = v_{rel,2}V_2A_2 \quad (2.13)$$

The relative curtain velocities $v_{rel,i}$ are set to 0.5 [-].

Using the ideal gas equation, the volume fluxes are scaled to standard liters per minute under standard conditions.

$$\dot{V}_{SLM,i,j} = \dot{V}_{i,j} \frac{273.15K}{T_{i,j}} \quad (2.14)$$

2.5. Controlling Units

2.5.1. Mass Flow Controllers

A mass flow controller (MFC) is a device used to measure and control a specific gas at a particular range of flow rates. Using the density of the gas, it calculates volumetric units out of mass units.

For the combustion experiments with the counterflow burner, several Teledyne Hastings mass flow controllers are used. They vary in their full scale range (1 to 100 standard liters per minute) and types (HFC-302 and HFC-303), allowing the user to operate each MFC in its specific range to achieve maximum accuracy. The MFCs are connected to the software via two Teledyne PowerPod 400 modules, providing voltages linear to the mass flow rate. By giving the closed loop system of the MFCs an input signal, they compare the value of the mass flow sensors to the signal and adjust the valves to achieve the desired flows.

Proper calibration of the mass flow controllers is crucial to obtain precise results in combustion experiments. To calibrate the MFCs a Ritter TG5/5-ER drum type wet test meter with a flow range of 0.167 l/min to 33.3 l/min is used. The gas flowing into the wet test meter causes a rotation of the measuring drum within the packing fluid (in this case distilled water), periodically filling and emptying the rigid measuring chambers. By setting the flow volume in standard liters per minute in the program, the wet test meter determines the volumetric flows of gas by measuring the positive displacement of the rotating chamber over time. [5]

The calibration can be controlled using the LabVIEW program, which processes the data received from the wet test meter. Out of the measured volumetric flow and the set volume the maximum flow rate is calculated. This process is repeated until the deviation of the flow is less than $\pm 1\%$.

2.5.2. Temperature Measurement

To measure the temperature during the combustion process thermoelectric effect sensors, short thermocouples, are used. Thermocouples consist of two dissimilar metal wires, joined at one end. The junction is placed at the position of temperature measurement. By heating or cooling the junction a voltage is induced, which is linked to the temperature change through a function.

Thermocouples are available in different combinations of metals or calibrations. The temperatures in the extinction experiments are measured using Omega type E thermocouples (nickel-chromium vs. copper-nickel) with a range of -200°C to $+900^{\circ}\text{C}$. [6] The fuel duct temperature is measured by a thermocouple placed at the duct exit below the screen, whereas the oxidizer duct temperature is determined by measuring the ambient temperature.

Chapter 3

Extinction Experiments

3.1. Experimental Procedure and Preparation

To prepare the extinction experiments, the extinction top must be aligned and leveled on the lower part of the burner. The 3 pins mounted to the bottom of the extinction top are adjusted to ensure the fuel and oxidizer ducts are concentric and the distance between the last screens of both ducts is precisely 12.5mm.

Prior to the start of the experiments, the cooling water must be turned on to prevent the fuel duct from overheating and ensure that no further reactions take place in the exhaust.

To begin the extinction experiments, the fuel and oxidizer strain rates are slowly raised to ensure accurate flow rates. At a strain rate slightly below the predicted extinction strain rate a flame is established with a blow torch. The oxidizer strain rate a_2 is then increased until the flame extinguishes. In order to obtain precise results, the strain rate is increased at a very low rate of 1 s^{-1} every 5 seconds. This procedure is repeated at least 8 times or until the extinction strain rate does not change significantly. The strain rates at extinction, $a_{2,q}$ and $a_{1,q}$ are recorded as functions of ξ_{st} . The quantities $a_{2,q}$ and $a_{1,q}$ are the values of a_2 and a_1 at extinction.

At higher mixture fractions ($\xi_{st} > 0.2406$ at $T_{st} = 2000$ and $\xi_{st} > 0.1858$ at $T_{st} = 2100$ for CH_4) it is necessary to increase the strain rate of the fuel stream in intervals to ensure a safe experiment. At a low strain rate a flame is established using a low fuel mass fraction. The amount of nitrogen in the fuel stream is then slowly decreased and the fuel mass fraction increased while

slightly increasing the strain rate. Once the desired mixture fraction is attained the strain rate is further increased until the point of extinction.

In a diffusion flame, extinction occurs when the heat conduction from the reaction zone towards the lean (oxidizer) and rich (fuel) side exceeds the heat produced by the chemical reaction. Increasing the strain rate of the fuel and oxidizer streams therefore causes the flame to extinguish, as the heat produced by the reaction no longer balances the heat lost by conduction in the reaction zone. [1]

3.2. Adiabatic Flame Temperature

The adiabatic flame temperature is the theoretical temperature of a flame during a complete combustion process occurring without work, heat transfer to or from the reaction zone or changes in kinetic or potential energy, at either constant volume or constant pressure. This implies an ideal combustion process, the resulting products being only water and carbon dioxide and the absolute enthalpy of the reactants before the combustion equaling the absolute enthalpy of the products after combustion. The adiabatic flame temperature is therefore the maximum temperature that can be attained during combustion with the given reactants, since any heat transfer or energy losses would result in a lower temperature of the flame. The adiabatic temperature is determined by the initial temperature and composition of the reactants as well as the pressure. [3, 9]

3.2.1. Adiabatic Flame Temperature of Methane

If the diffusivity of methane, oxygen and nitrogen are presumed to be equal to the thermal diffusivity, the adiabatic temperature is defined as

$$T_{st} = T_u + \frac{Q_F \xi_{st} Y_{F,1}}{W_F c_{p,st}} \quad (3.1)$$

with

$$T_u = T_2 + \xi_{st}(T_1 - T_2) \quad (3.2)$$

where W_F is the molecular weight of methane, ξ_{st} the stoichiometric mixture fraction, Q_F the heat release of the reaction $\text{CH}_4 + 2\text{O}_2 \rightarrow \text{CO}_2 + 2\text{H}_2\text{O}$, and $c_{p,st}$ the heat capacity per unit mass of the products [10]. Subscript 1 denotes the fuel stream and subscript 2 the oxidizer stream.

3.2.2. Adiabatic Flame Temperature of Dimethyl Ether

Professor Seshadri developed an asymptotic formulation where the adiabatic flame temperature is fixed and the corresponding mass fractions of DME and oxygen can be calculated. In this formulation the Damköhler numbers are presumed to be high due to the assumption that the reaction takes place simultaneously with the fuel. The adiabatic flame temperature T_{st} is then given by

$$T_{st} = T_u + \frac{m}{c_p W_{N_2}} Q_{dme} \xi_{st} (1 - \xi_{st}) \quad (3.3)$$

with

$$\frac{1}{Le_{dme}} \frac{dX_{dme}}{d\xi} = \frac{1}{\sqrt{Le_{dme}}} \frac{X_{dme,1}}{1 - \xi_{dme,st}} \left\{ \exp \left[\frac{x_{st}^2 (1 - Le_{dme})}{2} \right] \right\} = m \quad (3.4)$$

where W_{N_2} is the molecular weight of Nitrogen, $Q_{dme} = 1328 \cdot 10^3$ J/mol is the heat release of dimethyl ether, $c_p = 1300$ J/(kgK) the heat capacity, X_{dme} the mole fraction of DME, Le_{dme} the Lewis number and x_{st} the location of the flame sheet.

3.3. Mixture Fraction

The mixture fraction ξ is a very important variable in combustion theory, especially when considering diffusion flames. It allows the quantification of the state of local composition before combustion in a known mixture of fuel and oxidizer flows. The value ξ of the mixture fraction ranges between zero and one, one being the mixture fraction in the fuel stream and zero the mixture fraction in the oxidizer stream.

In a homogeneous system, where a fuel stream with mass flux \dot{m}_1 is mixed with an oxidizer stream with mass flux \dot{m}_2 , the mixture fraction is given by

$$\xi = \frac{\dot{m}_1}{\dot{m}_1 + \dot{m}_2} \quad (3.5)$$

The mass fraction $Y_{F,u}$ of the fuel in the mixture is proportional to the mass fraction in the original fuel stream [7], so

$$Y_{F,u} = Y_{F,1}\xi_{st} \quad (3.6)$$

$Y_{F,1}$ being the mass fraction of fuel in the fuel stream. The mass fraction of the oxidizer stream in the mixture is represented by $(1 - \xi)$, leading to

$$Y_{O_2,u} = Y_{O_2,2}(1 - \xi_{st}) \quad (3.7)$$

$Y_{O_2,u}$ being the mass fraction of oxygen in the mixture and $Y_{O_2,2}$ the mass fraction of oxygen in the oxidizer stream ($Y_{O_2,2} = 0.233$ for air).

For a stoichiometric mixture, one obtains

$$\xi_{st} = \left[1 + \frac{\nu Y_{F,1}}{Y_{O_2,2}} \right]^{-1} \quad (3.8)$$

using

$$\nu Y_F = Y_{O_2} \quad (3.9)$$

where ν is the stoichiometric oxygen-to-fuel mass ratio.

The flamelet model, developed by Burke and Schumann in 1928, assumes that combustion in a diffusion flame takes place at the location of the stoichiometric mixture fraction. Fuel and oxidizer diffuse into the flame area from opposite sides and immediately vanish, while the products and the temperature reach a maximum. It is therefore assumed that the characteristic chemical reaction time is significantly smaller than the characteristic times of convection and diffusion. From a mathematical point of view it is assumed that the reactions take place under infinite residence time and under complete combustion for a one-step reaction. Considering these conditions, the following figures can be obtained. [1, 7, 12]

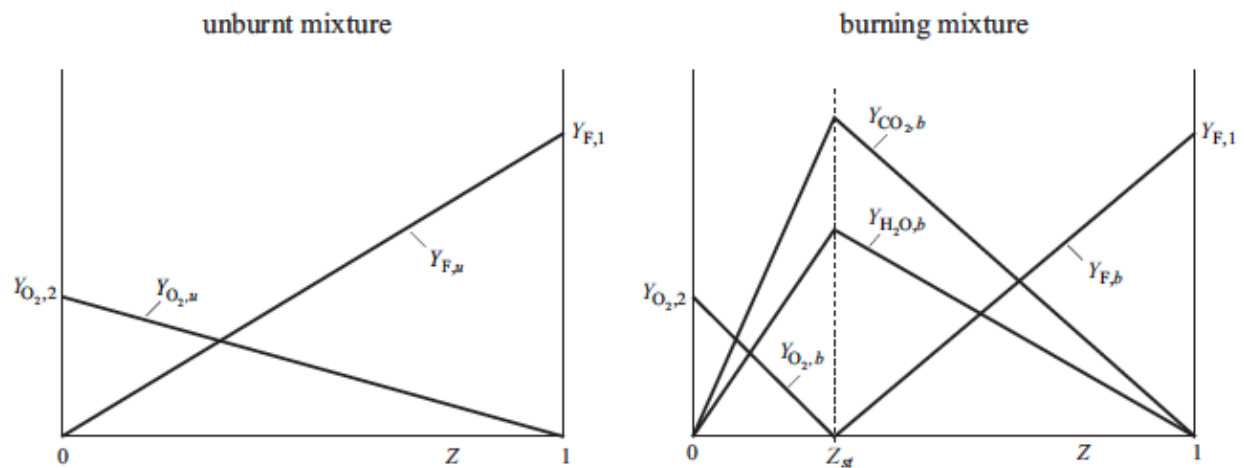


Figure 3.1: Left: Profiles of $Y_{F,u}$ and $Y_{O_2,u}$ in the unburnt gas mixture

Right: Profiles of $Y_{F,b}$, $Y_{O_2,b}$, $Y_{CO_2,b}$ and $Y_{H_2O,b}$ in the burnt gas mixture [1]

The left side of figure 3.1 shows the fuel and oxidizer mass fractions as a function of the mixture fraction in the unburnt mixture. The right side shows the reactants and products in the burning mixture. The stoichiometric mixture fraction Z_{St} or ξ_{St} represents the point where fuel and oxidizer are mixed in

such way that the mass fractions are in a stoichiometric ratio. From this follows that both fuel and oxidizer are consumed entirely and react to their products water and carbon dioxide.

3.4. Determining the Mass Fractions

3.4.1. Boundary Values at $T_{st} = 2000\text{K}$ for non-premixed Methane Flames

The extinction experiments are conducted with $T_1 = T_2 = 298\text{K}$. Therefore the initial temperature of the reactants is $T_u = 298\text{K}$, hence $Q_F = 803000$ J per mole of methane consumed [13]. Experimental data on critical conditions of extinction are obtained with the values $Y_{F,1}$ and $Y_{O_2,2}$ so chosen that $T_{st} = 2000\text{K}$. At these conditions, the average heat capacity $c_{p,st} = 1300$ J/kgK [13]. It follows from Eq. (3.1) that

$$Y_{F,st} = Y_{F,1}\xi_{st} = 0.044 \quad (3.10)$$

and Eq. (3.8) that

$$Y_{O_2,st} = Y_{O_2,2}(1 - \xi_{st}) = 0.177 \quad (3.11)$$

These results can also be obtained from the Chemical Equilibrium Calculator [14], pressure 1.0atm, initial temperature 298K, fuel initial mole = 1.0, oxygen = 2.0, nitrogen = 10.055. The final Temperature = 2001.6K.

Table 3.1: Initial and final mole and mass fractions for $T_{st} = 2002\text{K}$

Species	Initial State		Equilibrium State	
	X_i	Y_i	X_i	Y_i
CH4	7.6599×10^{-2}	4.4353×10^{-2}	8.7086×10^{-9}	5.0425×10^{-9}
O2	1.5320×10^{-1}	1.7693×10^{-1}	1.7417×10^{-8}	2.0115×10^{-8}
N2	7.7020×10^{-1}	7.7872×10^{-1}	7.7020×10^{-1}	7.7872×10^{-1}
CO2	0.00	0.00	7.6599×10^{-2}	1.2167×10^{-1}
H2O	0.00	0.00	1.5320×10^{-1}	9.9611×10^{-2}

Using these results and Eq. (3.10) and (3.11), the mass fractions at the boundaries for various values of ξ_{st} for $T_{st} = 2002\text{K}$ can be obtained. The experiments are conducted for values of $0.044 < \xi_{st} < 0.823$. For $\xi_{st} = 0.044$, $Y_{F,1} = 1$, and for $\xi_{st} = 0.823$, $Y_{O_2,2} = 1$.

Table 3.2: Calculated fuel and oxidizer mass fractions for selected values of ξ_{st} at $T_{st} = 2002\text{K}$

	ξ_{st}	$Y_{F,1}$	$Y_{O_2,2}$
1	0.044353	1.000	0.185
2	0.055	0.806	0.18723
3	0.07	0.634	0.1902
4	0.1	0.44353	0.1966
5	0.2	0.2218	0.2212
6	0.2406	0.1843	0.233
7	0.4	0.111	0.295
8	0.5	0.089	0.354
9	0.6	0.0739	0.4423
10	0.7	0.0634	0.590
11	0.8	0.05544	0.88465
12	0.82307	0.05389	1.000

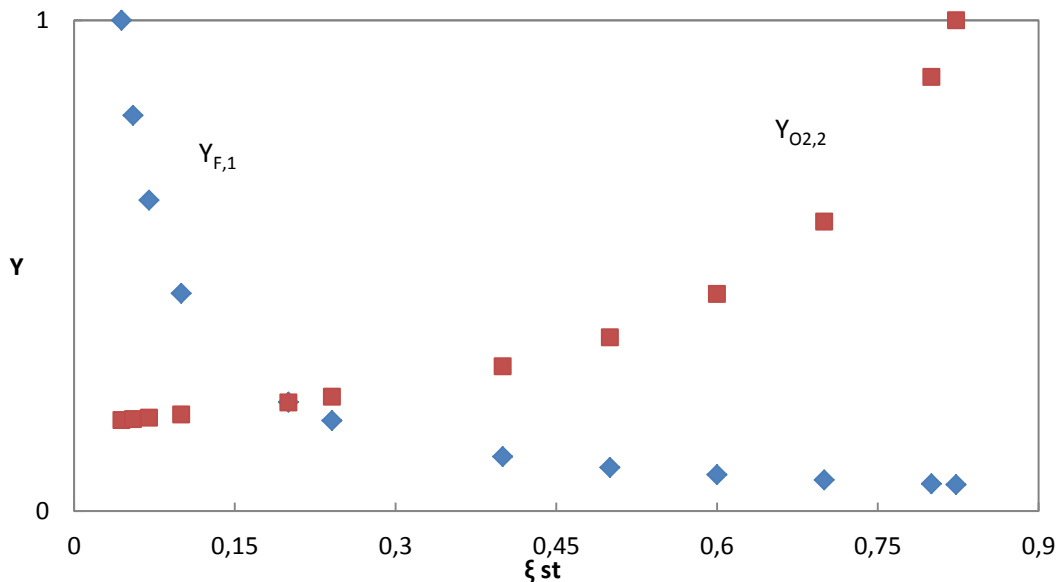


Figure 3.2: Fuel and oxidizer mass fractions over the stoichiometric mixture fraction at $T_{st} = 2002\text{K}$

3.4.2. Boundary Values at $T_{st} = 2100\text{K}$ for non-premixed Methane Flames

The mass fractions for different adiabatic flame temperatures are determined in the same fashion. By changing the input values in the Chemical Equilibrium Calculator to pressure 1.0atm, initial temperature 298K, fuel initial mole = 1.0, oxygen = 2.0, nitrogen = 9.185 the following conditions are obtained. The final Temperature = 2100.4K.

Table 3.3: Initial and final mole and mass fractions for $T_{st} = 2100\text{K}$

Species	Initial State		Equilibrium State	
	X_i	Y_i	X_i	Y_i
CH4	8.2068×10^{-2}	4.7557×10^{-2}	1.9967×10^{-8}	1.1571×10^{-8}
O2	1.6414×10^{-1}	1.8971×10^{-1}	3.9935×10^{-8}	4.6157×10^{-8}
N2	7.5380×10^{-1}	7.6273×10^{-1}	7.5380×10^{-1}	7.6273×10^{-1}
CO2	0.00	0.00	8.2068×10^{-2}	1.3046×10^{-1}
H2O	0.00	0.00	1.6414×10^{-1}	1.0681×10^{-1}

Using Eq. (3.10) and (3.11) the mass fractions at the boundaries are calculated. The experiments are conducted for values of $0.048 < \xi_{st} < 0.81$. For $\xi_{st} = 0.048$, $Y_{F,1} = 1$, and for $\xi_{st} = 0.81$, $Y_{O2,2} = 1$.

Table 3.4: Calculated fuel and oxidizer mass fractions for selected values of ξ_{st} at $T_{st} = 2100\text{K}$

	ξ_{st}	$Y_{F,1}$	$Y_{O2,2}$
1	0.047557	1	0.1992
2	0.055	0.865	0.2008
3	0.07	0.679	0.2040
4	0.1	0.4756	0.2108
5	0.1858	0.2560	0.233
6	0.25	0.1902	0.2529
7	0.4	0.119	0.3162
8	0.5	0.095	0.3794
9	0.6	0.0793	0.4743
10	0.7	0.0679	0.6324
11	0.76	0.06258	0.7905
12	0.81029	0.05869	1.000

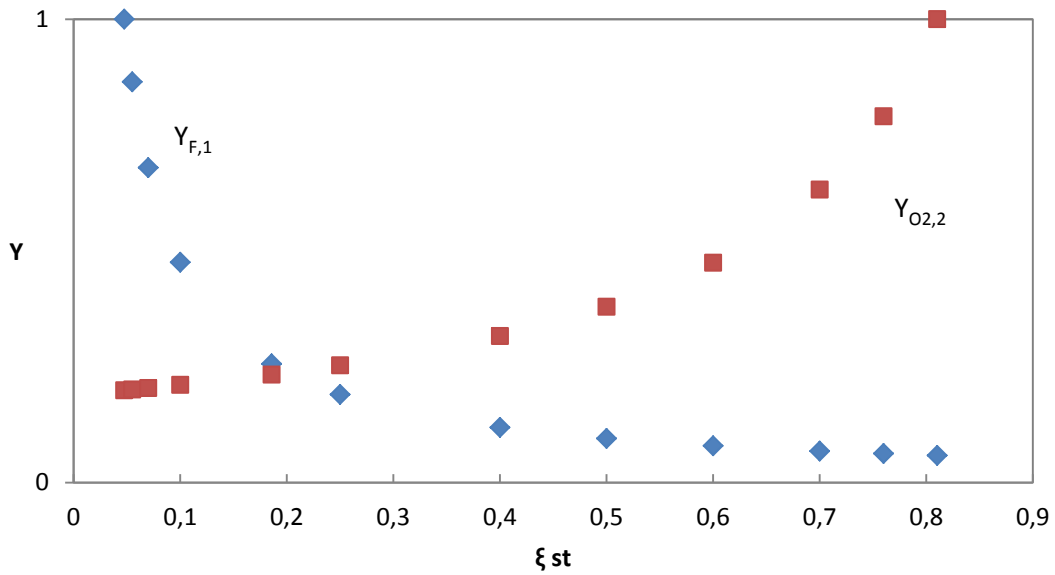


Figure 3.3: Fuel and oxidizer mass fractions over the stoichiometric mixture fraction at $T_{st} = 2100K$

3.4.3. Boundary Values at $T_{st} = 2000K$ for non-premixed Dimethyl Ether Flames

Professor Seshadri developed an asymptotic formulation for the calculation of the mass fractions of DME and oxygen. The equations shown in this chapter are the result of the asymptotic model, which is attached in appendix B.

The extinction experiments are conducted with $T_1 = T_2 = 298K$. Therefore the initial temperature of the reactants is $T_u = 298K$, hence the heat release $Q_{DME} = 1328000 \text{ J/mole}$ [13]. The Lewis number $Le_{dme} = 1.5$ and the adiabatic flame Temperature T_{st} is selected to be $2000K$. At these conditions, the average heat capacity $c_{p,st} = 1300 \text{ J/kgK}$ [13]. The mass fraction of dimethyl ether in the fuel stream is $Y_{dme,1}$ and the mass fraction of oxygen in the oxidizer stream is $Y_{O2,2}$, respectively.

The value of ξ_{st} for $Y_{O2,2} = 1$ is

$$\xi_{st} = 1 - \frac{3c_p(T_{st} - T_u)W_{O_2}}{Q_{dme}} \quad (3.12)$$

The value of ξ_{st} for $Y_{dme,1} = 1$ can be obtained from the solution to the equation

$$\frac{\xi_{st}(1 - \xi_{st})}{1 - \xi_{dme,st}} = \frac{c_p W_{C_2H_6O} \sqrt{Le_{dme}} (T_{st} - T_u)}{Q_{dme}} \left\{ \exp \left[\frac{x_{st}^2 (Le_{dme} - 1)}{2} \right] \right\} \quad (3.13)$$

The fuel and oxidizer mass fractions have to be calculated individually for each stoichiometric mixture fraction. From

$$\xi_{st} = \frac{1}{2} \operatorname{erfc} \left(x_{st} \sqrt{\frac{1}{2}} \right) \quad (3.14)$$

it follows that

$$x_{st} = \sqrt{2} [\operatorname{erfc}^{-1}(2\xi_{st})] \quad (3.15)$$

where erfc^{-1} is the inverse of the complementary error function and not the reciprocal.

The stoichiometric mixture fraction can be calculated with

$$\xi_{dme,st} = \frac{1}{2} \operatorname{erfc} \left(x_{st} \sqrt{\frac{Le_{dme}}{2}} \right) \quad (3.16)$$

The introduction of

$$m = \frac{c_p(T_{st} - T_u)}{Q_{dme}\xi_{st}(1 - \xi_{st})} \quad (3.17)$$

leads to the equations for the fuel and oxidizer mass fractions.

$$Y_{O_2,2} = 3m\xi_{st}W_{O_2} \quad (3.18)$$

$$Y_{dme,1} = mW_{C_2H_6O}\sqrt{Le_{dme}}(1 - \xi_{dme,st}) \left\{ \exp \left[\frac{x_{st}^2(Le_{dme} - 1)}{2} \right] \right\} \quad (3.19)$$

Table 3.5: Calculated fuel and oxidizer mass fractions for selected values of ξ_{st} at $T_{st} = 2000K$ and $Le = 1.5$

	ξ_{st}	$Y_{F,1}$	$Y_{O_2,2}$
1	0.13432	1	0.1848
2	0.16	0.7945	0.1904
3	0.19	0.6351	0.1975
4	0.22	0.5256	0.2051
5	0.3136	0.3349	0.2330
6	0.4	0.2471	0.2666
7	0.5	0.1877	0.3199
8	0.6	0.1503	0.3999
9	0.7	0.1247	0.5332
10	0.8	0.1060	0.7997
11	0.82	0.1028	0.8886
12	0.84005	0.0998	1

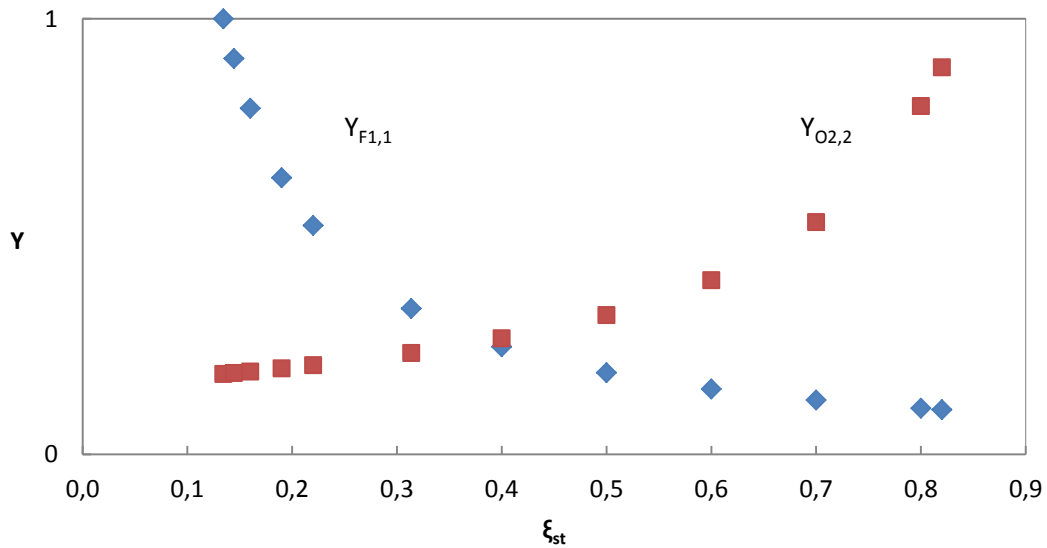


Figure 3.4: DME and oxidizer mass fractions over the stoichiometric mixture fraction at $T_{st} = 2000K$

To analyze the specific behavior of Dimethyl Ether strain rates at low mixture fractions, the calculations and experiments are repeated using different Lewis numbers. The effect of the Lewis number variation on the fuel mass fraction is shown in figure 3.5.

Table 3.6: Calculated DME mass fractions for selected ξ_{st} with varying Lewis numbers

	ξ_{st}	$Y_{DME,1}$		
		Le 1.4	Le 1.5	Le 1.6
0	0.12366	1.00	-	-
1	0.13432	0.9012	1.00	-
2	0.14443	0.8228	0.9088	1.00
3	0.16	0.7239	0.7945	0.8693
4	0.19	0.5847	0.6351	0.6879
5	0.22	0.4880	0.5256	0.5646
6	0.3136	0.3168	0.3349	0.3531

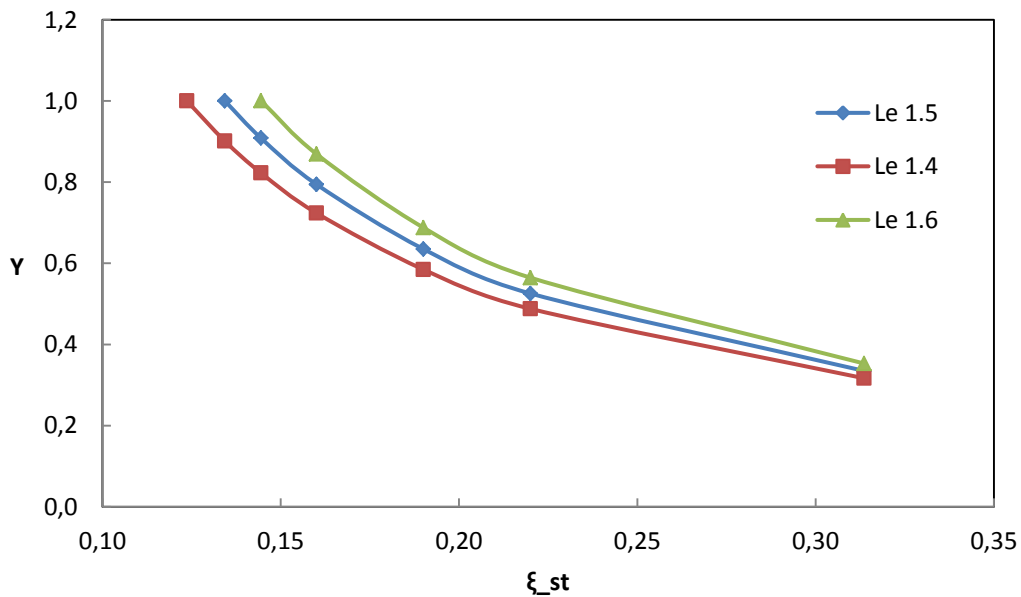


Figure 3.5: The effect of Lewis number variation on DME mass fractions

Chapter 4

Computational Simulations

4.1. Numerical Computations

Computational modeling and simulations have become increasingly important throughout the years in all fields of engineering. Enhanced computing power and performance has enabled the simulation of detailed chemical kinetics in the area of combustion research. The recent rise of computational simulations can also be attributed to the fact that they are not restricted to physical limitations. Complex computations however are very time consuming and require extremely powerful and costly processors. In order to reduce the necessary time and therefore the costs, the complexity and the dimensions of kinetic mechanisms are reduced by making simplifying assumptions and adopting analogy rules.

The numerical computations for non-premixed methane flames were carried out using the open source FlameMaster code [27]. The computations for the extinction of methane were performed by Dr. Reinhard Seiser of University of California, San Diego. The most recent version of the San Diego Mechanism (20141004) was used, which can be found at [28], as well as a one-step mechanism, described in Eq. (5.2).

The numerical computations for non-premixed dimethyl ether flames were conducted by the Indian Institute of Technology Madras using a dimethyl ether mechanism developed by Prof. Pitsch [33]. The flame is axisymmetric and the mass fractions of fuel, oxygen and inert gases are imposed on the left and right ends of the domain. For a value of mass flux on the oxidizer side, the mass flux on the fuel side is obtained by satisfying the momentum

balance. After achieving a small flame for a value of one mass flux, the value is increased manually (and the other mass flux changed accordingly) until the solution no longer converges. The strain rate at this point is noted down as the extinction strain rate obtained numerically.

4.2. Rate-Ratio Asymptotic Analysis

Combustion problems can seldom be linearized. Analytical strategies therefore require mathematical tools capable of dealing with nonlinearities. The most suitable tool has proven to be asymptotics, requiring only a large parameter or coordinate for its foundation [15].

Rate-ratio asymptotics were developed to account for elementary chemical reactions occurring due to deflagration. These methods involve several steps:

1. Introducing steady-state and partial-equilibrium assumptions in order to reduce an elementary mechanism analytically to a small number of global reactions
2. Identifying disparate layers in the flame structure where not more than two of these global reactions are active
3. Establishing a complete picture of the flame structure by linking the layers through appropriate matching conditions.

Previous rate-ratio asymptotic analyses of methane flames were applied to problems where ξ_{st} was small [10]. Professor Kalyanasundaram Seshadri developed the following extended analysis to include values of $\xi_{st} > 0.5$. Computations were performed by the Division of Fluid Mechanics, Department of Energy Sciences, Lund University.

For convenience, the following equations are introduced:

$$X_i \equiv \frac{Y_i W_{N_2}}{W_i} \quad (4.1)$$

$$\tau \equiv \frac{c_p W_{N_2} (T - T_u)}{Q_F} \quad (4.2)$$

Here Y_i and W_i are respectively the mass fraction and molecular weight of species i and W_{N_2} is the molecular weight of nitrogen.

The Lewis number of species i is defined as

$$Le_i = \frac{\lambda}{\rho c_p D_i} \quad (4.3)$$

for CH_4 , O_2 , CO_2 , H_2O and N_2 , where D_i is the coefficient of diffusion of species i .

The mixture fraction is used as the independent variable, therefore the profile of temperature as well as the profiles of mass fractions of all species are evaluated as a function of ξ . Chemical reactions are presumed to be located in a thin reaction zone, located at ξ_{st} . The regions $0 < \xi < \xi_{st}$ as well as $\xi_{st} < \xi < 1.0$ are inert and represent the outer structure. Through analysis of the outer structure, matching conditions for the equations describing the structure of the reaction zone are provided.

4.2.1. The Outer Structure

The outer structure of the flame is represented by the profile of the temperature, T , as well as the profiles of mass fractions of the reactants CH_4 and O_2 , as well as the products CO_2 and H_2O . These profiles are linear functions of ξ , and for constant c_p the Temperature T is also a linear function of ξ . The mass fractions of CH_4 and O_2 are zero at the reaction zone, located at $\xi = \xi_{st}$. In the region $\xi > \xi_{st}$, $Y_{O_2} = 0$, and in the region $\xi < \xi_{st}$, $Y_F = 0$. The gradients of X_i with respect to ξ and the gradient of τ are discontinuous at $\xi = \xi_{st}$. These gradients in the region $\xi > \xi_{st}$, represented by the subscript "+", are defined as following:

$$\left(\frac{dX_F}{d\xi}\right)_+ = \frac{X_{F,1}}{(1 - \xi_{st})} = g \quad (4.4)$$

$$\left(\frac{d\tau}{d\xi}\right)_+ = \frac{-\tau_{st}}{(1 - \xi_{st})} = -p \quad (4.5)$$

In the region $\xi < \xi_{st}$, represented by the subscript “-“, the gradients are

$$\left(\frac{dX_{O_2}}{d\xi}\right)_- = \frac{-X_{O_2,2}}{(\xi_{st})} = -2g \quad (4.6)$$

$$\left(\frac{d\tau}{d\xi}\right)_- = \frac{\tau_{st}}{(\xi_{st})} = s \quad (4.7)$$

Element balance gives the following relations [16]:

$$X_{CO_2,st} = g\xi_{st}(1 - \xi_{st}) \quad (4.8)$$

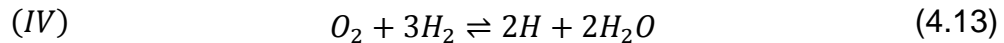
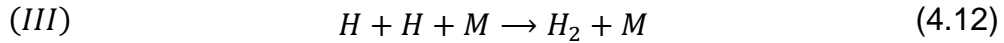
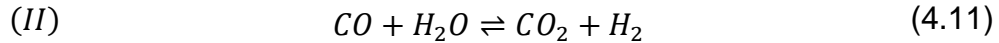
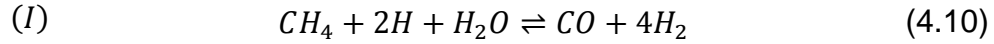
$$X_{H_2O,st} = 2g\xi_{st}(1 - \xi_{st}) \quad (4.9)$$

4.2.2. Reduced Mechanism

Flame chemistry for most hydrocarbon reactions proceeds in reaction chains, where only a few major reactions produce and consume the intermediate species. Thereby algebraic expressions can be derived from their steady-state relations. However, the presence of other steady-state species in these expressions leads to non-linear systems of algebraic equations. Consequently, the solutions are not unique. The difficulties that accompany the non-uniqueness of these algebraic equations can be overcome by the truncation of some steady-state equations [1, 7].

Reduced mechanisms offer benefits by reducing the computational effort in numerical calculations of flames. Algebraic relations are used to substitute differential equations of intermediate species assumed as being steady-state. In addition they help in the identification of kinetic parameters that influence global properties such as extinction strain rates or the burning velocity by enabling the analysis of flame structure by asymptotic methods.

For the extinction experiments in this thesis a reduced four-step mechanism is employed to describe the chemical reactions taking place in the thin reaction zone at $\xi = \xi_{st}$.



Global step I represents reactions between fuel and radicals to form the intermediate products CO and H₂. Step II represents the formation of CO₂ from CO, global step III describes the chain breaking reactions and global step IV chain branching reactions. Since radicals participate in all elementary steps, global step IV is active in the entire reaction zone.

Table 4.1: Rate Data of elementary reactions. Units are moles, cm³, seconds, kJoules, Kelvin.

Number	Reaction	A_n	β_n	E_n
1f	$O_2 + H \rightarrow OH + O$	2.000×10^{14}	0.00	70.30
5	$H + O_2 + M \rightarrow HO_2 + M$	2.300×10^{18}	-0.80	0.00
6f	$CO + OH \rightarrow CO_2 + H$	4.400×10^6	1.50	-3.10
7f	$CH_4 + H \rightarrow CH_3 + H_2$	2.200×10^4	3.00	36.60
8	$CH_3 + H \rightarrow CH_4$ k_0	6.257×10^{23}	-1.80	0.00
	k_∞	2.108×10^{14}	0.00	0.00
9	$CH_3 + O \rightarrow CH_2O + H$	7.000×10^{13}	0.00	0.00

Table 3 shows the elementary reactions that contribute to the rate of these global steps of the reduced mechanism. The symbol f appearing in the first column denotes the forward step of a reversible elementary reaction n , and subscript b will later refer to the reverse step. Reactions 5, 8 and 9 are presumed to be irreversible.

The rate constant of elementary step n is defined as

$$k_n = A_n T^{\beta_n} e^{-\frac{E_n}{\hat{R}T}} \quad (4.14)$$

where \hat{R} is the universal gas constant.

4.2.3. The Structure of the Reaction Zone

The global reactions of the reduced four-step mechanism take place in various layers within the reaction zone [16]. The reaction zone is presumed to be made up of two layers. Figure 4.1 depicts the structure of the reaction zone and shows the profile of the temperature as well as the profiles of CH_4 , O_2 , H_2 , CO and H . The temperature profiles shown by the dashed lines are projections from the outer structure into the reaction zone. The quantity T^0 is the peak temperature in the reaction zone. The chemical reactions take place with finite rates, so $T^0 < T_{st}$.

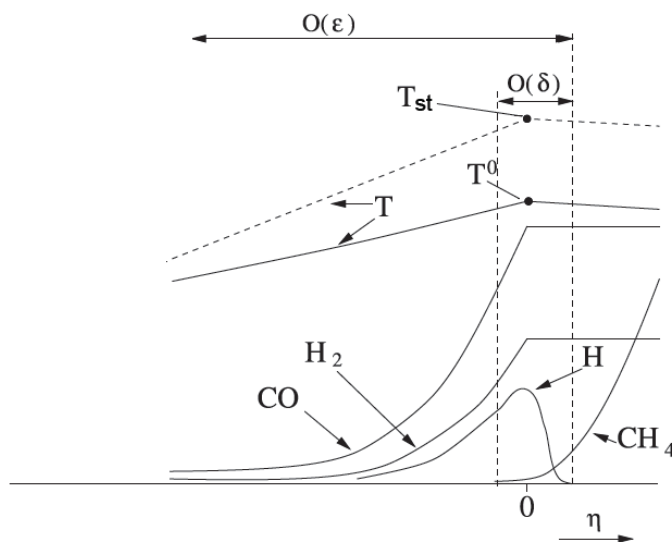
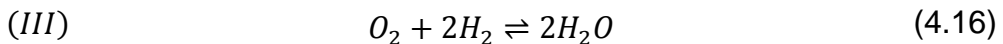
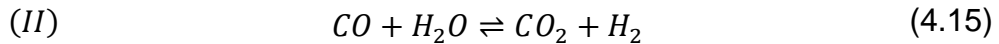


Figure 4.1: Schematic illustration of the structure of the reaction zone at ξ_{st} . The figure shows the inner layer and the oxidation layer

The two layers of the reaction zone are the inner layer of thickness of the order of $\bar{\delta}$ and the oxidation layer of the thickness of the order of ϵ , where $\bar{\delta} \ll \epsilon \ll 1$ is presumed. The relative locations of these layers is shown in terms of the stretched coordinate η , which is the independent variable in the analysis of the oxidation layer. It is defined such as that the inner layer is located around $\eta = 0$, with the temperature and scalar dissipation rate at this point being T^0 and χ^0 , respectively. Superscript 0 represents values in the inner layer, where global steps I and IV are active. In the inner layer, CH_4 is completely consumed and intermediate species H_2 and CO are formed. In the oxidation layer, global steps II, III and IV are formed and the products of the inner layer are oxidized to CO_2 and H_2O . Oxygen is consumed mainly in the oxidation layer. As a consequence, in the reaction zone X_{O_2} , X_{H_2} and X_{CO} are of the order of ϵ . Asymptotic analysis of the oxidation layer gives values of these quantities at the inner layer, required for characterizing its structure and calculating the scalar dissipation rate, χ^0 , at extinction. In the analysis, all rate constants and equilibrium constants are evaluated at T^0 , and changes in the values of these rate parameters with changes in the temperature are neglected [17]. The value of T^0 is also obtained in the analysis.

4.2.3.1. The Oxidation Layer

In the oxidation layer the concentration of fuel is negligible and H is presumed to maintain steady-state. These approximations reduce the four-step mechanism to a two-step mechanism:



The expansions

$$\xi - \xi_{st} = \epsilon(\eta + \eta^0) \quad (4.17)$$

$$x_{CO} = \epsilon 2g z_{CO} \quad (4.18)$$

$$x_{O_2} = \epsilon g [z_{O_2} - 2(\eta + \eta^0)] \quad (4.19)$$

Are introduced where ϵ is small and the variables η , z_{O_2} and z_{CO} are presumed to be of the order of unity. From coupling relations it follows [10] that

$$x_{H_2} = \epsilon 2g (z_{O_2} - z_{CO}) \quad (4.20)$$

$$\tau = \tau_{st} - \epsilon [2g q_{CO} z_{CO} + q_{O_2} z_{O_2} - s(\eta + \eta^0)] \quad (4.21)$$

The quantity q_{O_2} represents the fractional heat release in the steps III and IV and q_{CO} the fractional heat release in II. The small expansion parameter ϵ is so chosen that it can be calculated from the equation

$$\epsilon = D_{III}^{-1/4} \quad (4.22)$$

where D_{III} is the Damköhler number of global step III and is given by

$$D_{III} = 2^{5/2} \rho^0 g^2 k_5^0 C_M^0 (K_1^0 K_2^0 K_3^0)^{1/2} Le_{H_2}^{3/2} Le_{O_2}^{3/2} / (\chi^0 X_{H_2O,st} W_{N_2}) \quad (4.23)$$

It has been shown in [10] that the structure of the oxidation layer can be constructed from numerical integration of two-coupled second order differential equations, one for O_2 and another for CO. The boundary conditions for these equations are obtained from matching to the inert outer structure for large negative values of η and to the inner layer at $\eta = 0$. Figure 4.2 shows profiles of z_{O_2} and z_{CO} as functions of η .

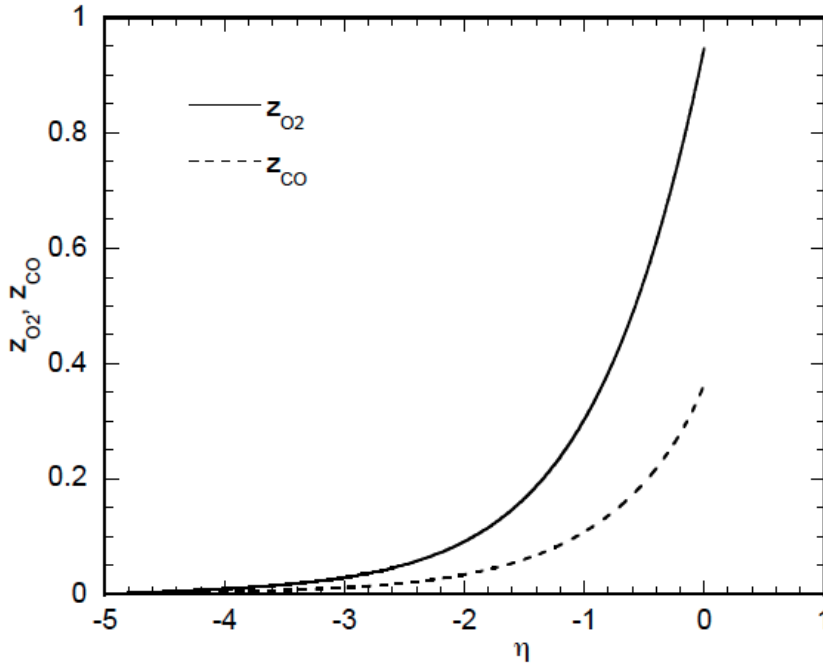


Figure 4.2: Profiles of z_{O_2} and z_{CO} as functions of η obtained from numerical integration of equations describing the structure of the oxidation layer for $\xi_{st} = 0.7$ and $\chi^0 = 0.9s^{-1}$

These profiles are used to obtain values of these quantities at $\eta = 0$ given by $z_{O_2}^0$ and z_{CO}^0 . They are then used to evaluate

$$X_{O_2}^0 = \epsilon g L e_{O_2} [z_{O_2}^0 - 2\eta^0] \quad (4.24)$$

$$X_{H_2}^0 = \epsilon 2g L e_{H_2} [z_{O_2}^0 - z_{CO}^0] \quad (4.25)$$

and the temperature T^0

$$T^0 = T_{st} - \epsilon (2gq_{CO}z_{CO}^0 + gq_{O_2}z_{O_2}^0 - s\eta^0)Q_F / (c_p W_{N_2}) \quad (4.26)$$

These quantities are required to characterize the structure of the inner layer and calculate the scalar dissipation rate at extinction.

4.2.3.2. The Structure of the Inner Layer

The analysis of the inner layer is identical to those in [10, 29]. The value of δ is

$$\delta^2 = \frac{2^{3/2} g^2 k_5^0 C_M^0 k_8^0 K_2^{0/2} Le_{H_2}^{3/2} Le_{O_2}^{3/2} \epsilon^4}{k_{7f}^0 k_9^0 K_2^{0/2} Le_F X_{O_2}^0 X_{H_2}^0} \quad (4.27)$$

Following the analysis in [29], two coupled second-order differential equations, one for CH_4 and one for H, are obtained. These equations include an eigenvalue ω given by

$$\omega^2 = \frac{2^{7/2} g^4 \epsilon^4 k_5^0 C_M^0 k_8^0 K_2^{0/2} X_{H_2O,st}^2 Le_H^2 Le_{O_2}^{3/2} Le_{H_2}^{3/2}}{k_{7f}^0 k_9^0 K_2^{0/2} K_3^{0/2} X_{O_2}^0 X_{H_2}^0 Le_F} \quad (4.28)$$

The coupled differential equations for CH_4 and H are required to satisfy five boundary conditions [29]. These equations are integrated numerically, with the additional boundary condition being used to obtain ω .

4.2.4. The Scalar Dissipation Rate

For given values of temperature and mass fractions of the reactants at the boundaries, the outer structure can be constructed. A value of η^0 is selected. The goal is to predict the scalar dissipation rate χ^0 , that is consistent with this selected value of η^0 . An iterative procedure is employed, beginning with selecting an appropriate value of T^0 . The equations describing the structure of the oxidation layer are integrated, and the results are used to obtain $X_{O_2}^0$ and $X_{H_2}^0$. The coupled differential equations for CH_4 and for H, describing the structure of the inner layer, are integrated and the value of ω is obtained. This

is compared with the value evaluated from Eq. (4.28). If they are not the same, the procedure is repeated with a different value of T^0 until the value of ω , obtained from integration of the coupled differential equations for CH_4 and H , agrees with that calculated using Eq. (4.28). The value of χ^0 that is consistent with the selected value of η^0 is calculated by recasting Eq. (4.23) as

$$\chi^0 = 2^{5/2} \rho^0 g^2 k_5^0 C_M^0 (K_1^0 K_2^0 K_3^{02})^{1/2} Le_{H_2}^{3/2} Le_{O_2}^{3/2} \epsilon^4 / (X_{H_2O,st} W_{N_2}) \quad (4.29)$$

The entire procedure is repeated with another selected value of η^0 .

The classical C-shaped curve is obtained when T^0 is plotted as a function of $(\chi^0)^{-1}$. The value of $(\chi^0)^{-1}$, where its derivative with respect to T^0 in the C-shaped curve is zero, represents the critical condition at extinction. At this critical condition, the value of χ^0 is denoted by χ_q^0 . To facilitate comparison of predictions of asymptotic analysis of critical conditions of extinction with experimental results, the scalar dissipation rate at ξ_{st} , denoted χ_{st} is calculated using the expression [30-32]

$$\chi_{st} = \chi^0 \exp[-2\epsilon\eta^0/\xi_{st}] \quad (4.30)$$

The value of χ_{st} at extinction is represented by $\chi_{st,q}$.

Chapter 5

Experimental and Computational Results

Chapter 5 summarizes the experimental results and compares them with the computations. The detailed experimental results and data can be found in appendix A, the approach for the computation is described in chapter 4.

5.1. Extinction of Methane

The extinction experiments with methane were carried out to investigate the influence of the stoichiometric mixture fractions ξ_{st} on the critical conditions of extinction. The scalar dissipation rate χ depends on the stoichiometric mixture fraction and the maximum flame temperature T_{st} . To elucidate the effect of ξ_{st} , the mass fractions of the reactants were so chosen that T_{st} is fixed.

Experiments were carried out from the lowest possible stoichiometric mixture fraction with a fuel mass fraction $Y_{F,1} = 1$, to the highest possible stoichiometric mixture fraction with an oxidizer mass fraction $Y_{O_2,2} = 1$. Two sets of experiments were conducted at different adiabatic flame temperatures, 2000K and 2100K.

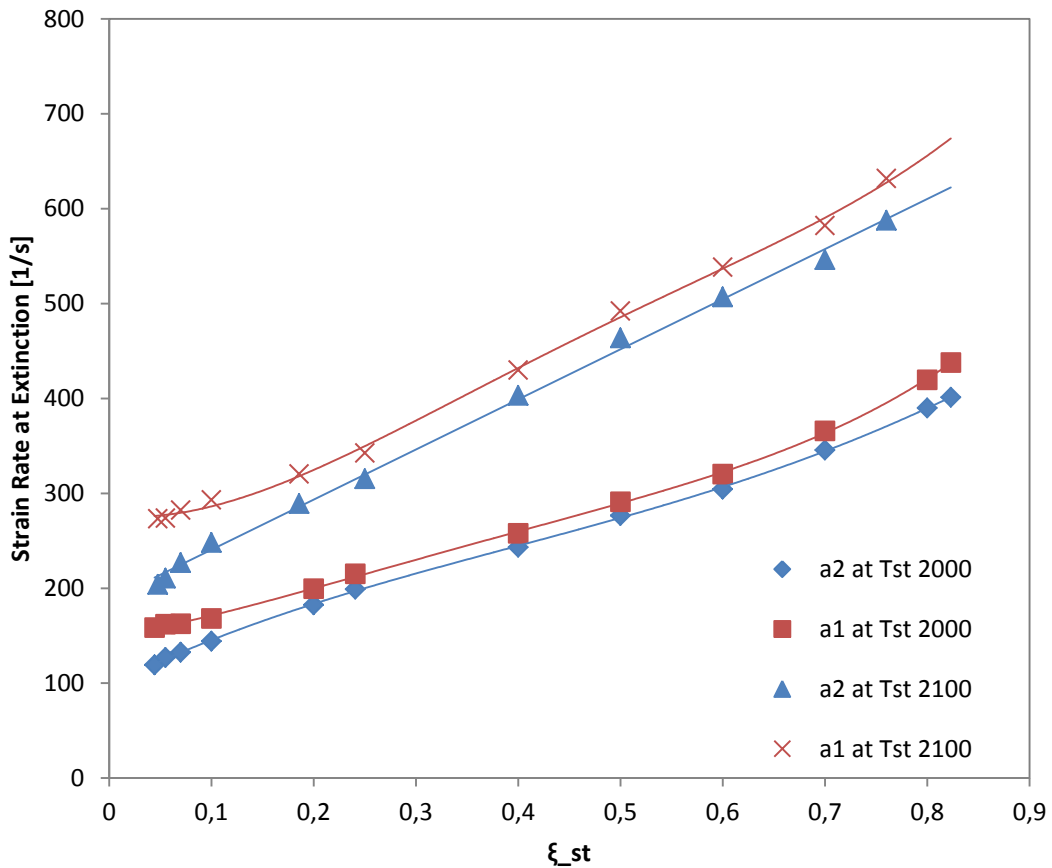


Figure 5.1: Extinction strain rates of methane over the stoichiometric mixture fraction at $T_{st} = 2000\text{K}$ and $T_{st} = 2100\text{K}$. The symbols represent the experimental data and the lines are best-fit curves based on polynomials fourth order.

As depicted in figure 5.1, the extinction strain rate of the fuel stream a_1 and the extinction strain rate of the oxidizer stream a_2 increase continually with increasing stoichiometric mixture fractions ξ_{st} . The lines (best-fit curves based on polynomials fourth order) are boundaries between the nonflammable and the flammable regions. In a system in a state above the lines, a flame cannot be ignited with an external energy source and stabilized. The flammable region can be reached either by decreasing the strain rate, which results in a downward shift, or by increasing the fuel mass fraction, equaling a horizontal shift to the left. The continuous increase in the extinction strain rates shows that it becomes harder to extinguish a flame with increasing oxygen mass fraction at constant energy content of the fuel-oxygen mixture.

Experiments at $T_{st} = 2100\text{K}$ were carried out only until a maximum $\xi_{st} = 0.76$ with a corresponding oxidizer mass fraction $Y_{O_2,2} = 0.7905$. This is attributed

to the high strain rates at these conditions, as the mass flows exceeded the limits of the mass flow controllers and the necessary flow rates could no longer be achieved.

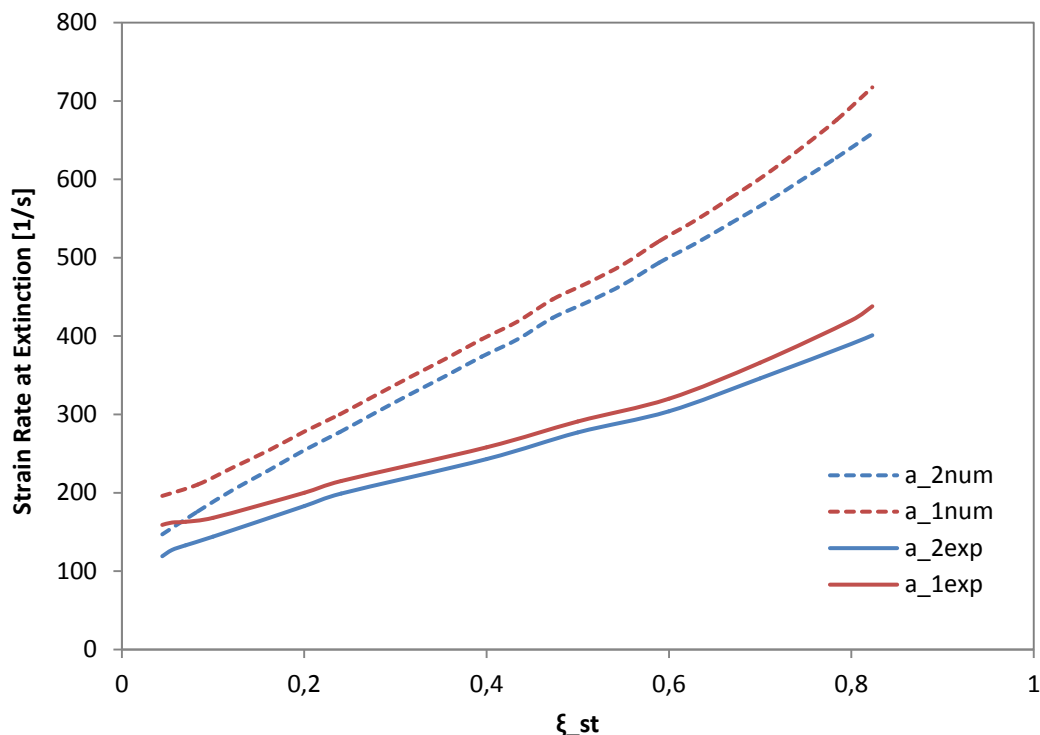


Figure 5.2: Comparison of extinction strain rates at $T_{st} = 2000K$: experimental results and numerical computations (detailed mechanism)

Figure 5.2 compares the strain rates of extinction of methane diffusion flames at an adiabatic temperature $T_{st} = 2000K$ with the numerical computations. It can be seen that for small ξ_{st} , the computational predictions of the strain rate of extinction are close to the measurements, whereas for larger ξ_{st} the predictions exceed the measurements by a factor of 1.5 and greater.

The numerical data was obtained from computations using the most recent version of the San Diego mechanism (20141004). The disagreement between the experimental data and the computations is fairly small considering the large number of reactions involved. Some reactions of the mechanism might not matter much for extinction or have minor errors and therefore may not match the measurements. In addition, the flow profile may not be exactly the same during low and high strain rates in the experiments. In order to improve

the mechanism over time it would be necessary to consider which reactions matter more at high strain rates in comparison to low strain rates.

As the separation of the ducts in the computations did not match the distance L in the experimental setup, a correctional factor was used to adjust the predictions.

$$a_{2,q\ num}^{corr} = \frac{a_{2,q\ num}}{1.25} \quad (5.1)$$

The corrected predictions are closer to the measurements for low ξ_{st} and match the experimental results well, however with increasing ξ_{st} the predicted extinction strain rates are still higher than the measurements (Figure 5.3).

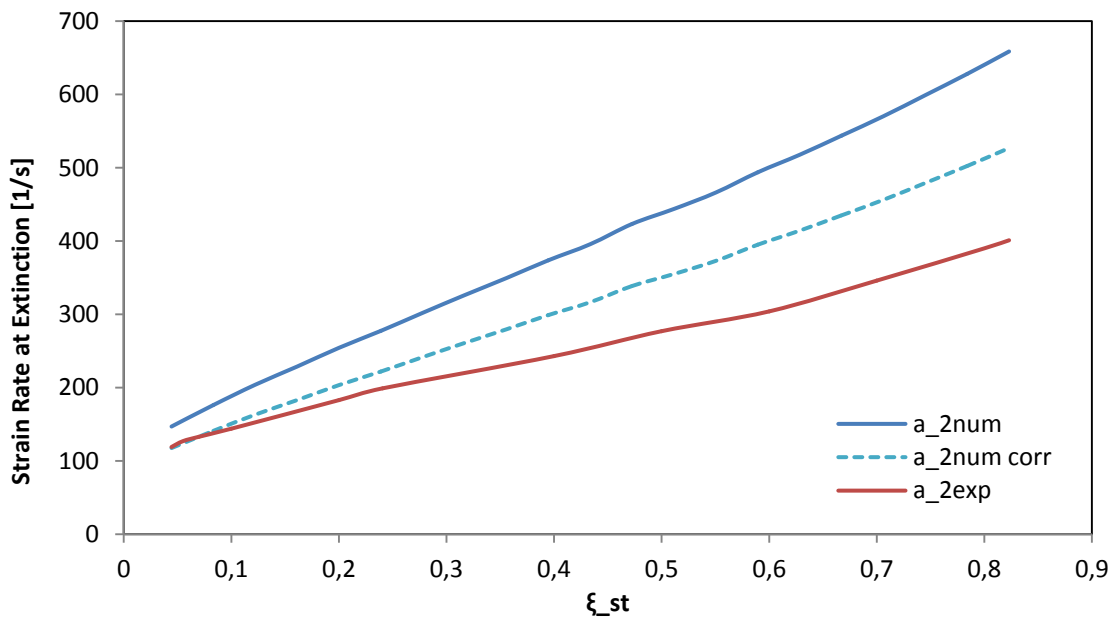


Figure 5.3: Extinction strain rates of methane at $T_{st} = 2000K$: A comparison of numerical and corrected numerical computations with experimental measurements

In order to examine the accuracy of the San Diego Mechanism in regard to the experimental measurements of methane extinction flames, further analysis was conducted at different adiabatic temperatures. By varying the fuel and oxidizer mass fractions in the streams in such way that the fuel to oxidizer-ratio and therefore the stoichiometric mixture fraction remains constant, extinction at various temperature conditions can be effectuated.

Figure 5.4 shows the corresponding numerical computations and experimental measurements at a constant stoichiometric mixture fraction and varying oxidizer mass fractions. There is good agreement between the computations and the measurements, however at higher strain rates and adiabatic temperatures the San Diego Mechanism begins to over predict the extinction strain rate.

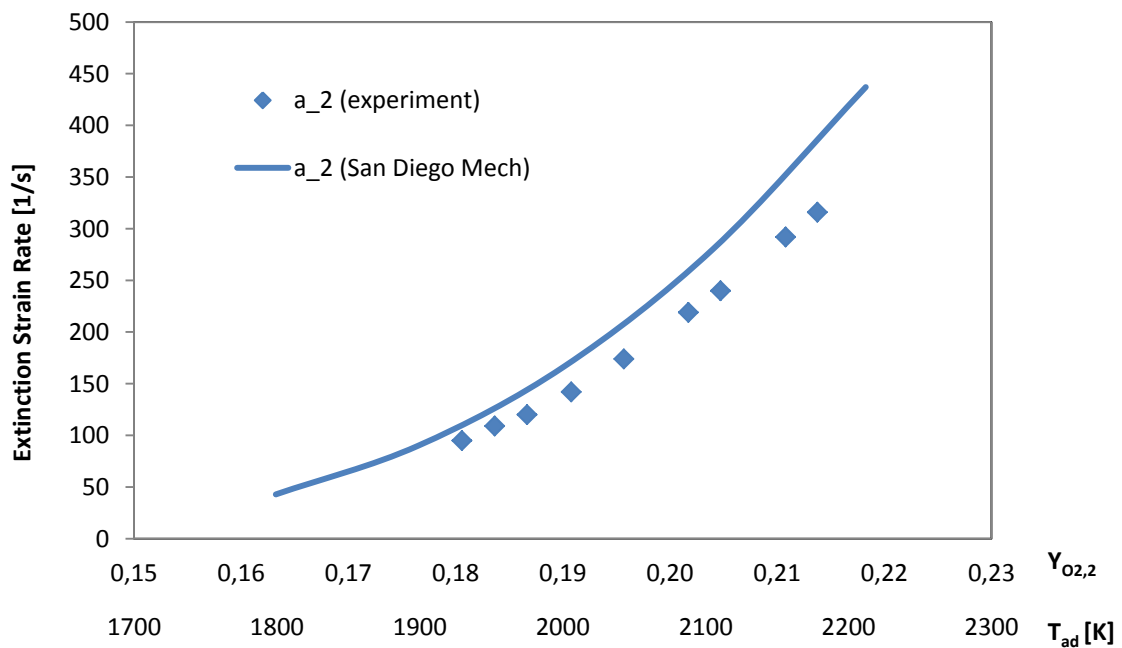


Figure 5.4: Experimental Data and numerical computations of extinction strain rates at constant $\xi_{st} = 0.07$ and varying fuel and oxidizer mass fractions

To illustrate the changes in the flame structure, calculations using one-step-chemistry were performed in addition to the San Diego Mechanism. A one-step overall reaction is assumed, with the overall rate constant

$$k = AT^\beta e^{-\frac{E_A}{RT}} \quad (5.2)$$

where $A = 1.123 \cdot 10^{14} \text{ cm}^3/(\text{mole} \cdot \text{s})$ and $E = 128 \text{ kJ/mole}$.

Figure 5.5 shows the comparison of the detailed San Diego Mechanism with the one-step mechanism. The one-step mechanism does not show a linear

increase of the extinction strain rate with increasing stoichiometric mixture fractions, but rather a decrease followed by an increase.

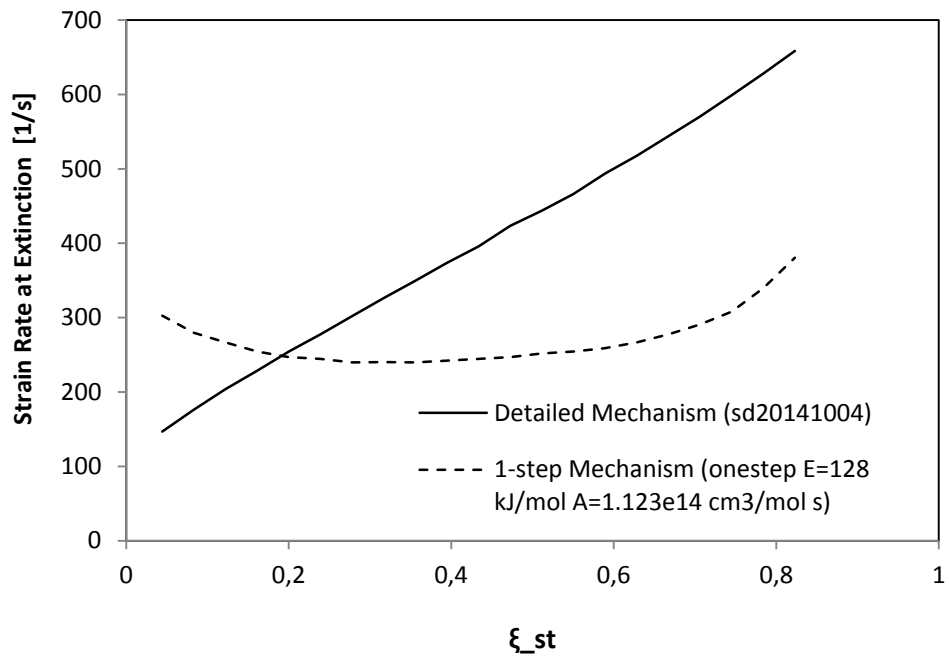


Figure 5.5: Comparison of extinction strain rates of detailed and one-step chemistry at varying ξ_{st}

The following figures illustrate the changes in the flame structure, the data is obtained from numerical computations.

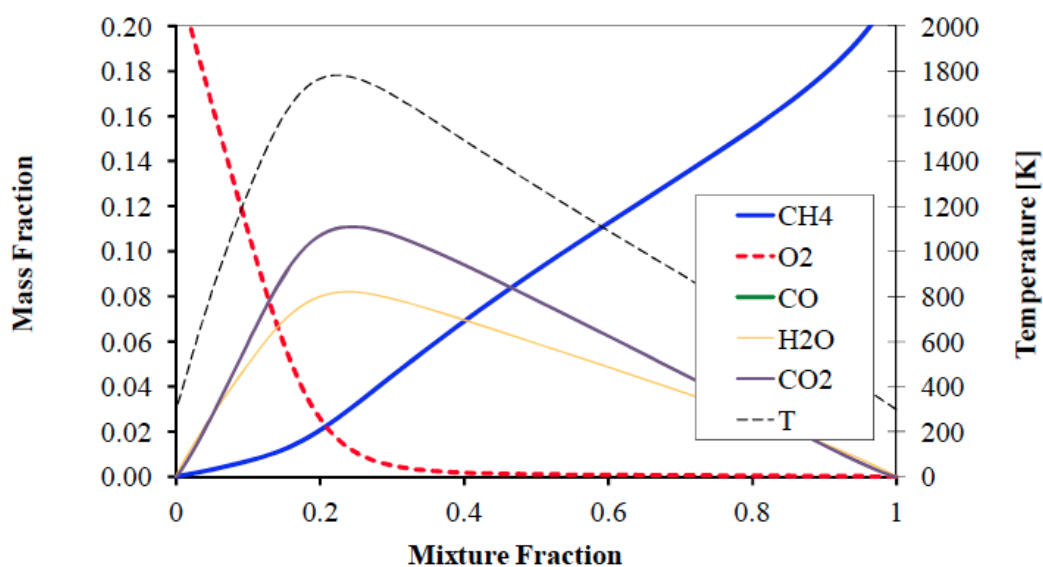


Figure 5.6: Numerical computation of flame structure at $\xi_{st} = 0.2$ and $T_{st} = 2000\text{K}$ using one-step mechanism

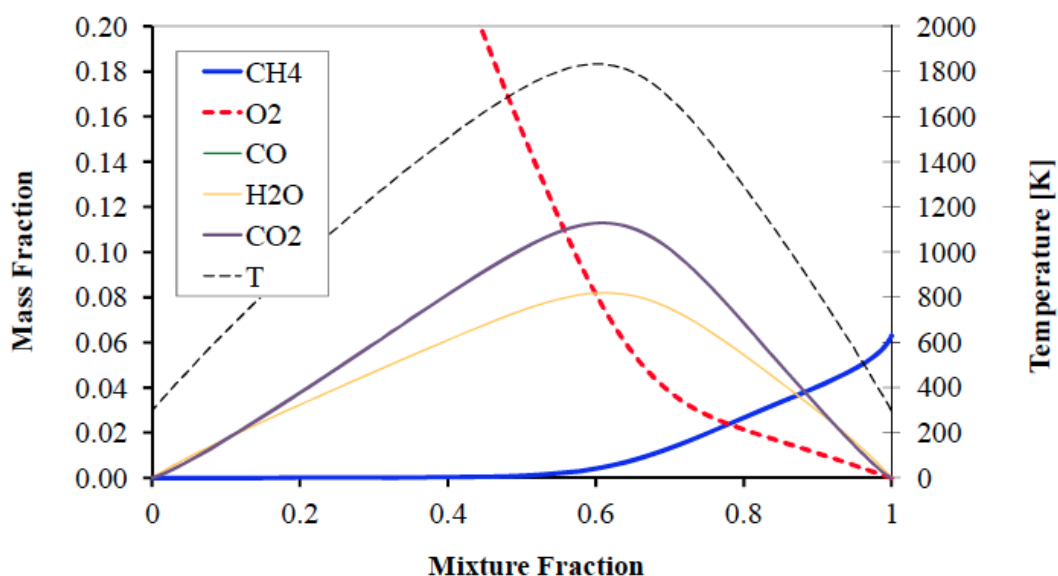


Figure 5.7: Numerical computation of flame structure at $\xi_{st} = 0.7$ and $T_{st} = 2000\text{K}$ using one step mechanism

Figures 5.6 and 5.7 show the flame structure at varying stoichiometric mixture fraction, computed using one-step chemistry. For small ξ_{st} a leakage of fuel can be observed and oxygen is completely consumed. For small $(1 - \xi_{st})$ however, there is a leakage of oxygen and fuel is completely consumed.

Furthermore, there are very little changes in the values of the strain rate at extinction with changes in the values of ξ_{st} .

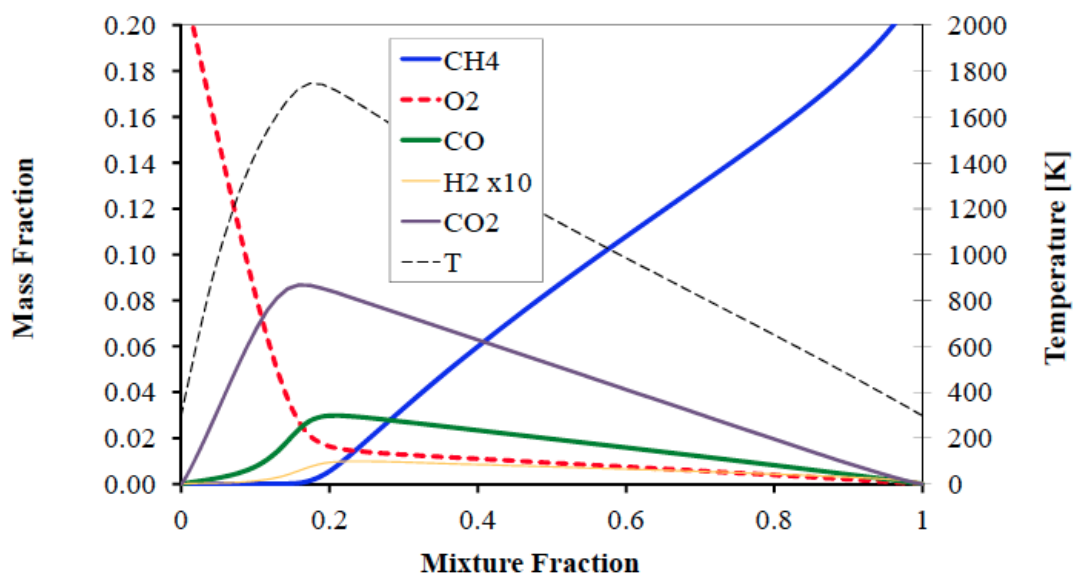


Figure 5.8: Numerical computation of flame structure at $\xi_{st} = 0.2$ and $T_{st} = 2000\text{K}$ using detailed chemistry

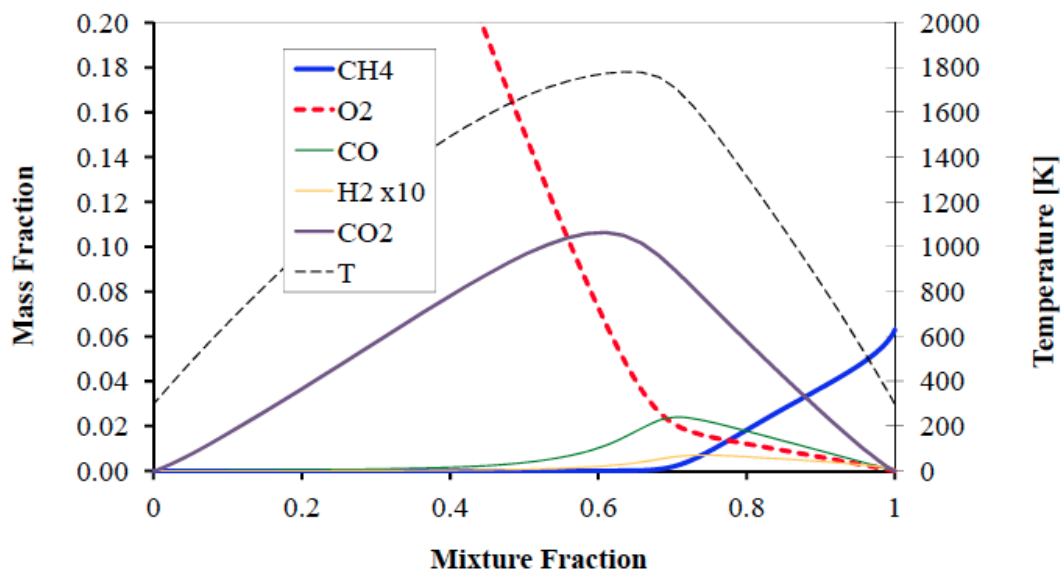


Figure 5.9: Numerical computation of flame structure at $\xi_{st} = 0.7$ and $T_{st} = 2000\text{K}$ using detailed chemistry

Figures 5.8 and 5.9 depict the flame structure at varying stoichiometric mixture fractions. The data was obtained from numerical computations using the detailed mechanism. For all values of ξ_{st} there was nearly complete

consumption of CH_4 , but there was leakage of O_2 from the reaction zone (measured as the value of the mass fraction of O_2 at ξ_{st}). Net rates of consumption of CH_4 and O_2 were calculated. With increasing ξ_{st} , the thickness of the regions where these reactants are consumed are found to increase, and leakage of oxygen at conditions close to extinction was found to increase.

At a mixture fraction slightly below ξ_{st} the formation of CO (green) and H_2 (yellow) through consumption of CH_4 is made visible, and Y_{CO} and Y_{H_2} increase until they reach their maximum in this layer. The temperature profile shows that the highest temperature occurs at a value ξ just slightly below ξ_{st} .

There are fundamental differences in predictions obtained employing detailed chemistry and one-step chemistry. A comparison with experimental data shows that numerical computations with the detailed mechanism are a better fit and more suitable for describing the extinction strain rate of non-premixed methane flames than one-step chemistry.

Figure 5.10 shows snapshots of the flame at the extinction strain rate, milliseconds before extinction occurred. The range of the stoichiometric mixture fraction ranges from $Y_{F,1} = 1$ to $Y_{O_2,2} = 1$. The change in the flame thickness and intensity can be observed with increasing ξ_{st} .

Figure 5.11 shows the flame at a constant oxidizer strain rate $a_2 = 150 \text{ s}^{-1}$ at $\xi_{st} = 0.2$ and $\xi_{st} = 0.7$. The vertical position of the flame shifts toward the fuel side with an increase in the stoichiometric mixture fraction. At low ξ_{st} , the oxidizer mass fraction is low and the stoichiometric mixture forms in a stagnation plane closer to the oxidizer duct. At high strain rates, the fuel mass fraction is very low and the reactants mix closer to the fuel duct, therefore the flame shifts toward the fuel side.

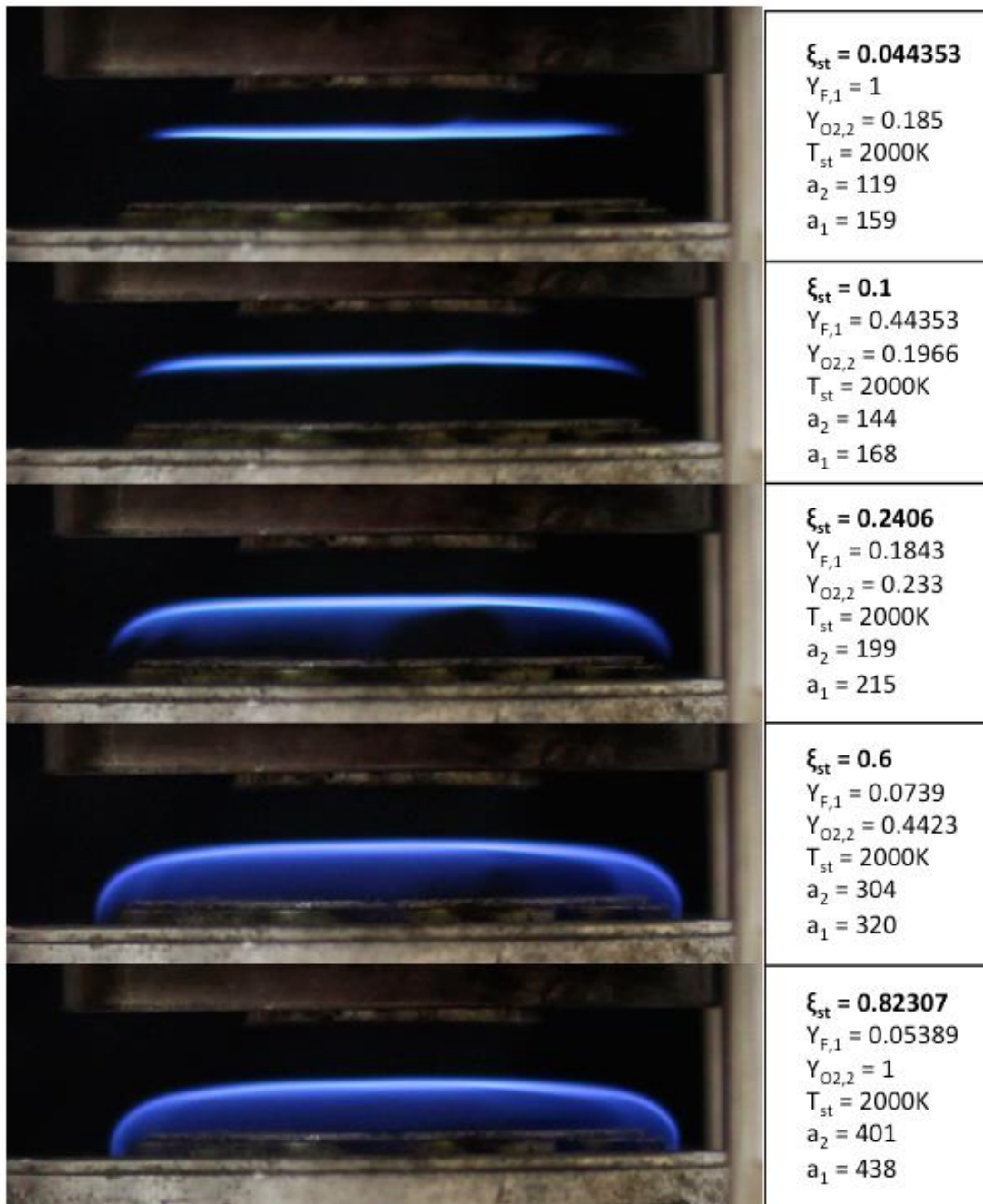


Figure 5.10: Flame appearance at extinction strain rate at varying ξ_{st} and $T_{st} = 2000K$

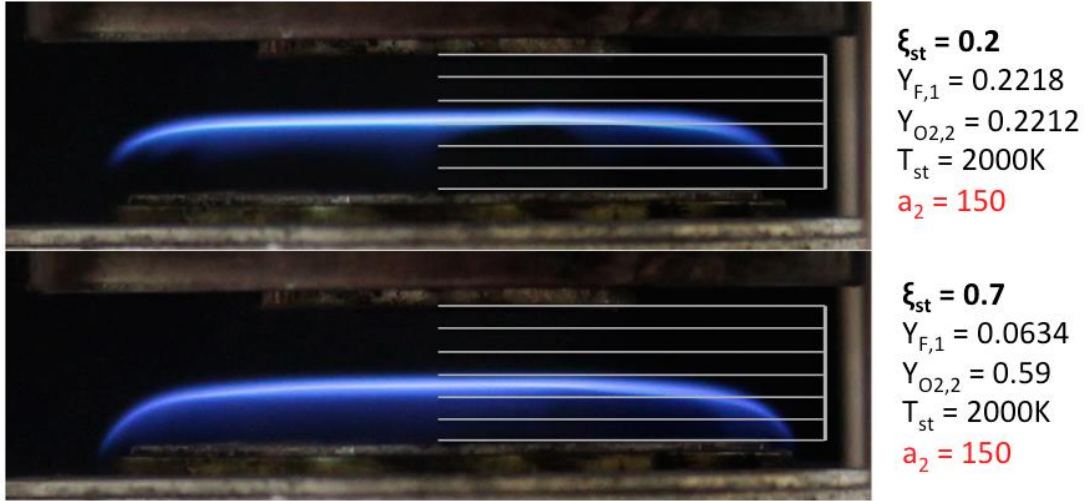


Figure 5.11: Flame position at constant oxidizer strain rate $a_2 = 150$ and varying stoichiometric mixture fraction at $T_{st} = 2000\text{K}$

5.1.1. Results of the Rate-Ratio Asymptotic Analysis

To facilitate a comparison of experimental measurements with results of the rate-ratio asymptotic analysis, the scalar dissipation rate at extinction $\chi_{st,q}$ is calculated from a_q using a relation derived by Prof. Seshadri from [24]. The scalar dissipation rate incorporates the influence of convection and diffusion normal to the surface of stoichiometric mixture [25] and is given by:

$$\chi_{st,q} = \frac{a_{2,q}}{2\pi} \frac{3 \left[(T_{st}/T_u)^{1/2} + 1 \right]^2}{2(T_{st}/T_u)^{1/2} + 1} * \exp\{-2[\text{erfc}^{-1}(2\xi_{st})]^2\} \quad (5.3)$$

for $\xi_{st} < 0.5$ and

$$\chi_{st,q} = \frac{a_{1,q}}{2\pi} \frac{3 \left[(T_{st}/T_u)^{1/2} + 1 \right]^2}{2(T_{st}/T_u)^{1/2} + 1} * \exp\{-2[\text{erfc}^{-1}(2(1 - \xi_{st}))]^2\} \quad (5.4)$$

for $\xi_{st} > 0.5$. Here erfc^{-1} is the inverse of the complimentary error function.

Figure 5.12 compares the ratio $\chi_{st,q}/\chi_{st,q,ref}$ of experiments, numerical calculations and RRA-analysis for various values of ξ_{st} at $T_{st} = 2000K$. Here the quantity $\chi_{st,q,ref}$ is the maximum value of $\chi_{st,q}$.

It is noteworthy that the scalar dissipation rate first increases and then decreases. In the asymptotic analysis, the peak value of $127s^{-1}$ is attained at $\xi_{st} = 0.7$, whereas the peak value of the experiments is reached at $\xi_{st} = 0.6$. Overall the numerical computations and the predictions of the asymptotic analysis agree well with the experimental data.

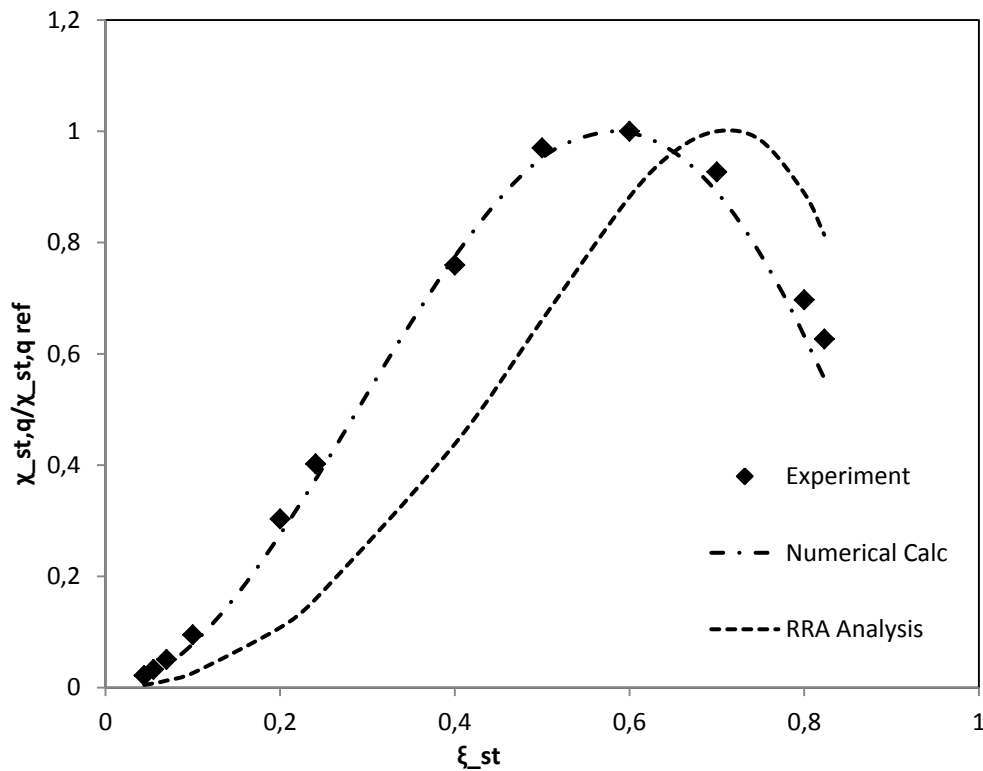


Figure 5.12: The ratio $\chi_{st,q}/\chi_{st,q,ref}$ for various values of ξ_{st} at $T_{st} = 2000K$

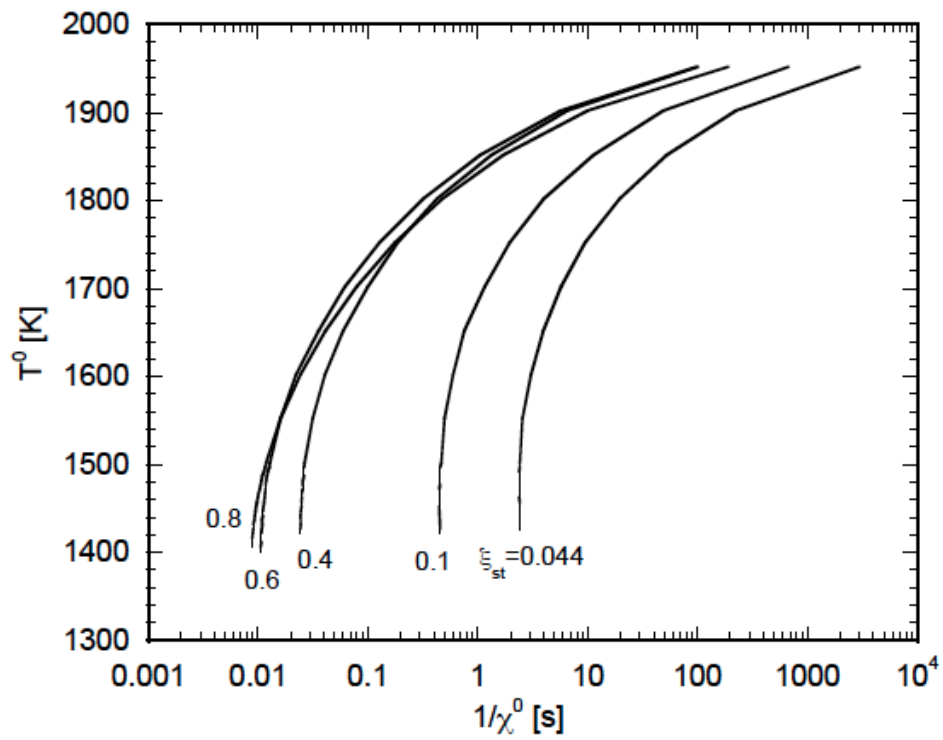


Figure 5.13: The flame temperature, T^0 , as a function of $(\chi^0)^{-1}$ [s], for various values of ξ_{st} at fixed $T_{st} = 2000\text{K}$

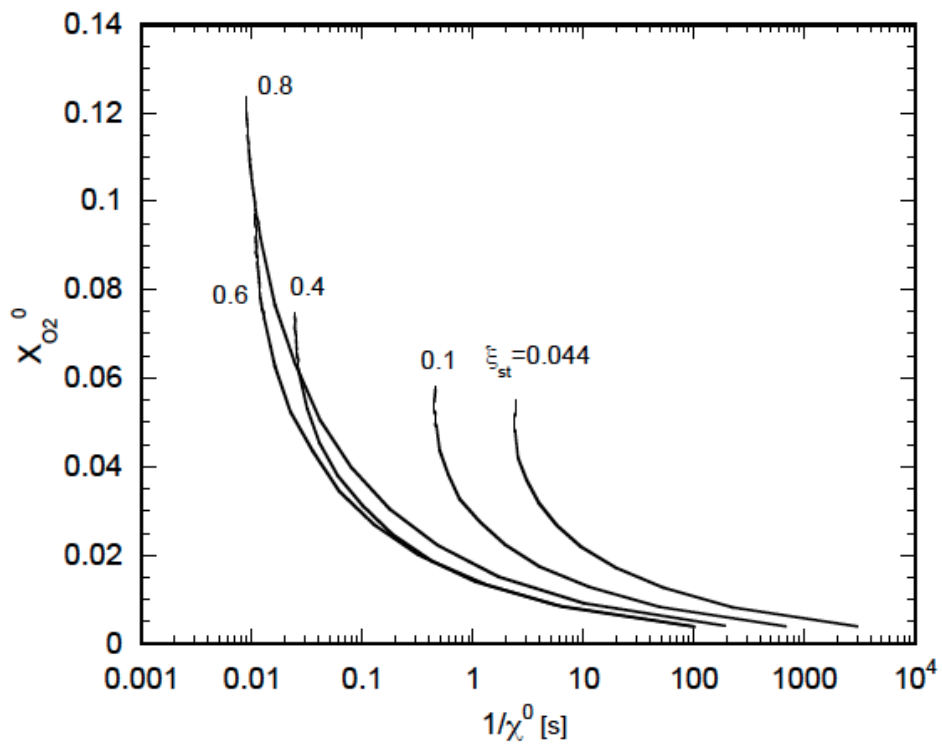


Figure 5.14: The normalized mass fraction of O_2 , $X_{\text{O}_2}^0$, as a function of $(\chi^0)^{-1}$ [s], for various values of ξ_{st} at fixed $T_{st} = 2000\text{K}$

Figure 5.13 shows T^0 and Figure 5.14 shows $X_{O_2}^0$ both as functions of $(\chi^0)^{-1}$ for various values of ξ_{st} . All show the classical C-shaped behavior. The upper branches of the C-shaped curves for T^0 vs. $(\chi^0)^{-1}$ and the lower branches for $X_{O_2}^0$ are stable. With decreasing values of $(\chi^0)^{-1}$, the flame temperature decreases and the oxidizer leakage represented by $X_{O_2}^0$ increases. All curves show that there is no solutions for values $(\chi^0)^{-1}$ below a critical value. This critical value of χ^0 is the scalar dissipation rate of extinction represented by χ_q^0 . It is noteworthy, that at extinction the values T^0 are nearly the same, while the value of $X_{O_2}^0$ increases with increasing ξ_{st} . The value of the scalar dissipation rate at extinction evaluated at ξ_{st} , $\chi_{st,q}$, is obtained from χ_q^0 using Equation (4.30).

Figure 5.15 shows values of ϵ and δ as a function of ξ_{st} . It can be seen that for all ξ_{st} , the value of δ is less than that of ϵ , and both are less than 0.1. This confirms the ordering $\delta \ll \epsilon \ll 1$ employed in the analysis. A key finding is that the values of ϵ and δ increase with ξ_{st} and are consistent with computational predictions of changes in thickness of the regions of oxygen consumption and fuel consumption.

Equation (4.29) shows that χ^0 depends on T^0 , ϵ , g and $X_{H_2O,st}$. Equation (4.26) shows that ϵ depends on g , $z_{O_2}^0$, z_{CO}^0 , and η^0 . At fixed $T_{st} = 2000K$ considered here, $\tau_{st} = 0.0772$, $g = 0.077/[\xi_{st}(1 - \xi_{st})]$, $X_{H_2O,st} = 0.1552$, and $s/g \approx (1 - \xi_{st})$. Results of the asymptotic analysis described here show that at conditions close to extinction, changes in values of T^0 , $z_{O_2}^0$, z_{CO}^0 , and η^0 are small, and their values are $T^0 = 1400K$, $z_{O_2}^0 = 0.9$, $z_{CO}^0 = 0.4$, $\eta^0 = -1.2$. Hence it follows that

$$\epsilon \approx 0.33 [\xi_{st}(1 - \xi_{st})]/(2.0 - 1.3\xi_{st}) \quad (5.5)$$

$$X_{O_2}^0 = 0.09/(2.0 - 1.3\xi_{st}) \quad (5.6)$$

The peak value of ϵ is around $\xi_{st} = 0.63$. The value of ϵ obtained from Eq. (5.5) is plotted in Figure 5.15 and is close to the values obtained from the asymptotic analysis.

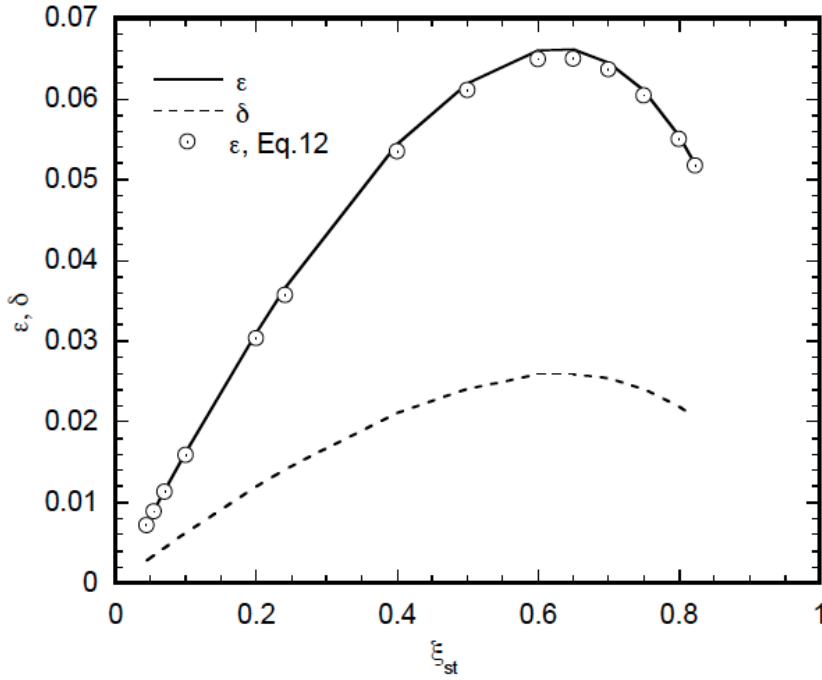


Figure 5.15: Predicted values of ϵ and δ as a function of ξ_{st} . The figure also shows the approximate value of ϵ calculated using Eq. (5.5)

Equation (5.6) shows that the leakage of oxygen from the reaction zone increases with increasing ξ_{st} . This is in agreement with the results shown in Figure 5.14 and with the predictions using detailed chemistry in Figures 5.8 and 5.9. Equation (4.27) shows that δ is proportional to ϵ . Therefore the changes in the thickness of the inner layer are similar to those of the oxidation layer. For fixed $(T_{st} - T_u)$ the quantity $\xi_{st}(1 - \xi_{st})$ is inversely proportional to the sum of the absolute values of the temperature gradients in the outer structure. Equation (4.29) predicts that

$$\chi_{st} \propto \epsilon^4 \quad (5.7)$$

showing that the scalar dissipation rate is proportional to the thickness of the reaction zone. Thus, changes in values of $\chi_{st,q}$ are similar to those of ϵ . With increasing ξ_{st} , the value of ϵ first increases and then decreases, and the peak is around $\epsilon = 0.63$. Thus with increasing ξ_{st} at first the flame thickness increases and the sum of the absolute values of the temperature gradients in the outer structure decreases, this increases the overall reactivity. This means that the flame gets stronger with rising χ_{st} and then weakens as the thickness decreases.

5.2. Extinction of Dimethyl Ether

The extinction experiments with dimethyl ether were carried out to investigate the influence of the stoichiometric mass fractions ξ_{st} on the critical conditions of extinction. As with the methane experiments, the mass fractions of the reactants were so chosen that T_{st} is fixed to elucidate the effect of ξ_{st} . Extinction strain rates of non-premixed dimethyl ether flames were predicted to decrease with increasing stoichiometric mixture fraction, and therefore differ from those of non-premixed methane flames. This trend is to be reconfirmed with these experiments.

For this purpose, three sets of experiments were carried out with different Lewis numbers, ranging from 1.4 to 1.6. The first set of experiments, using $Le = 1.5$, was carried out from the lowest possible stoichiometric mixture fraction with a fuel mass fraction $Y_{F,1} = 0.7945$, to the highest possible stoichiometric mixture fraction with an oxidizer mass fraction $Y_{O_2,2} = 0.7997$. The second and third sets of experiments were executed up to an oxidizer mass fraction $Y_{O_2,2} = 0.233$ (see Table 3.6).

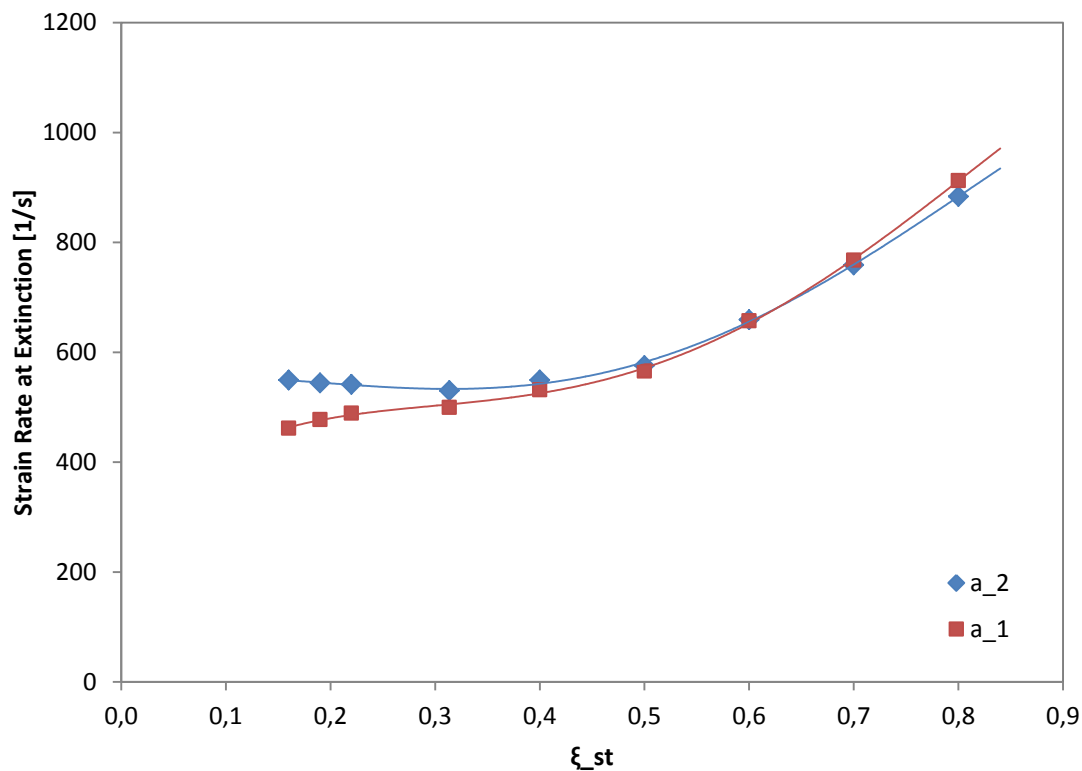


Figure 5.16: Extinction strain rates of non-premixed dimethyl ether flames at varying ξ_{st} and $Le = 1.5$. The symbols represent the experimental data and the lines are best-fit curves based on polynomials fourth order.

Figure 5.16 shows the extinction strain rates of non-premixed dimethyl ether flames at $Le = 1.5$ and $T_{st} = 2000K$. The oxidizer strain rate decreases until it reaches its minimum at $\xi_{st} = 0.3136$, which corresponds to an oxidizer mass fraction $Y_{O_2,2} = 0.233$. Experiments at low ξ_{st} using a fuel mass fraction $Y_{F,1} = 1$ were not successful due to technical difficulties resulting from the high demand of fuel at this point. Moreover, experiments with $Y_{O_2,2} > 0.7997$ were not carried out to avoid turbulence, as the counter-flow setup is not designed for such high strain rates.

Figure 5.17 compares the extinction strain rates of non-premixed DME flames obtained using different Lewis numbers in the calculation of the mass fractions. It can be seen that there is a trend of a decrease in the extinction strain rates until a minimum is reached with increasing ξ_{st} , independent of the Lewis number. A higher Lewis number indicates a higher extinction strain rate.

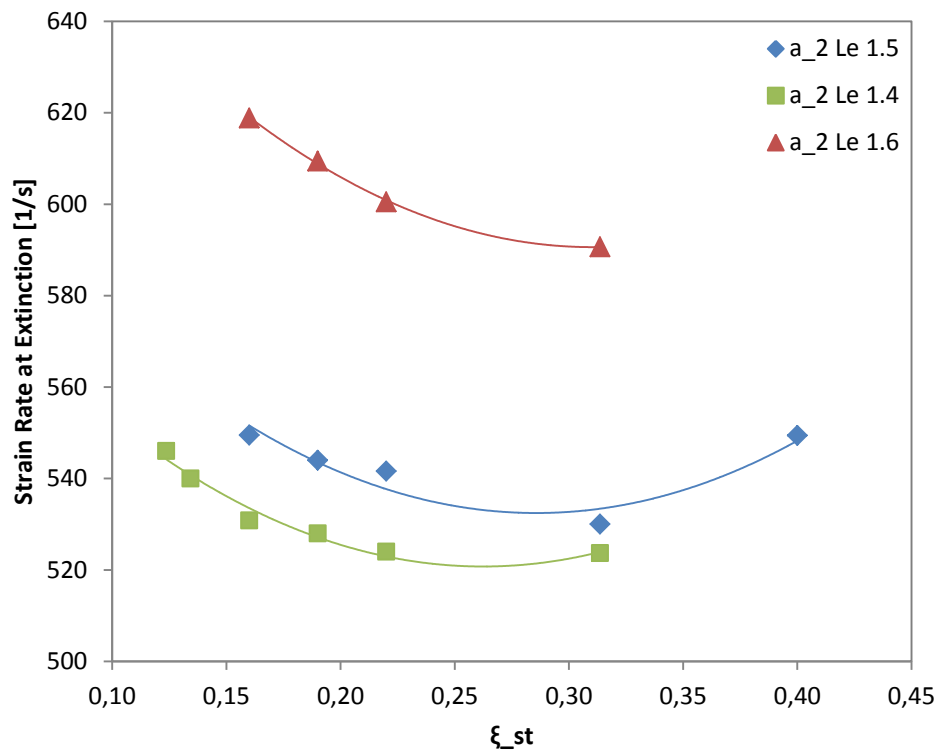


Figure 5.17: Extinction strain rates of non-premixed DME flames at varying ξ_{st} and Le . The symbols represent the experimental data and the lines are best-fit curves based on polynomials second order.

A comparison of the extinction strain rates of non-premixed DME flames with the numerical computations shows a strong discrepancy in the results. As shown in Figure 5.18, the predictions also show a decrease of $a_{2,q}$ with increasing ξ_{st} . However, extinction was predicted to occur at a higher strain rate at a low stoichiometric mixture fraction and continually decreases with an increase in the oxygen mass fraction. After reaching a minimum at $\xi_{st} = 0.61$ there is a slight increase in the extinction strain rate.

The separation distance between the fuel and oxidizer ducts in the computations was set to 10mm. The experiments, however, were conducted with a separation distance of 12.5mm. This may explain the mismatch between experimental data and numerical computations, is however not a sufficient justification for the discrepancy. Further numerical analysis and a review of the computational parameters is necessary.

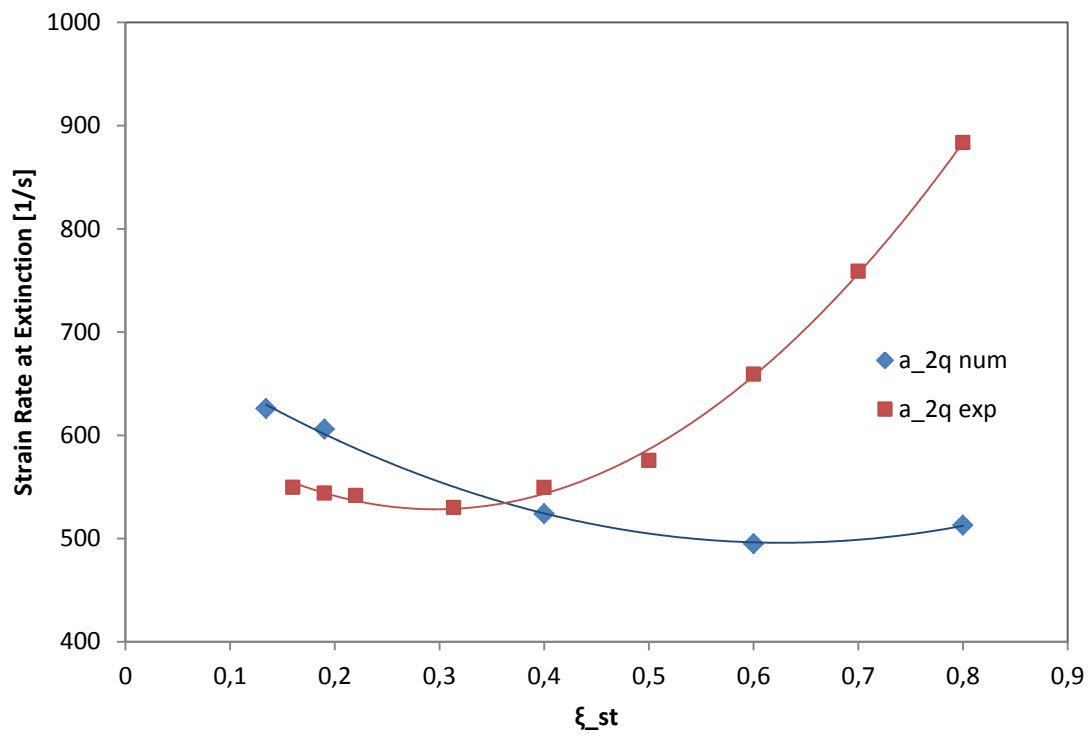


Figure 5.18: Comparison of strain rates of extinction of non-premixed DME flames with numerical computations at constant T_{st} and $Le = 1.5$. The symbols represent the experimental data and the lines are best-fit curves based on polynomials second order.

Chapter 6

Concluding Remarks

The main focus of this diploma thesis was to gain a better understanding of the influence of the stoichiometric mixture fraction ξ_{st} on the critical conditions of extinction of non-premixed methane and non-premixed dimethyl ether flames.

For methane flames, the experimental studies show a constant increase in the extinction strain rate with increasing stoichiometric mixture fractions at constant adiabatic temperature. Thus, extinction of non-premixed methane flames is delayed with increasing amounts of oxygen and decreasing amounts of methane. This is confirmed by the numerical computations, carried out using the San Diego Mechanism. In addition, computations were performed with chemistry represented by a one-step irreversible reaction Fuel + Oxygen \rightarrow Products. It was found that for small ξ_{st} there was a leakage of fuel from the reaction zone and for small $(1 - \xi_{st})$ there was a leakage of oxygen, whereas the San Diego mechanism shows that for all values of ξ_{st} there was complete consumption of fuel and a leakage of oxygen. In addition, one step chemistry shows very little changes in the values of the strain rate at extinction with changes in the values of the stoichiometric mixture fraction. Thus, there are fundamental differences in predictions obtained using detailed chemistry and one-step chemistry.

The predictions of the rate-ratio asymptotic analysis show that at fixed adiabatic temperature, starting from small ξ_{st} , the scalar rate of dissipation at extinction, $\chi_{st,q}$, first increases, attains a peak value and then decreases with increasing ξ_{st} . A noteworthy observation is that with increasing stoichiometric

mixture fraction, the sum of the absolute values of the temperature gradient in the outer structure first increases and then decreases. As a consequence, the thickness of the reaction zones first increases and then decreases. Another important prediction is that with an increase in values of ξ_{st} , the leakage of oxygen through the reaction zone increases. This is due to the shallower concentration gradient on the oxygen side, which affects its evolution through the oxygen consumption layer ϵ .

Experimental studies on extinction of non-premixed dimethyl ether flames show the influence of the stoichiometric mixture fraction on the extinction strain rate. With increasing ξ_{st} , $a_{2,q}$ first decreases, attains a minimum value, and then increases. This behavior was observed at various fuel and oxidizer mass fractions obtained using different Lewis numbers in the calculation. Numerical computations were performed but do not match the experimental results, showing a much more significant decrease in strain rates at extinction. Further research is necessary to eliminate the offset between the experimental results and the predictions of the numerical computations.

References

- [1] Peters, N. 2010. *Combustion Theory. CEFRC Summer School, Princeton.* RWTH Aachen University
- [2] Tsuji, H. 1982. *Counterflow diffusion flames.* Progress in Energy and Combustion Science. 8, 2 (1982), 93–119.
- [3] Humer, S. 2007. *Development of a Surrogate Diesel Fuel.* PhD Thesis, Vienna, Austria.
- [4] Seshadri, K., Williams, F.A. 1978. Laminar flow between parallel plates with injection of a reactant at high Reynolds number. *International Journal of Heat and Mass Transfer*, 21(2): 251-253.
- [5] Ritter TG-Series Operation Instructions V2.0, Rev. 02/2011. URL <http://www.ritter.de/fileadmin/download/public/EN/Manuals/RITTER-EN-Manual-P01-TG.pdf>. Accessed: 2015-11-12.
- [6] Omega Revised Thermocouple Reference Tables, Type E, N.I.S.T Monograph 175 Revised to ITS-90. URL <http://www.omega.com/temperature/Z/pdf/z206.pdf>. Accessed 2015-11-04
- [7] Peters, N. 1992. *Fifteen Lectures on Laminar and Turbulent Combustion.* Ercoftac Summer School, RWTH Aachen
- [8] Connors, K. A. 1990. *Chemical kinetics. The study of reaction rates in solution.* VCH, New York, N.Y.
- [9] Turns, S. 2011. *An Introduction to Combustion: Concepts and Applications.* McGraw-Hill Science/Engineering/Math.
- [10] K. Seshadri, X. S. Bai. 2015. *Combustion Science and Technology* 187, 3-26.
- [11] K. Seshadri, F. A. Williams. 1978. *International Journal of Heat and Mass Transfer* 21, 251-253.
- [12] Peters, N. *Technische Verbrennung I*, RWTH Aachen.
- [13] NIST-JANAF Thermochemical Tables, <http://kinetics.nist.gov/janaf/>, 2013.
- [14] Chemical Equilibrium Calculator, Colorado State University, Copyright David Dandy

<http://navier.engr.colostate.edu/~dandy/code/code-4/>. Accessed 2015-10-7

[15] Buckmaster, J., Clavin, P., Linan, A., Matalon, M., Peters, N., Sivashinsky, G., Williams, F. A. 2005. *Combustion Theory and Modeling*. Proceedings of the Combustion Institute, 30, 1, 1-19

[16] Peters, N. 1993. *Reduced Kinetic Mechanisms for Applications in Combustion Systems*, Springer Verlag Berlin Heidelberg

[17] Seshadri, K. 1996. *Proceedings of the Combustion Institute* 26, 831-846.

[18] National Institute of Standards and Technology. 2005. *NIST Chemistry WebBook Standard Reference Database Number 69*.
<http://webbook.nist.gov/chemistry/>. Accessed 23 October 2015.

[19] Semelsberger, T. A., Borup, R. L., and Greene, H. L. 2006. *Dimethyl ether (DME) as an alternative fuel*. Journal of Power Sources 156, 2, 497–511.

[20] McCandless, J., 2001. *DME as an Automotive Fuel: Technical, Economical and Social Perspectives*, Energy Frontiers Conference

[21] Erdener, H., Arinan, A. and Orman, S. 2012. *Future Fossil Fuel Alternative; DME (A review)*. International Journal of Renewable Energy Research (IJRER). 1, 4 (2012), 252–258.

[22] Ogawa, T., Inoue, N., Shikada, T. and Ohno, Y. 2003. *Direct dimethyl ether synthesis*. Journal of natural gas chemistry. 12, 4 (2003), 219–227.

[23] Goyal, P., Sidharta, 2003. *Present scenario of air quality in Delhi: a case study of CNG implementation*. Atmospheric Environment, 37 (2003), 5423-5431

[24] J. S. Kim, F. A. Williams. 1993. *SIAM Journal on Applied Mathematics* 53 (1993) 1551-1566.

[25] Pitsch, H. 2014. *Laminar Diffusion Flames*. CEFRC Summer School, Princeton. RWTH Aachen University

[26] Gehmlich, R. 2015. *Experimental Studies on Nonpremixed Combustion at Atmospheric and Elevated Pressure*. PhD Thesis, University of California San Diego

- [27] Pitsch, H. 2014. *FlameMaster: A C++ computer program for 0D combustion and 1D laminar flame calculations*
- [28] The San Diego Mechanism, Chemical-Kinetic Mechanisms for Combustion Applications. UC San Diego
<http://web.eng.ucsd.edu/mae/groups/combustion/mechanism.html>
Accessed 2015-12-05
- [29] X. S. Bai, K. Seshadri. 1999. *Combustion Theory and Modelling* 3 (1999) 51-75
- [30] N. Peters. 1984. *Progress in Energy and Combustion Science* 10 (1984) 319-339
- [31] K. Seshadri, N. Peters. 1988. *Combustion and Flame* 73 (1988) 23-44
- [32] B. Yang, K. Seshadri. 1992. *Combustion Science and Technology* 88 (1992)115-132
- [33] Cai, L., H. Pitsch. 2014. *Tailoring fuels for a shockless explosion combustor*, In R. King, ed., *Active Flow and Combustion Control 2014*, vol 127 of NNFM, 299-316. Springer International Publishing, 2015.

List of Figures

Figure 1.1: DME Production Methods: Direct and Indirect Synthesis.....	6
Figure 1.2: Schematic illustration of the counterflow burner with an established flame.....	8
Figure 1.3: The maximum temperature T_{max} as a function of the Damköhler number - the characteristic S-shaped curve. T_1 is the temperature of the fuel boundary, T_2 the temperature of the oxidizer boundary, T_{ad} the adiabatic flame temperature, D_{al} the Damköhler number at ignition, D_{aE} the Damköhler number at extinction.	11
Figure 2.1: Schematic illustration of the experimental setup, showing the counterflow burner, the mass flow controllers and the gas supply.....	14
Figure 2.2: Section view of the lower part of the burner.....	16
Figure 2.3: Section view of the extinction top.....	17
Figure 2.4: Experiment control screen of the Lab View program. The user can control reactant mass fractions, gaseous flow rates, temperatures and data saving routines.....	18
Figure 2.5: Control setup screen of the Lab View software. The User can select the computation program for the desired experiments, assign the gas inputs to the different ports and start the calibration procedure for the mass flow controllers.	19
Figure 3.1: Left: Profiles of $Y_{F,u}$ and $Y_{O_2,u}$ in the unburnt gas mixture	29
Figure 3.2: Fuel and oxidizer mass fractions over the stoichiometric mixture fraction at $T_{st} = 2002K$	32
Figure 3.3: Fuel and oxidizer mass fractions over the stoichiometric mixture fraction at $T_{st} = 2100K$	34
Figure 3.4: DME and oxidizer mass fractions over the stoichiometric mixture fraction at $T_{st} = 2000K$	36
Figure 3.5: The effect of Lewis number variation on DME mass fractions	37
Figure 4.1: Schematic illustration of the structure of the reaction zone at ξ_{st} . The figure shows the inner layer and the oxidation layer.....	43

Figure 4.2: Profiles of z_{O_2} and z_{CO} as functions of η obtained from numerical integration of equations describing the structure of the oxidation layer for $\xi_{st} = 0.7$ and $\chi^0 = 0.9s^{-1}$	46
Figure 5.1: Extinction strain rates of methane over the stoichiometric mixture fraction at $T_{st} = 2000K$ and $T_{st} = 2100K$. The symbols represent the experimental data and the lines are best-fit curves based on polynomials fourth order.	50
Figure 5.2: Comparison of extinction strain rates at $T_{st} = 2000K$: experimental results and numerical computations (detailed mechanism)	51
Figure 5.3: Extinction strain rates of methane at $T_{st} = 2000K$: A comparison of numerical and corrected numerical computations with experimental measurements	52
Figure 5.4: Experimental Data and numerical computations of extinction strain rates at constant $\xi_{st} = 0.07$ and varying fuel and oxidizer mass fractions	53
Figure 5.5: Comparison of extinction strain rates of detailed and one-step chemistry at varying ξ_{st}	54
Figure 5.6: Numerical computation of flame structure at $\xi_{st} = 0.2$ and $T_{st} = 2000K$ using one-step mechanism.....	55
Figure 5.7: Numerical computation of flame structure at $\xi_{st} = 0.7$ and $T_{st} = 2000K$ using one step mechanism.....	55
Figure 5.8: Numerical computation of flame structure at $\xi_{st} = 0.2$ and $T_{st} = 2000K$ using detailed chemistry	56
Figure 5.9: Numerical computation of flame structure at $\xi_{st} = 0.7$ and $T_{st} = 2000K$ using detailed chemistry	56
Figure 5.10: Flame appearance at extinction strain rate at varying ξ_{st} and $T_{st} = 2000K$	58
Figure 5.11: Flame position at constant oxidizer strain rate $a_2 = 150$ and varying stoichiometric mixture fraction at $T_{st} = 2000K$	59
Figure 5.12: The ratio $\chi_{st,q}/\chi_{st,q,ref}$ for various values of ξ_{st} at $T_{st} = 2000K$	60
Figure 5.13: The flame temperature, T^0 , as a function of $(\chi^0)^{-1}$ [s], for various values of ξ_{st} at fixed $T_{st} = 2000K$	61
Figure 5.14: The normalized mass fraction of O2, $X_{O_2}^0$, as a function of $(\chi^0)^{-1}$ [s], for various values of ξ_{st} at fixed $T_{st} = 2000K$	61

Figure 5.15: Predicted values of ϵ and δ as a function of ξ_{st} . The figure also shows the approximate value of ϵ calculated using Eq. (5.5)63

Figure 5.16: Extinction strain rates of non-premixed dimethyl ether flames at varying ξ_{st} and $Le = 1.5$. The symbols represent the experimental data and the lines are best-fit curves based on polynomials fourth order.65

Figure 5.17: Extinction strain rates of non-premixed DME flames at varying ξ_{st} and Le . The symbols represent the experimental data and the lines are best-fit curves based on polynomials second order.66

Figure 5.18: Comparison of strain rates of extinction of non-premixed DME flames with numerical computations at constant T_{st} and $Le = 1.5$ 67

List of Tables

Table 1.1: Properties of Methane and Dimethyl Ether [18,19]	3
Table 3.1: Initial and final mole and mass fractions for $T_{st} = 2002\text{K}$	31
Table 3.2: Calculated fuel and oxidizer mass fractions for selected values of ξ_{st} at $T_{st} = 2002\text{K}$	32
Table 3.3: Initial and final mole and mass fractions for $T_{st} = 2100\text{K}$	33
Table 3.4: Calculated fuel and oxidizer mass fractions for selected values of ξ_{st} at $T_{st} = 2100\text{K}$	33
Table 3.5: Calculated fuel and oxidizer mass fractions for selected values of ξ_{st} at $T_{st} = 2000\text{K}$ and $Le = 1.5$	36
Table 3.6: Calculated DME mass fractions for selected ξ_{st} with varying Lewis numbers.....	37
Table 4.1: Rate Data of elementary reactions. Units are moles, cm^3 , seconds, kJoules, Kelvin.....	42

Appendix A

A.1 Experimental Data: Extinction of Methane at $T_{st} = 2000\text{K}$

ξ_{st}	a_2 (1/s)	a_1 (1/s)	rho_2 (kg/m ³)	rho_1 (kg/m ³)	V2 (m/s)	V1 (m/s)	T2 (K)	T1 (K)	P (Pa)	Y2,1	Y2,Inert	Y1,1	Y1,Inert
0.044353	122	163	1.185617	0.667748	0.305	0.406411	294.543005	292.4	101231	0.185	0.814	1	0
0.044353	119	159	1.185937	0.663129	0.2975	0.39785	294.536641	294.5	101231	0.185	0.814	1	0
0.044353	119	159	1.185937	0.663129	0.2975	0.39785	294.463709	294.5	101231	0.185	0.814	1	0
0.044353	119	159	1.185937	0.663129	0.2975	0.39785	294.444609	294.5	101231	0.185	0.814	1	0
0.044353	120	160	1.185464	0.663129	0.3	0.401113	294.733874	294.5	101231	0.185	0.814	1	0
0.044353	118	158	1.185528	0.663129	0.295	0.394438	294.533368	294.5	101231	0.185	0.814	1	0
0.044353	118	158	1.185528	0.663129	0.295	0.394438	294.386923	294.5	101231	0.185	0.814	1	0
0.055	129	165	1.185662	0.723086	0.3225	0.412967	294.488804	294.5	101231	0.18723	0.81277	0.806	0.194
0.055	128	164	1.185611	0.723086	0.32	0.409757	294.507906	294.5	101231	0.18723	0.81277	0.806	0.194
0.055	128	164	1.185611	0.723086	0.32	0.409757	294.488804	294.5	101231	0.18723	0.81277	0.806	0.194
0.055	127	163	1.186059	0.723086	0.3175	0.406632	294.406216	294.5	101231	0.18723	0.81277	0.806	0.194
0.055	125	160	1.185905	0.723086	0.3125	0.400203	294.384016	294.5	101231	0.18723	0.81277	0.806	0.194
0.055	124	159	1.185623	0.723086	0.31	0.396954	294.517548	294.5	101231	0.18723	0.81277	0.806	0.194
0.055	127	163	1.185854	0.723086	0.3175	0.406597	294.517548	294.5	101231	0.18723	0.81277	0.806	0.194
0.055	128	164	1.185996	0.723086	0.32	0.409823	294.482443	294.5	101231	0.18723	0.81277	0.806	0.194
0.07	137	168	1.186469	0.790127	0.3425	0.419701	294.527005	293	101231	0.1902	0.8098	0.634	0.366
0.07	132	162	1.185649	0.790127	0.33	0.404244	294.791104	293	101231	0.1902	0.8098	0.634	0.366
0.07	133	163	1.186085	0.786102	0.3325	0.408423	294.74968	294.5	101231	0.1902	0.8098	0.634	0.366
0.07	133	163	1.186085	0.786102	0.3325	0.408423	294.644823	294.5	101231	0.1902	0.8098	0.634	0.366
0.07	132	162	1.18561	0.786102	0.33	0.405271	294.613007	294.5	101231	0.1902	0.8098	0.634	0.366
0.07	131	161	1.185214	0.786102	0.3275	0.402133	294.628827	294.5	101231	0.1902	0.8098	0.634	0.366

ξ_{st}	a_2 (1/s)	a_1 (1/s)	rho_2 (kg/m ³)	rho_1 (kg/m ³)	V2 (m/s)	V1 (m/s)	T2 (K)	T1 (K)	P (Pa)	Y2,1	Y2,Inert	Y1,1	Y1,Inert
0.07	131	161	1.185214	0.786102	0.3275	0.402133	294.558827	294.5	101231	0.1902	0.8098	0.634	0.366
0.07	131	161	1.185214	0.786102	0.3275	0.402133	294.571556	294.5	101231	0.1902	0.8098	0.634	0.366
0.1	144	168	1.188308	0.876906	0.36	0.419074	294.273024	294.64	101231	0.1966	0.8034	0.44353	0.55647
0.1	146	170	1.188488	0.876906	0.365	0.424926	294.126421	294.64	101231	0.1966	0.8034	0.44353	0.55647
0.1	143	166	1.188308	0.876906	0.3575	0.416163	294.075406	294.64	101231	0.1966	0.8034	0.44353	0.55647
0.1	144	168	1.188	0.876906	0.36	0.419019	294.244049	294.64	101231	0.1966	0.8034	0.44353	0.55647
0.1	145	169	1.188333	0.876906	0.3625	0.421989	294.075406	294.64	101231	0.1966	0.8034	0.44353	0.55647
0.1	144	168	1.188386	0.876906	0.36	0.419087	294.218558	294.64	101231	0.1966	0.8034	0.44353	0.55647
0.1	144	168	1.188386	0.876906	0.36	0.419087	294.202721	294.64	101231	0.1966	0.8034	0.44353	0.55647
0.1	143	166	1.187794	0.876906	0.3575	0.416074	294.263365	294.64	101231	0.1966	0.8034	0.44353	0.55647
0.2	181	198	1.192559	1.00143	0.4525	0.493797	294.049895	294.64	101231	0.2212	0.7788	0.2218	0.7782
0.2	183	200	1.191991	1.00143	0.4575	0.499134	294.177424	294.64	101231	0.2212	0.7788	0.2218	0.7782
0.2	183	200	1.191991	1.00143	0.4575	0.499134	294.285765	294.64	101231	0.2212	0.7788	0.2218	0.7782
0.2	183	200	1.191991	1.00143	0.4575	0.499134	294.285765	294.64	101231	0.2212	0.7788	0.2218	0.7782
0.2	182	199	1.192172	1.00143	0.455	0.496444	294.081786	294.64	101231	0.2212	0.7788	0.2218	0.7782
0.2	183	200	1.192003	1.00143	0.4575	0.499137	294.155209	294.64	101231	0.2212	0.7788	0.2218	0.7782
0.2406	201	217	1.194024	1.019805	0.5025	0.543731	294.279393	294	101231	0.233	0.767	0.1843	0.8157
0.2406	200	216	1.193868	1.019805	0.5	0.54099	294.273024	294	101231	0.233	0.767	0.1843	0.8157
0.2406	199	215	1.194334	1.019805	0.4975	0.53839	294.132798	294	101231	0.233	0.767	0.1843	0.8157
0.2406	199	215	1.194334	1.019805	0.4975	0.53839	294.158297	294	101231	0.233	0.767	0.1843	0.8157
0.2406	198	214	1.193881	1.019805	0.495	0.535583	294.403712	294	101231	0.233	0.767	0.1843	0.8157
0.2406	199	215	1.193648	1.019805	0.4975	0.538236	294.250819	294	101231	0.233	0.767	0.1843	0.8157
0.2406	197	213	1.192834	1.019805	0.4925	0.532645	294.29234	294	101231	0.233	0.767	0.1843	0.8157
0.2406	199	215	1.193338	1.019805	0.4975	0.538166	294.416449	294	101231	0.233	0.767	0.1843	0.8157
0.4	242	256	1.203388	1.071336	0.605	0.641203	294.200034	294	101231	0.295	0.705	0.111	0.889
0.4	242	256	1.203388	1.071336	0.605	0.641203	294.149037	294	101231	0.295	0.705	0.111	0.889
0.4	243	258	1.203336	1.071336	0.6075	0.643838	294.101317	294	101231	0.295	0.705	0.111	0.889

ξ_{st}	a_2 (1/s)	a_1 (1/s)	rho_2 (kg/m ³)	rho_1 (kg/m ³)	V2 (m/s)	V1 (m/s)	T2 (K)	T1 (K)	P (Pa)	Y2,1	Y2,Inert	Y1,1	Y1,Inert
0.4	242	256	1.203179	1.071336	0.605	0.641147	294.267054	294	101231	0.295	0.705	0.111	0.889
0.4	245	260	1.203035	1.071336	0.6125	0.649056	294.155623	294	101231	0.295	0.705	0.111	0.889
0.4	245	260	1.203035	1.071336	0.6125	0.649056	294.152537	294	101231	0.295	0.705	0.111	0.889
0.4	243	258	1.203609	1.071336	0.6075	0.643911	294.232111	294	101231	0.295	0.705	0.111	0.889
0.5	278	294	1.213034	1.087834	0.695	0.733905	294.079316	294	101231	0.354	0.646	0.089	0.911
0.5	276	291	1.213218	1.087834	0.69	0.728681	294.273852	294	101231	0.354	0.646	0.089	0.911
0.5	276	291	1.213218	1.087834	0.69	0.728681	294.069859	294	101231	0.354	0.646	0.089	0.911
0.5	277	291	1.213218	1.087834	0.69	0.728681	294.152537	294	101231	0.354	0.646	0.089	0.911
0.5	276	291	1.213218	1.087834	0.69	0.728681	294.107905	294	101231	0.354	0.646	0.089	0.911
0.5	277	292	1.212261	1.087834	0.6925	0.731032	294.365908	294	101231	0.354	0.646	0.089	0.911
0.5	276	291	1.212523	1.087834	0.69	0.728472	294.251229	294	101231	0.354	0.646	0.089	0.911
0.6	304	322	1.227357	1.097066	0.76	0.803864	294.210123	294.64	101231	0.4423	0.5577	0.0739	0.9261
0.6	303	320	1.226506	1.097066	0.7575	0.800942	294.108122	294.64	101231	0.4423	0.5577	0.0739	0.9261
0.6	306	324	1.226798	1.097066	0.765	0.808968	294.24199	294.64	101231	0.4423	0.5577	0.0739	0.9261
0.6	303	320	1.226532	1.097066	0.7575	0.800951	294.292967	294.64	101231	0.4423	0.5577	0.0739	0.9261
0.6	304	321	1.226692	1.097066	0.76	0.803646	294.267476	294.64	101231	0.4423	0.5577	0.0739	0.9261
0.6	305	323	1.227383	1.097066	0.7625	0.806517	294.050724	294.64	101231	0.4423	0.5577	0.0739	0.9261
0.6	306	324	1.227078	1.097066	0.765	0.809061	294.174956	294.64	101231	0.4423	0.5577	0.0739	0.9261
0.6	303	320	1.226945	1.097066	0.7575	0.801085	294.225949	294.64	101231	0.4423	0.5577	0.0739	0.9261
0.6	306	323	1.226002	1.097066	0.765	0.808706	294.397963	294.64	101231	0.4423	0.5577	0.0739	0.9261
0.7	345	367	1.249725	1.105464	0.8625	0.917052	294.560633	294.59	101231	0.59	0.41	0.0634	0.9366
0.7	346	368	1.249834	1.105464	0.865	0.91975	294.532105	294.59	101231	0.59	0.41	0.0634	0.9366
0.7	344	366	1.250415	1.105464	0.86	0.914647	294.341078	294.59	101231	0.59	0.41	0.0634	0.9366
0.7	346	368	1.250199	1.105464	0.865	0.919885	294.620978	294.59	101231	0.59	0.41	0.0634	0.9366
0.7	344	366	1.249348	1.105464	0.86	0.914256	294.496979	294.59	101231	0.59	0.41	0.0634	0.9366
0.7	347	369	1.25047	1.105464	0.8675	0.922643	294.382149	294.59	101231	0.59	0.41	0.0634	0.9366
0.7	347	369	1.25047	1.105464	0.8675	0.922643	294.350304	294.59	101231	0.59	0.41	0.0634	0.9366

ξ_{st}	a_2 (1/s)	a_1 (1/s)	rho_2 (kg/m ³)	rho_1 (kg/m ³)	V2 (m/s)	V1 (m/s)	T2 (K)	T1 (K)	P (Pa)	Y2,1	Y2,Inert	Y1,1	Y1,Inert
0.7	343	365	1.249821	1.105464	0.8575	0.911771	294.503132	294.59	101231	0.59	0.41	0.0634	0.9366
0.7	348	370	1.249591	1.105464	0.87	0.924977	294.576437	294.59	101231	0.59	0.41	0.0634	0.9366
0.8	383	414	1.300512	1.11147	0.9575	1.035732	294.690962	294.67	101231	0.88465	0.11535	0.05544	0.94456
0.8	384	416	1.301412	1.11147	0.96	1.038795	294.550978	294.67	101231	0.88465	0.11535	0.05544	0.94456
0.8	386	418	1.301088	1.11147	0.965	1.044075	294.423874	294.67	101231	0.88465	0.11535	0.05544	0.94456
0.8	388	420	1.300681	1.11147	0.97	1.049321	294.506422	294.67	101231	0.88465	0.11535	0.05544	0.94456
0.8	392	424	1.301243	1.11147	0.98	1.060368	294.566996	294.67	101231	0.88465	0.11535	0.05544	0.94456
0.8	397	429	1.300793	1.11147	0.9925	1.073707	294.5828	294.67	101231	0.88465	0.11535	0.05544	0.94456
0.8	392	424	1.301876	1.11147	0.98	1.060626	294.350514	294.67	101231	0.88465	0.11535	0.05544	0.94456
0.8	392	424	1.301876	1.11147	0.98	1.060626	294.299553	294.67	101231	0.88465	0.11535	0.05544	0.94456
0.8	393	425	1.301778	1.11147	0.9825	1.063291	294.296261	294.67	101231	0.88465	0.11535	0.05544	0.94456
0.8	392	424	1.302314	1.11147	0.98	1.060804	294.30571	294.67	101231	0.88465	0.11535	0.05544	0.94456
0.82307	401	438	1.324115	1.11214	1.0025	1.093875	294.232537	294.82	101231	1	0	0.05389	0.94611
0.82307	397	433	1.323427	1.11214	0.9925	1.082682	294.25495	294.82	101231	1	0	0.05389	0.94611
0.82307	399	435	1.323054	1.11214	0.9975	1.087983	294.238913	294.82	101231	1	0	0.05389	0.94611
0.82307	398	434	1.323455	1.11214	0.995	1.085421	294.28352	294.82	101231	1	0	0.05389	0.94611
0.82307	397	433	1.323442	1.11214	0.9925	1.082688	294.382149	294.82	101231	1	0	0.05389	0.94611
0.82307	405	442	1.323083	1.11214	1.0125	1.104355	294.296261	294.82	101231	1	0	0.05389	0.94611
0.82307	405	442	1.323083	1.11214	1.0125	1.104355	294.277148	294.82	101231	1	0	0.05389	0.94611
0.82307	406	443	1.323942	1.11214	1.015	1.107442	294.331408	294.82	101231	1	0	0.05389	0.94611
0.82307	403	440	1.323154	1.11214	1.0075	1.098931	294.433312	294.82	101231	1	0	0.05389	0.94611

A.2 Experimental Data: Extinction of Methane at $T_{st} = 2100K$

ξ_{st}	a_2 (1/s)	a_1 (1/s)	rho_2 (kg/m ³)	rho_1 (kg/m ³)	V2 (m/s)	V1 (m/s)	T2 (K)	T1 (K)	P (Pa)	Y2,1	Y2,Inert	Y1,1	Y1,Inert
0.047557	201	269	1.18889	0.662409	0.5025	0.6732	294.149895	294.82	101230.8577	0.1992	0.8008	1	0
0.047557	205	275	1.188402	0.662409	0.5125	0.686455	294.254734	294.82	101230.8577	0.1992	0.8008	1	0
0.047557	204	273	1.188363	0.662409	0.51	0.683096	294.229245	294.82	101230.8577	0.1992	0.8008	1	0
0.047557	204	273	1.188363	0.662409	0.51	0.683096	294.382361	294.82	101230.8577	0.1992	0.8008	1	0
0.047557	206	276	1.187232	0.662409	0.515	0.689465	294.439677	294.82	101230.8577	0.1992	0.8008	1	0
0.055	213	277	1.188566	0.702971	0.5325	0.692409	294.121312	294.82	101230.8577	0.2008	0.7992	0.865	0.135
0.055	212	276	1.188271	0.702971	0.53	0.689072	294.43002	294.82	101230.8577	0.2008	0.7992	0.865	0.135
0.055	209	272	1.189404	0.702971	0.5225	0.679645	294.105042	294.82	101230.8577	0.2008	0.7992	0.865	0.135
0.055	209	272	1.189404	0.702971	0.5225	0.679645	294.003216	294.82	101230.8577	0.2008	0.7992	0.865	0.135
0.055	210	273	1.189016	0.702971	0.525	0.682786	294.172314	294.82	101230.8577	0.2008	0.7992	0.865	0.135
0.07	229	285	1.188164	0.767744	0.5725	0.712206	294.503132	294.82	101230.8577	0.204	0.796	0.679	0.321
0.07	226	281	1.188447	0.767744	0.565	0.702959	294.461861	294.82	101230.8577	0.204	0.796	0.679	0.321
0.07	225	280	1.187998	0.767744	0.5625	0.699716	294.604964	294.82	101230.8577	0.204	0.796	0.679	0.321
0.07	226	281	1.188074	0.767744	0.565	0.702849	294.579945	294.82	101230.8577	0.204	0.796	0.679	0.321
0.07	229	285	1.188049	0.767744	0.5725	0.712171	294.487324	294.82	101230.8577	0.204	0.796	0.679	0.321
0.1	253	299	1.190637	0.853322	0.6325	0.747126	294.18484	294.91	101230.8577	0.2108	0.7892	0.476	0.524
0.1	250	295	1.190109	0.853322	0.625	0.738103	294.273852	294.91	101230.8577	0.2108	0.7892	0.476	0.524
0.1	247	292	1.190482	0.853322	0.6175	0.72936	294.248579	294.91	101230.8577	0.2108	0.7892	0.476	0.524
0.1	247	292	1.190482	0.853322	0.6175	0.72936	294.369625	294.91	101230.8577	0.2108	0.7892	0.476	0.524
0.1	246	290	1.189594	0.853322	0.615	0.726136	294.550978	294.91	101230.8577	0.2108	0.7892	0.476	0.524
0.1	246	290	1.189594	0.853322	0.615	0.726136	294.608252	294.91	101230.8577	0.2108	0.7892	0.476	0.524
0.1858	290	321	1.192186	0.970975	0.725	0.803352	294.334706	294.91	101230.8577	0.233	0.767	0.256	0.744
0.1858	290	321	1.192186	0.970975	0.725	0.803352	294.388953	294.91	101230.8577	0.233	0.767	0.256	0.744
0.1858	287	318	1.192508	0.970975	0.7175	0.795149	294.566996	294.91	101230.8577	0.233	0.767	0.256	0.744

ξ_{st}	a_2 (1/s)	a_1 (1/s)	rho_2 (kg/m ³)	rho_1 (kg/m ³)	V2 (m/s)	V1 (m/s)	T2 (K)	T1 (K)	P (Pa)	Y2,1	Y2,Inert	Y1,1	Y1,Inert
0.1858	288	319	1.191968	0.970975	0.72	0.797739	294.550978	294.91	101230.8577	0.233	0.767	0.256	0.744
0.1858	291	322	1.191955	0.970975	0.7275	0.806044	294.614615	294.91	101230.8577	0.233	0.767	0.256	0.744
0.25	302	328	1.197134	1.013872	0.755	0.820402	294.328333	294.58	101230.8577	0.253	0.747	0.1902	0.8098
0.25	303	329	1.196992	1.013872	0.7575	0.82307	294.178467	294.58	101230.8577	0.253	0.747	0.1902	0.8098
0.25	318	345	1.196577	1.013872	0.795	0.863666	294.331629	294.58	101230.8577	0.253	0.747	0.1902	0.8098
0.25	315	342	1.196072	1.013872	0.7875	0.855337	294.408064	294.58	101230.8577	0.253	0.747	0.1902	0.8098
0.25	314	341	1.197341	1.013872	0.785	0.853075	294.044787	294.58	101230.8577	0.253	0.747	0.1902	0.8098
0.25	315	342	1.196771	1.013872	0.7875	0.855587	294.255171	294.58	101230.8577	0.253	0.747	0.1902	0.8098
0.25	315	342	1.196771	1.013872	0.7875	0.855587	294.236056	294.58	101230.8577	0.253	0.747	0.1902	0.8098
0.4	407	433	1.205459	1.063327	1.0175	1.083371	294.343935	294.61	101230.8577	0.3162	0.6838	0.1189	0.8811
0.4	404	430	1.206189	1.063327	1.01	1.075711	294.522229	294.61	101230.8577	0.3162	0.6838	0.1189	0.8811
0.4	401	427	1.206033	1.063327	1.0025	1.067654	294.458567	294.61	101230.8577	0.3162	0.6838	0.1189	0.8811
0.4	405	431	1.2046	1.063327	1.0125	1.077663	294.611327	294.61	101230.8577	0.3162	0.6838	0.1189	0.8811
0.4	399	425	1.205419	1.063327	0.9975	1.062059	294.557341	294.61	101230.8577	0.3162	0.6838	0.1189	0.8811
0.4	404	430	1.205146	1.063327	1.01	1.075246	294.379074	294.61	101230.8577	0.3162	0.6838	0.1189	0.8811
0.5	463	492	1.219426	1.080784	1.1575	1.229502	293.519349	294.68	101230.8577	0.3794	0.6206	0.095	0.905
0.5	465	494	1.220665	1.080784	1.1625	1.23544	293.154364	294.68	101230.8577	0.3794	0.6206	0.095	0.905
0.5	468	497	1.220319	1.080784	1.17	1.243234	293.384737	294.68	101230.8577	0.3794	0.6206	0.095	0.905
0.5	460	489	1.219587	1.080784	1.15	1.221616	293.532133	294.68	101230.8577	0.3794	0.6206	0.095	0.905
0.5	463	492	1.218658	1.080784	1.1575	1.229115	293.666329	294.68	101230.8577	0.3794	0.6206	0.095	0.905
0.6	508	540	1.234224	1.092743	1.27	1.349714	293.535498	294.68	101230.8577	0.4743	0.5257	0.0793	0.9207
0.6	507	539	1.234518	1.092743	1.2675	1.347217	293.580237	294.68	101230.8577	0.4743	0.5257	0.0793	0.9207
0.6	511	543	1.234625	1.092743	1.2775	1.357905	293.58663	294.68	101230.8577	0.4743	0.5257	0.0793	0.9207
0.6	505	537	1.234948	1.092743	1.2625	1.342137	293.458781	294.68	101230.8577	0.4743	0.5257	0.0793	0.9207
0.6	504	536	1.234666	1.092743	1.26	1.339326	293.551308	294.68	101230.8577	0.4743	0.5257	0.0793	0.9207
0.6	507	539	1.234465	1.092743	1.2675	1.347189	293.589323	294.68	101230.8577	0.4743	0.5257	0.0793	0.9207
0.7	545	581	1.261454	1.111704	1.3625	1.451369	293.577219	294.67	101230.8577	0.6324	0.3676	0.0679	0.9321

ξ_{st}	a_2 (1/s)	a_1 (1/s)	rho_2 (kg/m ³)	rho_1 (kg/m ³)	V2 (m/s)	V1 (m/s)	T2 (K)	T1 (K)	P (Pa)	Y2,1	Y2,Inert	Y1,1	Y1,Inert
0.7	544	580	1.261071	1.109803	1.36	1.449725	293.682471	294.67	101230.8577	0.6324	0.3676	0.0679	0.9321
0.7	545	581	1.260755	1.109803	1.3625	1.452208	293.733569	294.67	101230.8577	0.6324	0.3676	0.0679	0.9321
0.7	551	587	1.260658	1.109803	1.3775	1.468139	293.561066	294.67	101230.8577	0.6324	0.3676	0.0679	0.9321
0.8	584	627	1.287883	1.115921	1.46	1.568463	293.577219	294.81	101230.8577	0.7905	0.2095	0.06258	0.93742
0.8	589	633	1.288612	1.115921	1.4725	1.582339	293.580237	294.81	101230.8577	0.7905	0.2095	0.06258	0.93742
0.8	589	633	1.288163	1.115921	1.4725	1.582063	293.676081	294.81	101230.8577	0.7905	0.2095	0.06258	0.93742
0.8	589	633	1.288163	1.115921	1.4725	1.582063	293.682471	294.81	101230.8577	0.7905	0.2095	0.06258	0.93742

A.3 Experimental Data: Extinction of Dimethyl Ether with $Le = 1.5$

ξ_{st}	a_2 (1/s)	a_1 (1/s)	rho_2 (kg/m ³)	rho_1 (kg/m ³)	V2 (m/s)	V1 (m/s)	T2 (K)	T1 (K)	P (Pa)	Y2,1	Y2, Inert	Y1,1	Y1, Inert
0.13432	546	431.21025	1.188669	1.90576	1.365	1.078026	293.770865	294.326056	101230.8577	0.1848	0.8152	1	0
0.13432	547	431.845406	1.188424	1.906732	1.3675	1.079614	293.720055	294.128909	101230.8577	0.1848	0.8152	1	0
0.13432	562	443.069423	1.186737	1.90934	1.405	1.107674	294.214102	293.774165	101230.8577	0.1848	0.8152	1	0
0.13432	549	432.752523	1.187547	1.911245	1.3725	1.081881	293.716719	293.440745	101230.8577	0.1848	0.8152	1	0
0.16	554	463.667155	1.188418	1.690467	1.3825	1.159168	294.051947	293	101230.8577	0.1904	0.8096	0.7945	0.2055
0.16	557	468.045839	1.18874	1.683529	1.3925	1.170115	294.023386	294.186337	101230.8577	0.1904	0.8096	0.7945	0.2055
0.16	558	467.837208	1.188481	1.684663	1.3925	1.169593	293.947125	293.987317	101230.8577	0.1904	0.8096	0.7945	0.2055
0.16	543	456.023085	1.187305	1.683403	1.3575	1.140058	294.279534	294.262818	101230.8577	0.1904	0.8096	0.7945	0.2055
0.16	547	459.060217	1.186764	1.684999	1.3675	1.147651	294.283112	293.936037	101230.8577	0.1904	0.8096	0.7945	0.2055
0.16	540	453.26448	1.187859	1.685966	1.35	1.133161	294.152316	293.746161	101230.8577	0.1904	0.8096	0.7945	0.2055
0.16	541	453.770402	1.187549	1.688005	1.3525	1.134426	294.190308	293.455256	101230.8577	0.1904	0.8096	0.7945	0.2055
0.16	529	443.560721	1.188411	1.690332	1.3225	1.108902	294.104634	293.045777	101230.8577	0.1904	0.8096	0.7945	0.2055
0.19	549	481.257752	1.189422	1.542203	1.37	1.203144	294.129874	294.434096	101230.8577	0.1975	0.8025	0.6351	0.3649
0.19	544	477.539811	1.18861	1.542475	1.36	1.19385	294.113808	294.416483	101230.8577	0.1975	0.8025	0.6351	0.3649
0.19	544	477.414217	1.188045	1.542553	1.36	1.193536	294.269844	294.383141	101230.8577	0.1975	0.8025	0.6351	0.3649
0.19	539	472.921662	1.189514	1.545143	1.3475	1.182304	294.027583	293.900757	101230.8577	0.1975	0.8025	0.6351	0.3649
0.22	546	493.559906	1.190847	1.457342	1.365	1.2339	293.91964	294.696995	101230.8577	0.2051	0.7949	0.5256	0.4744
0.22	546	492.599976	1.190587	1.457355	1.3625	1.2315	294.136511	294.732161	101230.8577	0.2051	0.7949	0.5256	0.4744
0.22	539	487.334908	1.191001	1.456916	1.3475	1.218337	293.906874	294.820071	101230.8577	0.2051	0.7949	0.5256	0.4744
0.22	534	481.61271	1.189517	1.456898	1.3325	1.204032	294.228806	294.833926	101230.8577	0.2051	0.7949	0.5256	0.4744
0.22	543	489.865342	1.190187	1.457003	1.355	1.224663	294.097733	294.846814	101230.8577	0.2051	0.7949	0.5256	0.4744
0.3136	529	500.470074	1.195043	1.330133	1.32	1.251175	294.009501	295.170811	101230.8577	0.233	0.767	0.3349	0.6651
0.3136	526	497.550531	1.194498	1.329933	1.3125	1.243876	293.964842	295.16989	101230.8577	0.233	0.767	0.3349	0.6651
0.3136	523	495.684774	1.194383	1.329646	1.3075	1.239212	294.11101	295.300217	101230.8577	0.233	0.767	0.3349	0.6651

ξ_{st}	a_2 (1/s)	a_1 (1/s)	rho_2 (kg/m ³)	rho_1 (kg/m ³)	V2 (m/s)	V1 (m/s)	T2 (K)	T1 (K)	P (Pa)	Y2,1	Y2, Inert	Y1,1	Y1, Inert
0.3136	525	497.637905	1.194551	1.329525	1.3125	1.244095	294.133727	295.262364	101230.8577	0.233	0.767	0.3349	0.6651
0.3136	534	504.187704	1.194124	1.3295	1.33	1.260469	294.123763	295.278019	101230.8577	0.233	0.767	0.3349	0.6651
0.3136	532	502.232832	1.194306	1.330016	1.325	1.255582	293.868851	295.18186	101230.8577	0.233	0.767	0.3349	0.6651
0.4	546	529.00864	1.199751	1.278059	1.365	1.322522	293.880825	295.500822	101230.8577	0.2666	0.7334	0.2471	0.7529
0.4	553	534.53763	1.198712	1.278311	1.38	1.336344	294.148743	295.384293	101230.8577	0.2666	0.7334	0.2471	0.7529
0.4	550	532.506965	1.198725	1.278775	1.375	1.331267	294.218861	295.320475	101230.8577	0.2666	0.7334	0.2471	0.7529
0.4	548	529.450627	1.198323	1.27908	1.3675	1.323627	294.444628	295.275088	101230.8577	0.2666	0.7334	0.2471	0.7529
0.4	550	532.406584	1.198829	1.279368	1.375	1.331016	294.266274	295.221436	101230.8577	0.2666	0.7334	0.2471	0.7529
0.5	583	572.963982	1.206628	1.244987	1.455	1.43241	294.109978	295.743002	101230.8577	0.3199	0.6801	0.1877	0.8123
0.5	584	575.210365	1.207963	1.245163	1.46	1.438026	294.291516	295.644967	101230.8577	0.3199	0.6801	0.1877	0.8123
0.5	575	565.894928	1.206629	1.24577	1.4375	1.414737	294.403109	295.467444	101230.8577	0.3199	0.6801	0.1877	0.8123
0.5	581	570.767221	1.207282	1.246656	1.45	1.426918	294.243845	295.286166	101230.8577	0.3199	0.6801	0.1877	0.8123
0.5	570	560.438091	1.206133	1.247641	1.425	1.401095	294.466788	295.081734	101230.8577	0.3199	0.6801	0.1877	0.8123
0.5	575	564.156234	1.206108	1.248565	1.435	1.410391	294.485644	294.861491	101230.8577	0.3199	0.6801	0.1877	0.8123
0.5	561	551.213551	1.206602	1.249828	1.4025	1.378034	294.403109	294.554291	101230.8577	0.3199	0.6801	0.1877	0.8123
0.6	664	662.472432	1.220083	1.225716	1.66	1.656181	294.020348	295.694495	101230.8577	0.3999	0.6001	0.1503	0.8497
0.6	660	657.678296	1.221048	1.225961	1.6475	1.644196	294.157601	295.623324	101230.8577	0.3999	0.6001	0.1503	0.8497
0.6	658	656.465039	1.220573	1.226287	1.645	1.641163	293.870543	295.508654	101230.8577	0.3999	0.6001	0.1503	0.8497
0.6	661	658.23898	1.220558	1.227097	1.65	1.645597	293.723988	295.361662	101230.8577	0.3999	0.6001	0.1503	0.8497
0.6	653	651.291526	1.221473	1.227889	1.6325	1.628229	293.944081	295.179415	101230.8577	0.3999	0.6001	0.1503	0.8497
0.7	762	770.980591	1.242875	1.210905	1.9025	1.927451	294.092688	296.112168	101230.8577	0.5332	0.4668	0.1247	0.8753
0.7	759	769.087436	1.243779	1.211366	1.8975	1.922719	293.74837	296.017941	101230.8577	0.5332	0.4668	0.1247	0.8753
0.7	759	768.552923	1.242132	1.211445	1.8975	1.921382	293.850525	295.99668	101230.8577	0.5332	0.4668	0.1247	0.8753
0.7	758	767.068161	1.240895	1.211729	1.895	1.91767	294.354279	295.945835	101230.8577	0.5332	0.4668	0.1247	0.8753
0.7	752	760.386105	1.242521	1.212035	1.8775	1.900965	294.029763	295.793398	101230.8577	0.5332	0.4668	0.1247	0.8753
0.7	752	756.49144	1.242558	1.221325	1.875	1.891229	293.979325	293.63358	101230.8577	0.5332	0.4668	0.1247	0.8753
0.7	770	779.606674	1.244894	1.214402	1.925	1.949017	293.440359	295.310929	101230.8577	0.5332	0.4668	0.1247	0.8753

ξ_{st}	a_2 (1/s)	a_1 (1/s)	rho_2 (kg/m ³)	rho_1 (kg/m ³)	V2 (m/s)	V1 (m/s)	T2 (K)	T1 (K)	P (Pa)	Y2,1	Y2, Inert	Y1,1	Y1, Inert
0.8	885	915.075938	1.286969	1.203761	2.2125	2.28769	294.257622	295.587838	101230.8577	0.7997	0.2003	0.106	0.894
0.8	884	912.943079	1.287176	1.204126	2.2075	2.282358	293.753933	295.510207	101230.8577	0.7997	0.2003	0.106	0.894
0.8	889	918.485666	1.286244	1.204986	2.2225	2.296214	294.366194	295.272511	101230.8577	0.7997	0.2003	0.106	0.894
0.8	877	904.74634	1.286912	1.206433	2.19	2.261866	294.209956	294.981087	101230.8577	0.7997	0.2003	0.106	0.894
0.8	885	913.853898	1.28747	1.207452	2.2125	2.284635	294.312184	294.717427	101230.8577	0.7997	0.2003	0.106	0.894
0.8	881	908.995384	1.287524	1.209439	2.2025	2.272488	294.375883	294.247219	101230.8577	0.7997	0.2003	0.106	0.894

A.4 Experimental Data: Extinction of Dimethyl Ether with $Le = 1.4$

ξ_{st}	a_2 (1/s)	a_1 (1/s)	ρ_2 (kg/m ³)	ρ_1 (kg/m ³)	V2 (m/s)	V1 (m/s)	T2 (K)	T1 (K)	P (Pa)	Y2,1	Y2, Inert	Y1,1	Y1, Inert
0.12366	546	430.576868	1.186822	1.908401	1.365	1.076442	293.902752	293.928105	101230.8577	0.1825	0.8175	1	0
0.13432	537	437.027672	1.186923	1.792063	1.3425	1.092569	294.097733	294.256312	101230.8577	0.1848	0.8152	0.9012	0.0988
0.13432	545	443.685273	1.186911	1.790858	1.3625	1.109213	294.218861	294.423867	101230.8577	0.1848	0.8152	0.9012	0.0988
0.13432	538	438.211428	1.187928	1.790553	1.345	1.095529	293.944641	294.487736	101230.8577	0.1848	0.8152	0.9012	0.0988
0.16	524	448.539238	1.188569	1.615946	1.3075	1.121348	293.838953	294.660746	101230.8577	0.1904	0.8096	0.7239	0.2761
0.16	541	463.685545	1.187191	1.616099	1.3525	1.159214	294.237982	294.617314	101230.8577	0.1904	0.8096	0.7239	0.2761
0.16	530	454.428939	1.187911	1.61586	1.325	1.136072	294.014822	294.683949	101230.8577	0.1904	0.8096	0.7239	0.2761
0.16	532	456.292764	1.188594	1.615733	1.33	1.140732	294.097733	294.70801	101230.8577	0.1904	0.8096	0.7239	0.2761
0.16	525	450.487454	1.188698	1.614451	1.3125	1.126219	293.788128	294.92914	101230.8577	0.1904	0.8096	0.7239	0.2761
0.16	533	457.144379	1.187846	1.61476	1.3325	1.142861	293.931878	294.883826	101230.8577	0.1904	0.8096	0.7239	0.2761
0.19	525	467.126887	1.189307	1.502253	1.3125	1.167817	293.848908	294.533091	101230.8577	0.1975	0.8025	0.5847	0.4153
0.19	534	475.299156	1.19025	1.502404	1.335	1.188248	293.970421	294.493332	101230.8577	0.1975	0.8025	0.5847	0.4153
0.19	526	467.253855	1.189591	1.501795	1.3125	1.168135	293.833083	294.620112	101230.8577	0.1975	0.8025	0.5847	0.4153
0.19	526	467.821827	1.190427	1.504919	1.315	1.169555	293.747813	294.026881	101230.8577	0.1975	0.8025	0.5847	0.4153
0.19	529	470.894811	1.191178	1.503282	1.3225	1.177237	293.540583	294.269534	101230.8577	0.1975	0.8025	0.5847	0.4153
0.22	527	478.508499	1.191615	1.439886	1.315	1.196271	293.86386	292.86349	101230.8577	0.2051	0.7949	0.488	0.512
0.22	528	480.702729	1.191512	1.437517	1.32	1.201757	293.755328	293.370383	101230.8577	0.2051	0.7949	0.488	0.512
0.22	516	470.176776	1.192471	1.436234	1.29	1.175442	293.627571	293.652005	101230.8577	0.2051	0.7949	0.488	0.512
0.22	529	481.920547	1.190684	1.434686	1.3225	1.204801	293.940447	293.934481	101230.8577	0.2051	0.7949	0.488	0.512
0.22	522	477.45416	1.19044	1.43386	1.31	1.193635	293.806408	294.053008	101230.8577	0.2051	0.7949	0.488	0.512
0.22	522	475.950611	1.191875	1.433665	1.305	1.189877	293.902161	294.142823	101230.8577	0.2051	0.7949	0.488	0.512
0.3136	526	498.84657	1.195057	1.328697	1.315	1.247116	294.044339	293.109412	101230.8577	0.233	0.767	0.3168	0.6832
0.3136	527	500.106595	1.19472	1.326667	1.3175	1.250266	294.088986	293.516159	101230.8577	0.233	0.767	0.3168	0.6832
0.3136	517	490.670401	1.194486	1.326119	1.2925	1.226676	294.012448	293.648623	101230.8577	0.233	0.767	0.3168	0.6832

ξ_{st}	a_2 (1/s)	a_1 (1/s)	rho_2 (kg/m ³)	rho_1 (kg/m ³)	V2 (m/s)	V1 (m/s)	T2 (K)	T1 (K)	P (Pa)	Y2,1	Y2, Inert	Y1,1	Y1, Inert
0.3136	530	502.27954	1.194201	1.32464	1.3225	1.255699	294.082608	293.989443	101230.8577	0.233	0.767	0.3168	0.6832
0.3136	525	497.886953	1.194927	1.323556	1.31	1.244717	293.990279	294.20336	101230.8577	0.233	0.767	0.3168	0.6832
0.3136	517	491.508197	1.194655	1.321789	1.2925	1.22877	294.00607	294.589335	101230.8577	0.233	0.767	0.3168	0.6832

A.5 Experimental Data: Extinction of Dimethyl Ether with $Le = 1.6$

ξ_{st}	a_2 (1/s)	a_1 (1/s)	ρ_2 (kg/m ³)	ρ_1 (kg/m ³)	V2 (m/s)	V1 (m/s)	T2 (K)	T1 (K)	P (Pa)	Y2,1	Y2, Inert	Y1,1	Y1, Inert
0.16	610	501.177175	1.188876	1.76122	1.525	1.252943	293.549216	293.711913	101230.8577	0.1904	0.8096	0.8693	0.1307
0.16	617	505.654055	1.189174	1.759093	1.5375	1.264135	293.855952	293.963486	101230.8577	0.1904	0.8096	0.8693	0.1307
0.16	622	508.369676	1.1888	1.768207	1.55	1.270924	293.880564	292.590163	101230.8577	0.1904	0.8096	0.8693	0.1307
0.16	614	503.812968	1.189938	1.76735	1.535	1.259532	293.644587	292.716292	101230.8577	0.1904	0.8096	0.8693	0.1307
0.16	628	513.900402	1.190391	1.766365	1.565	1.284751	293.641241	292.917406	101230.8577	0.1904	0.8096	0.8693	0.1307
0.16	622	512.256798	1.189439	1.753668	1.555	1.280642	293.66902	295	101230.8577	0.1904	0.8096	0.8693	0.1307
0.19	593	512.531604	1.191142	1.594526	1.4825	1.281329	293.52365	292.859488	101230.8577	0.1975	0.8025	0.6879	0.3121
0.19	605	521.209704	1.190598	1.593583	1.5075	1.303024	293.616183	293.063359	101230.8577	0.1975	0.8025	0.6879	0.3121
0.19	610	527.472146	1.193418	1.596074	1.525	1.31868	293.060044	292.591278	101230.8577	0.1975	0.8025	0.6879	0.3121
0.19	615	532.703096	1.193431	1.595836	1.54	1.331758	293.139622	292.64404	101230.8577	0.1975	0.8025	0.6879	0.3121
0.19	614	531.553994	1.190539	1.588495	1.535	1.328885	293.601727	294.016844	101230.8577	0.1975	0.8025	0.6879	0.3121
0.19	613	530.535063	1.189571	1.58812	1.5325	1.326338	293.885777	294.015894	101230.8577	0.1975	0.8025	0.6879	0.3121
0.19	616	531.707012	1.189895	1.586721	1.535	1.329268	293.681734	294.230753	101230.8577	0.1975	0.8025	0.6879	0.3121
0.22	599	534.768062	1.19114	1.494465	1.4975	1.33692	293.875777	293.045918	101230.8577	0.2051	0.7949	0.5646	0.4354
0.22	606	539.423491	1.191749	1.494167	1.51	1.348559	293.776688	293.131148	101230.8577	0.2051	0.7949	0.5646	0.4354
0.22	600	534.434442	1.192359	1.492864	1.495	1.336086	293.665053	293.368382	101230.8577	0.2051	0.7949	0.5646	0.4354
0.22	590	526.796249	1.190237	1.492973	1.475	1.316991	294.12403	293.382183	101230.8577	0.2051	0.7949	0.5646	0.4354
0.22	606	541.260519	1.189864	1.491523	1.515	1.353151	294.053616	293.66375	101230.8577	0.2051	0.7949	0.5646	0.4354
0.22	602	538.065122	1.190509	1.49024	1.505	1.345163	294.063313	293.899016	101230.8577	0.2051	0.7949	0.5646	0.4354
0.3136	592	558.381897	1.195665	1.343972	1.48	1.395955	293.43829	294.492623	101230.8577	0.233	0.767	0.3531	0.6469
0.3136	589	555.525052	1.195796	1.344251	1.4725	1.388813	293.655333	294.450922	101230.8577	0.233	0.767	0.3531	0.6469
0.3136	590	556.587696	1.196603	1.344581	1.475	1.391469	293.594494	294.371291	101230.8577	0.233	0.767	0.3531	0.6469
0.3136	588	554.465417	1.196095	1.345152	1.47	1.386164	293.993695	294.273186	101230.8577	0.233	0.767	0.3531	0.6469
0.3136	593	559.092983	1.19476	1.34407	1.4825	1.397732	294.015345	294.501711	101230.8577	0.233	0.767	0.3531	0.6469

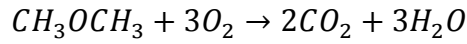
ξ_{st}	a_2 (1/s)	a_1 (1/s)	rho_2 (kg/m ³)	rho_1 (kg/m ³)	V2 (m/s)	V1 (m/s)	T2 (K)	T1 (K)	P (Pa)	Y2,1	Y2, Inert	Y1,1	Y1, Inert
0.3136	588	552.374529	1.194423	1.344268	1.465	1.380936	294.059994	294.446171	101230.8577	0.233	0.767	0.3531	0.6469
0.3136	594	560.061653	1.194656	1.343829	1.485	1.400154	294.149264	294.569279	101230.8577	0.233	0.767	0.3531	0.6469
0.3136	580	547.075857	1.195329	1.343533	1.45	1.36769	293.945162	294.685889	101230.8577	0.233	0.767	0.3531	0.6469
0.3136	602	567.463914	1.193659	1.343373	1.505	1.41866	294.139832	294.675732	101230.8577	0.233	0.767	0.3531	0.6469

Appendix B

Professor K. Seshadri (2015) developed the following asymptotic formulation for extinction of dimethyl ether under non-premixed conditions.

Chemical Reaction

The overall chemical reaction for dimethyl ether (CH_3OCH_3) and O_2 is



the reaction rate, ω_{dme} with units of $1 / (\text{m}^3 \text{ s})$.

Formulation

Consider two counterflowing streams flowing toward a stagnation plane. One stream called the fuel stream is injected toward the stagnation plane from the fuel boundary. It is made up of CH_3OCH_3 and N_2 . The other stream, called the oxidizer stream, is injected from the oxidizer boundary. It is made up of O_2 , and N_2 . The mass fractions of dimethyl ether at the fuel boundary is represented by $Y_{dme,1}$, and the mass fraction of O_2 at the oxidizer boundary is represented by $Y_{\text{O}_2,2}$.

The species balance equations are

$$\rho a \hat{x} \frac{dY_{dme}}{d\hat{x}} + \rho D_{dme} \frac{d^2 Y_{dme}}{d\hat{x}^2} = W_{dme} \omega_{dme} \quad (1)$$

$$\rho a \hat{x} \frac{dY_{\text{O}_2}}{d\hat{x}} + \rho D_{\text{O}_2} \frac{d^2 Y_{\text{O}_2}}{d\hat{x}^2} = 3W_{\text{O}_2} \omega_{dme}$$

Here D_{dme} , and D_{O_2} are respectively the coefficient of diffusion for CH_3OCH_3 and O_2 . The energy conservation equation is

$$\rho c_p a \hat{x} \frac{dT}{d\hat{x}} + \lambda \frac{d^2T}{d\hat{x}^2} + \sum_{i=1}^n \rho D_i c_{p,i} \frac{dY_i}{d\hat{x}} \frac{dT}{d\hat{x}} = -Q_{dme} \omega_{dme} \quad (2)$$

Here λ is the coefficient of thermal conductivity, c_p is the heat capacity of the mixture, $c_{p,i}$ is the heat capacity of species i , D_i is the coefficient of diffusion of species i , and Q_{dme} is the heat released per mole of CH_3OCH_3 consumed.

Define the independent variable

$$x = \hat{x} \left(\frac{\rho c_p a}{\lambda} \right)^{1/2} \quad (3)$$

For convenience, the definitions

$$\begin{aligned} X_i &\equiv Y_i W_{N_2} / W_i \\ \tau &\equiv (T - T_{ref}) / \Delta T_{ref} \\ M_{dme} &\equiv W_{N_2} \omega_{dme} / (\rho a) \\ G_{dme} &\equiv Q_{dme} / (W_{N_2} c_p \Delta T_{ref}) \end{aligned} \quad (4)$$

are introduced. Here W_i is the molecular weight of species i , W_{N_2} is the molecular weight of nitrogen, T_{ref} is a reference temperature and ΔT_{ref} is a reference temperature difference.

Introducing Eqs. (3) and (4) into Eq. (1), the following equations are obtained

$$\begin{aligned} x \frac{dX_{dme}}{dx} + \frac{1}{Le_{dme}} \frac{d^2 X_{dme}}{dx^2} &= M_{dme} \\ x \frac{dX_{O_2}}{dx} + \frac{1}{Le_{O_2}} \frac{d^2 X_{O_2}}{dx^2} &= 3M_{dme} \end{aligned} \quad (5)$$

Introducing Eqs. (3) and (4) into Eq. (2), the following equation is obtained

$$x \frac{d\tau}{dx} + \frac{d^2 \tau}{dx^2} + \sum_{i=1}^n \frac{1}{Le_i} \frac{W_i}{W_{N_2}} \frac{c_{p,i}}{c_p} \frac{dX_i}{dx} \frac{d\tau}{dx} = -G_{dme} M_{dme} \quad (6)$$

The conserved scalar quantities ξ , ξ_{oct} , and ξ_{dme} are defined by the equations

$$x \frac{d\xi}{dx} + \frac{d^2\xi}{dx^2} = 0 \quad (7)$$

$$x \frac{d\xi_{dme}}{dx} + \frac{1}{Le_{dme}} \frac{d^2\xi_{dme}}{dx^2} = 0$$

Eq. (7) is constrained to satisfy the conditions

$$\begin{aligned} \xi = \xi_{dme} = 0; x = \infty \\ \xi = \xi_{dme} = 1; x = -\infty \end{aligned} \quad (8)$$

Integration of Eq. (7) together with Eq. (8) gives

$$\xi = \frac{1}{2} \operatorname{erfc} \left(x_{st} \sqrt{\frac{1}{2}} \right) \quad (9)$$

$$\xi_{dme} = \frac{1}{2} \operatorname{erfc} \left(x_{st} \sqrt{\frac{Le_{dme}}{2}} \right)$$

Differentiation of Eq. (9) gives

$$\frac{d\xi}{dx} = - \left(\sqrt{\frac{1}{2\pi}} \right) \exp \left(-\frac{x^2}{2} \right) \quad (10)$$

$$\frac{d\xi_{dme}}{dx} = - \left(\sqrt{\frac{Le_{dme}}{2\pi}} \right) \exp \left(-\frac{x^2 Le_{dme}}{2} \right)$$

It follows from Eq. (10)

$$\frac{d\xi_{dme}}{dx} = (\sqrt{Le_{dme}}) \frac{d\xi}{dx} \left\{ \exp \left[\frac{x^2(1 - Le_{dme})}{2} \right] \right\} \quad (11)$$

Coupling Relations at x_{st}

Let the flame sheet be located at $x = x_{st}$. At the flame sheet, $\xi = \xi_{st}$, and $\xi_{dme} = \xi_{dme,st}$. At x_{st} there is complete consumption of CH_3OCH_3 , and O_2 . At x_{st} the gradients are

$$\frac{1}{Le_{dme}} \frac{dX_{dme}}{dx} + \frac{1}{Le_{dme}} \frac{dX_{dme}}{d\xi_{dme}} \frac{d\xi_{dme}}{dx} = \frac{1}{Le_{dme}} \frac{X_{dme,1}}{1 - \xi_{dme,st}} \frac{d\xi_{dme}}{dx} \quad (12)$$

$$\frac{dX_{CO_2}}{dx} = \frac{dX_{CO_2}}{d\xi} \frac{d\xi}{dx} = - \frac{X_{CO_2,st}}{1 - \xi_{st}} \frac{d\xi}{dx}$$

$$\frac{dX_{H_2O}}{dx} = \frac{dX_{H_2O}}{d\xi} \frac{d\xi}{dx} = - \frac{X_{H_2O,st}}{1 - \xi_{st}} \frac{d\xi}{dx}$$

$$\frac{d\tau}{dx} = \frac{d\tau}{d\xi} \frac{d\xi}{dx} = - \frac{\tau_{st}}{1 - \xi_{st}} \frac{d\xi}{dx}$$

At x_{st+} the gradients are

$$\frac{dX_{O_2}}{dx} = \frac{dX_{O_2}}{d\xi} \frac{d\xi}{dx} = - \frac{X_{O_2,2}}{\xi_{st}} \frac{d\xi}{dx} \quad (13)$$

$$\frac{dX_{CO_2}}{dx} = \frac{dX_{CO_2}}{d\xi} \frac{d\xi}{dx} = \frac{X_{CO_2,st}}{\xi_{st}} \frac{d\xi}{dx}$$

$$\frac{dX_{H_2O}}{dx} = \frac{dX_{H_2O}}{d\xi} \frac{d\xi}{dx} = \frac{X_{H_2O,st}}{\xi_{st}} \frac{d\xi}{dx}$$

$$\frac{d\tau}{dx} = \frac{d\tau}{d\xi} \frac{d\xi}{dx} = \frac{\tau_{st}}{\xi_{st}} \frac{d\xi}{dx}$$

The gradients at ξ_{st+} are

$$\frac{1}{Le_{dme}} \frac{dX_{dme}}{d\xi} = \frac{1}{\sqrt{Le_{dme}}} \frac{X_{dme,1}}{1 - \xi_{dme,st}} \left\{ \exp \left[\frac{x^2(1 - Le_{dme})}{2} \right] \right\} = m \quad (14)$$

$$\frac{dX_{CO_2}}{d\xi} = - \frac{X_{CO_2,st}}{1 - \xi_{st}}$$

$$\frac{dX_{H_2O}}{d\xi} = - \frac{X_{H_2O,st}}{1 - \xi_{st}}$$

$$\frac{d\tau}{d\xi} = -\frac{\tau}{1 - \xi_{st}} = -p$$

At ξ_{st} - the gradients are

$$\frac{dX_{O_2}}{d\xi} = -\frac{X_{O_2,2}}{\xi_{st}} = -c \quad (15)$$

$$\frac{dX_{CO_2}}{d\xi} = \frac{X_{CO_2,st}}{\xi_{st}}$$

$$\frac{dX_{H_2O}}{d\xi} = \frac{X_{H_2O,st}}{\xi_{st}}$$

$$\frac{d\tau}{d\xi} = \frac{\tau_{st}}{\xi_{st}} = s$$

Balance equation for carbon across the reaction zone at $x = x_{st}$ is

$$\left(\frac{2}{Le_{dme}} \frac{dX_{dme}}{dx} + \frac{dX_{CO_2}}{dx} \right)_{\pm} = 0 \quad (16)$$

Balance equation for oxygen across the reaction zone at $x = x_{st}$ is

$$\left(\frac{1}{Le_{dme}} \frac{dX_{dme}}{dx} + 2 \frac{dX_{O_2}}{dx} + 2 \frac{dX_{CO_2}}{dx} + \frac{dX_{H_2O}}{dx} \right)_{\pm} = 0 \quad (17)$$

Balance equation for hydrogen across the reaction zone at $x = x_{st}$ is

$$\left(\frac{3}{Le_{dme}} \frac{dX_{dme}}{dx} + \frac{dX_{H_2O}}{dx} \right)_{\pm} = 0 \quad (18)$$

It follows from Eqs. (16), (17) and (18)

$$\left(\frac{3}{Le_{dme}} \frac{dX_{dme}}{dx} - \frac{dX_{O_2}}{dx} \right)_{\pm} = 0 \quad (19)$$

Use of Eqs. (14), and (15), into Eq. (19) gives

$$3m = c \quad (20)$$

Coupling relations for temperature gives

$$\left(\frac{d\tau}{dx} \frac{G_{dme}}{Le_{dme}} - \frac{dX_{dme}}{dx} \right)_{\pm} = 0 \quad (21)$$

This gives

$$\tau_{st} = mG_{dme}\xi_{st}(1 - \xi_{st}) \quad (22)$$

The adiabatic flame temperature T_{st} is

$$T_{st} = T_u + \frac{m}{c_p W_{N_2}} Q_{dme} \xi_{st} (1 - \xi_{st}) \quad (23)$$